CHAPTER THREE

Quantum Control in Multilevel Systems

Ignacio R. Sola*, Bo Y. Chang†, Svetlana A. Malinovskaya‡, Vladimir S. Malinovsky§

*Universidad Complutense de Madrid, Madrid, Spain
†School of Chemistry (BK21), Seoul National University, Seoul, Republic of Korea
‡Stevens Institute of Technology, Hoboken, NJ, United States
§US Army Research Laboratory, Adelphi, MD, United States

Contents

Advances in Atomic, Molecular, and Optical Physics, Volume 67
ISSN 1049-250X
https://doi.org/10.1016/bs.aamop.2018.02.003

Abstract

Quantum control originated in the mid-1980s as a set of different laser schemes designed to manipulate chemical reactions and excite the molecule in specific quantum states. In the last four decades it has enlarged its scope to optimize any type of process in quantum systems. In this chapter we analyze in a stepwise manner how the different laser parameters: pulse area, optical phase, duration, timing, frequency and intensity, affect the dynamics, motivating different quantum control mechanisms. We explain the control setups in simple scenarios that involve a few particles, mostly a trapped ion, a quantum dot or a diatomic molecule. Using examples from our own publications, we show how the different control schemes can be used to prepare the system in specific quantum states, or prepare quantum gates, or manipulate the position and width of the wave function, or control the geometry, photophysics, and photochemistry of the molecule in the excited state. Finally, we give an introduction to the techniques of optimal control theory that allow to generalize and globally optimize the dynamics of the system by using a variational approach.

1. INTRODUCTION

Atomic and molecular physics were first studied from a static or structural point of view, by which ever more precise or computationally efficient theoretical methods were developed for determining the electronic structure, and then there was a nondynamic view of processes in excited states based on scattering theory. Laser sources and molecular beams tested the Hamiltonian eigenvalues and state-to-state cross sections. The first dynamical theories were proposed to explain the relaxation processes that limited the precision that could be achieved by measuring those observables. And then came the development of dynamic spectroscopy to resolve in time the dynamics. But how and in what sense the new field of quantum control (QC) emerged and why was it needed?

The usual narrative starts with the story of a failure: the application of lasers tuned to fundamental frequencies of vibrational modes of molecules to selectively break the chemical bonds did not produce the desired fragments. In spite of the large energy deposited with strong continuous wave laser sources in the selected bond, most energy was effectively dissipated as

heat. This led to the development of ultrashort laser pulses and Femtochemistry (Rosker et al., 1988; Zewail, 1988, 2000). The key experimental realization of a pump-probe experiment allowed to probe a time-slice of the dynamics of the molecule out of equilibrium, allowing the characterization of the transition states. While scanning different time delays allows to follow the evolution of the wave packet in the excited potential, one can select the particular frame with the largest overlap of the wave packet to the desired state or location in the ground potential. By using a probe pulse acting as a Stokes pulse at the right time delay one can restore the wave packet to the ground potential at the desired position. This is the underlying principle of the Tannor–Rice–Kosloff control scheme (Tannor and Rice, 1985; Tannor et al., 1986). As more complex systems were studied and higher yields demanded, the control was exerted not only in the timing of the electronic transitions, but also in the wave packet motion within each electronic state. That required the use of stronger fields or pulse bandwidths comprising the infrared and visible parts of the spectrum and algorithms that could find the right parameters in the high-dimensional space of solutions, paving the way to optimization strategies (Judson and Rabitz, 1992; Peirce et al., 1988).

However, this is only one leg of the story. For the other one, we should pay attention to progress in nonlinear laser spectroscopy (Berman and Malinovsky, 2011). In general, the role of coherence and henceforth the relative phases (or time delays) between laser pulses or frequency components, revealed as a key principle to drive quantum systems. Adiabatic control (Bergmann et al., 1998) and coherent control (Shapiro and Brumer, 1999) emerged from nonlinear high-finesse spectroscopic techniques in order to overcome the difficulties in observing population inversion by resonant absorption, the so-called Rabi oscillations. Essentially, the relative phase between the pulses and the sequence by which isolated Hamiltonian resonances act in the dynamics play the essential role in determining the outcome of the desired molecular process, which is predesigned by the controller. For instance, quantum control is needed to improve the yield of a Raman transition avoiding fluorescence in the stimulated Raman adiabatic passage or STIRAP scheme of Gaubatz et al. (1990). It is also needed to select a target state from a set of degenerate quantum states in the coherent control schemes of Brumer and Shapiro (1986). The control is thus exerted mainly in the frequency domain, by focusing several phase-locked laser beams or designing specific sequences of pulses. Interesting theoretical concepts, like the dressed states, have their roots in these original ideas.

From the experimental point of view QC grew side by side with pulse modulation or pulse shaping techniques. An ultrashort, minimal time-width pulse implies a transform-limited maximally coherent pulse, but the phase relation between different spectral components can be manipulated in pulse-shapers, inducing temporal profiles in the pulses as complex as demanded (Brixner and Gerber, 2001; Spano et al., 1987; Weiner et al., 1986). In the simplest case, the phase varies quadratically with the pulse, inducing a linear chirp (the pulse frequency shifts from red to blue or blue to red as the pulse proceeds). In the adiabatic rapid passage or ARP scheme (Bergmann et al., 1998; Shore, 2011; Vitanov et al., 2001, 2017) the yield of an optical transition is greatly enhanced using chirped pulses where the frequency sweeps across the resonance. On the other hand, several frequency components can work in parallel with certain phase relationships, as in the Shapiro and Brumer (1999). Other phases have been used to modulate, mask certain frequencies or split the original pulse into subpulses (Brixner et al., 2005; Silberberg, 2009; Wollenhaupt et al., 2005).

Besides the time or frequency domain properties of the pulses, the laser intensity constitutes another essential control knob that is recently gaining a leading role in new control scenarios. Beyond intensities larger than the TW cm^{-2} but below intensities that ionize the molecule, many nonlinear multiphoton transitions may occur. Additionally, Autler–Townes resonances and strong Stark shifts modify the electronic forces and reshape the potential energy surfaces. Yuan and George (1978) and Bandrauk and Sink (1981) introduced a "chemical" picture of light-induced processes, where the slow effects of the field on the nuclei (averaged over the radiation cycles) are incorporated in the dressed (energy shifted and distorted) molecular potentials, which are called light-induced potentials or LIPs. Static phenomena like bond hardening in a laser-free dissociative state (Zavriyev et al., 1993) or bond softening of the ground state (Bucksbaum et al., 1990) were first interpreted in the light of the LIPs, and the dynamics of photodissociation or multiphoton processes was recast in terms of predissociation, avoided crossings, or other topological features of the LIPs, with the important difference that now the position of the laser-induced avoided crossings, LIACs (Gonzalez-Vazquez et al., 2009) or in general, of the laser-induced conical intersections, LICIs (Csehi et al., 2017; Demekhin and Cederbaum, 2013; Halász et al., 2012a,b, 2013a,b, 2014, 2015; Moiseyev et al., 2008; Sindelka et al., 2011) can be externally controlled. Much effort has been put recently in characterizing the LICIs and exploiting then to control molecular properties.

Many schemes of adiabatic control can be translated to this so-called moderately intense regime, allowing to control the selective transfer of vibronic population through the LIPs, as in the adiabatic passage by light-induced potentials or APLIP scheme (Chang et al., 2001c; Garraway and Suominen, 1998; Gonzalez-Vazquez et al., 2006a; Malinovsky et al., 2003; Rodriguez et al., 2000; Sola et al., 2000a,b), sometimes aided with frequency chirped pulses (Chang et al., 2000; Kallush and Band, 2000), or the selective population of dressed states or SPODS scheme (Bayer et al., 2008; Wollenhaupt and Baumert, 2006; Wollenhaupt et al., 2006, 2010). Not only one can control the population transfer between different electronic states, but also its structure and its photophysical (internal conversion, intersystem crossing) and photochemical processes. The development of the non-resonant dynamic stark effect scheme, by Sussman et al. (2006), stimulated novel approaches to control chemical reactions (Corrales et al., 2014, 2017; Kim et al., 2012).

While the nuclear wave function encodes the molecular structure, given by the shape or the geometry, the electronic distribution is responsible for the chemical properties. In particular, the dipole moment typically provides simplified information regarding the distribution of charges, so it is particularly interesting to create and manipulate the molecular dipoles. In principle, the laser field drives directly the charges, leading at sufficiently strong amplitudes to tunnel ionization and recombination (Lewenstein et al., 1994; Seideman et al., 1995). At lower intensities, however, it is sometimes possible (Albert et al., 2016; Calegari et al., 2014; Chang et al., 2015b; Falge et al., 2012a; Jiménez-Galán et al., 2014) to control the charge displacement while the electron–nuclear motions remain correlated.

In many ways one can regard QC as an additional set of tools that the experimentalist or theoretician in the atomic, molecular and optical physics (the AMO community) has at her disposal. Indeed one can claim that there is no experiment in laser physics without a careful design and tuning of the laser parameters, typically named in QC as the control knobs. And from the theoretical point of view, what can there be more than solving the time-dependent Schrödinger equation (TDSE) in the presence of an external field? However, as progress through this review will show, the goal of driving a quantum system to a predetermined target state (an eigenstate of the Hamiltonian or of a different operator), or to accomplish some process (like a photochemical process or the processing of quantum information), was more complex than initially expected. As the number of laser parameters or control knobs grew, the strategies to manipulate these parameters had to

evolve too. In general, one needs to synchronize the natural evolution of the Hamiltonian dynamics, determined by phase differences, with the multispectral nature of the driving pulse. A most effective experimental setup, usually referred as adaptive learning, was proposed by Judson and Rabitz (1992) which couples the pulse-shapers that modulate the control pulse with learning algorithms that retrieve the information from the probe in a closed-loop design.

The change in paradigm from solving the TDSE to an inversion (or rather a dynamical optimization process), and to a learning process, required the development of new theory to understand general features of the cost functionals and of the time-evolution operators. This corpse of theory is generally referred to as quantum optimal control theory (QOCT) and is a distinct feature of QC with respect to other approaches. In the last 15 years, many experimental results in the laser control of photofragmentation of complex molecules (Assion et al., 1998; Brixner and Gerber, 2003; Brixner et al., 2004; Daniel et al., 2003; Levis et al., 2001; Nuernberger et al., 2010; Wells et al., 2013) or control of photochemistry in the condensed phase (Brixner et al., 2001; Herek et al., 2002; Vogt et al., 2005) have validated this approach, but the challenge remains in interpreting the control mechanisms that lead to the general efficiency of the method (Daniel et al., 2003; Herek et al., 2002; Roslund and Rabitz, 2009; Trallero et al., 2008; Wells et al., 2013), and its applications to newer and wider domains.

The goal of this chapter is a broad overview of the different physical models and mathematical techniques regularly employed in quantum control, for a variety of purposes of growing complexity. The emphasis is on the general ideas, trying to display them in the simplest scenarios for pedagogical reasons, rather than the applications, which are typically selected from the work of the authors for illustration purposes.

After this introduction, the chapter follows by Section 2 on Rabi oscillations in a two-level system. Adiabatic control of a single-qubit and single-qubit quantum gates based on the geometrical phase are reviewed in Section 3. STIRAP methods of control are discussed in Section 4. Closed-loop system control is illustrated using a two-qubit system as an example in Section 5. Section 6 shows what conditions apply in order to extend the previous basic control strategies (Rabi oscillations and adiabatic passage) to molecules using short pulses, where the potential energy curve adds another dimension to the problem. In Section 7 we illustrate control ideas that rely on the use of pulses strong enough to modify the potential curves. We show how in these new potentials one can selectively

control population transfer, the geometry of the molecule, or the photophysical and photochemical processes of the excited states. Finally, Section 8 introduces the control techniques to deal with more complex systems that require a different, more numerical, approach based on the calculus of variations. We explain in detail some algorithms used to solve the equations and end the chapter with a short summary.

2. RABI OSCILLATIONS IN A TWO-LEVEL SYSTEM

In this section we consider fundamental features of quantum control in two-level system (TLS). Understanding population dynamics in TLS is a crucial factor in many areas of physics and chemistry. We will refer to the TLS as a qubit since later in this work we will address some problems of control directly related to the quantum information. For simplicity, we will mostly use wave function formalism, neglecting decoherence and dissipation effects.

The total wave function of the TLS system $|\Psi(t)\rangle = a_0(t)|0\rangle + a_1(t)|1\rangle$, where $a_{0,1}(t)$ are the probability amplitudes to be in the states $|0\rangle$ and $|1\rangle$, is governed by the time-dependent Schrödinger equation (TDSE). In the rotating wave approximation (RWA) the Hamiltonian describing dynamics of a TLS (Fig. 1) has the form

$$H = -\frac{\hbar}{2}\begin{pmatrix} 0 & \Omega(t)e^{i\phi_0} \\ \Omega(t)e^{-i\phi_0} & 2\Delta\omega \end{pmatrix}, \tag{1}$$

where $\Delta\omega = \omega_0 - E_1/\hbar$ is the detuning between the transition frequency and the center frequency, ω_0, of the laser field, taken as $\epsilon(t) = E(t)\cos(\omega_0 t + \phi_0)$, E_1 is the excited state energy, the $|0\rangle$ state energy is assumed equal to zero,

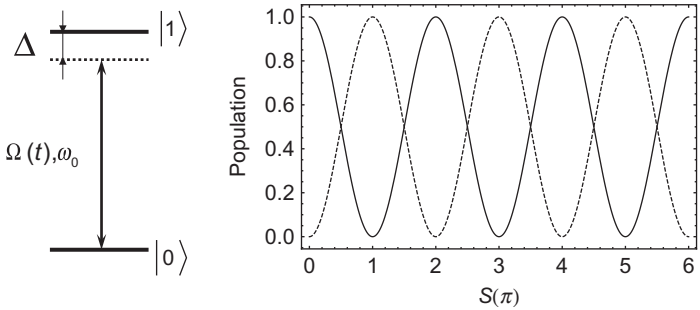

Fig. 1 Schematic of a two-level system. Population of the ground (*solid line*) and excited (*dashed line*) as a function of the pulse area of the Gaussian shape envelope.

$\Omega(t) = E(t)\mu_{01}/\hbar$ is the Rabi frequency, μ_{01} is the dipole moment, $E(t)$ is the pulse envelope, ϕ_0 is the initial phase.

In resonant conditions, $\Delta\omega = 0$, the expression for the evolution operator of the TLS is analytic,

$$\begin{aligned} \boldsymbol{U}(t) &= e^{-i\frac{S(t)}{2}(\boldsymbol{n}\cdot\boldsymbol{\sigma})} = \cos\left(\frac{S(t)}{2}\right)\boldsymbol{I} - i\sin\left(\frac{S(t)}{2}\right)(\boldsymbol{n}\cdot\boldsymbol{\sigma}) \\ &= \cos\left(\frac{S(t)}{2}\right)\boldsymbol{I} + i\sin\left(\frac{S(t)}{2}\right)\left[\cos(\phi_0)\boldsymbol{\sigma}_x - \sin(\phi_0)\boldsymbol{\sigma}_y\right] \\ &= \begin{pmatrix} \cos\left(\frac{S(t)}{2}\right) & ie^{i\phi_0}\sin\left(\frac{S(t)}{2}\right) \\ ie^{-i\phi_0}\sin\left(\frac{S(t)}{2}\right) & \cos\left(\frac{S(t)}{2}\right) \end{pmatrix}, \end{aligned} \tag{2}$$

where $S(t) = \int_0^t \Omega(t')dt'$ is the pulse area, $\boldsymbol{n} = (-\cos\phi_0, \sin\phi_0, 0)$, $\boldsymbol{\sigma}_{x,\,y,\,z}$ are the Pauli matrices.

As we can see from Eq. (2) population dynamics of the TLS is controlled by the pulse area, $S(t)$, which determines how much population is transferred from the ground to the excited state. A pulse area of π corresponds to complete population inversion, whereas a pulse area of $\pi/2$ gives a coherent superposition of the TLS states with equal amplitudes. Fig. 1 shows the Rabi oscillations of the population between the states.

The dynamics of the population in the TLS is more complex in the case of off-resonant excitation, $\Delta\omega \neq 0$ (Berman and Malinovsky, 2011). Under a field of constant amplitude and frequency, slightly detuned from the resonance, the excitation probability of the TLS undergoes Rabi oscillations $P_1(t) = |a_1(t)|^2 = \Omega_0^2 \sin^2(\Omega_{\text{eff}}t/2)/\Omega_{\text{eff}}^2$, where Ω_0 is the constant Rabi frequency, and the effective Rabi frequency, $\Omega_{\text{eff}} = \sqrt{\Omega_0^2 + \Delta\omega^2}$, takes into account the effect of the detuning. The detuning accelerates the rate of the population transfer but decreases the maximum that can reach the target state, hampering the efficiency and robustness of the preparation process. A general feature of detuning is to generate fast oscillating dynamical phases that modulate (and reduce) the coherent transfer induced by the Rabi frequency.

In the case of the pulsed excitation, for the off-resonance case, the population of the excited states may reach some nonzero value at the intermediate times, but will always decay to zero at the end of the pulse if the

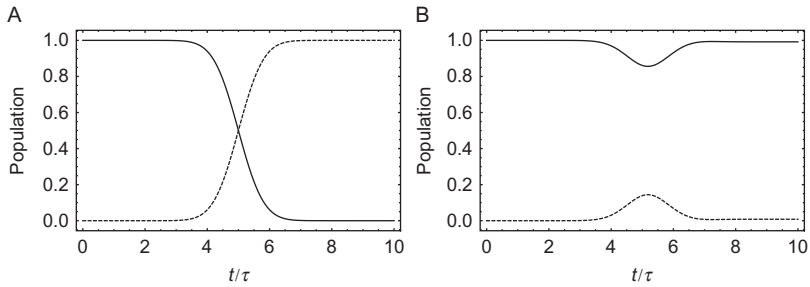

Fig. 2 Population of the ground (*solid line*) and excited (*dashed line*) as a function of time under excitation by a π-pulse with Gaussian envelope; (A) exact resonance and (B) off-resonant excitation.

pulse is turned on and off smoothly. This is known as an adiabatic population return. Fig. 2 shows the population dynamics in TLS under a π-pulse for resonant and off-resonant conditions.

From the control point of view, the Rabi oscillations provide an efficient and selective method of population transfer in quantum systems, with a variety of applications in chemistry, laser spectroscopy, quantum optics and quantum information processing. In some cases, the sensitivity of the final population distribution in the system to the field parameters is considered as a drawback of the method. In the next chapters we will consider several adiabatic passage techniques of population transfer in quantum systems which are substantially more robust against moderate variations in the interaction parameters.

3. ADIABATIC CONTROL IN A SINGLE QUBIT

Adiabatic control methods have been studied extensively during last few decades and found many applications in various areas of laser spectroscopy, physical chemistry, as well as in quantum information processing. In this section we consider application of the adiabatic passage (AP) to design an universal set of single-qubit quantum gates. We will consider the electron spin in a single quantum dot as one of the most promising realizations of a qubit for the implementation of a quantum computer (Press et al., 2008). During the last decade several control schemes that perform single gate operations on a single quantum dot spin were reported (Chen et al., 2004; Economou and Reinecke, 2007; Liu et al., 2010; Press et al., 2008). Here we consider a scheme that allows performing ultrafast arbitrary unitary operations on a single qubit represented by the electron spin. The idea of geometrically

manipulating the qubit wave function has been developed to the point of becoming a new research direction called geometric quantum computing (Falci et al., 2000; Jones et al., 2000; Zanardi and Rasetti, 1999). The main motivation of this development is the robustness of geometric quantum gates against noise (Chiara and Palma, 2003; Lupo and Aniello, 2009; Zanardi and Rasetti, 1999). Here, we demonstrate how to use the geometric phase, which the Bloch vector gains along the cyclic path, to prepare an arbitrary state of a single qubit. We show that the geometrical phase is fully controllable by the relative phase between the external fields.

Let us consider the coherent Raman excitation in the three-level Λ-type system consisting of the two lowest states of electron spin $|0\rangle$ and $|1\rangle$ coupled through an intermediate trion state $|T\rangle$ consisting of two electrons and a heavy hole (Bayer et al., 2002) (Fig. 3). Assuming that the trion state is far off-resonance with the external fields we neglect decoherence on the trion-qubit transitions. The electron spin states are split by an external magnetic field; the separation energy is $\hbar\omega_e$. The total wave function of the system

$$|\Psi(t)\rangle = a_0(t)|0\rangle + a_1(t)|1\rangle + b(t)|T\rangle, \tag{3}$$

where $a_{0,1}(t)$ and $b(t)$ are the probability amplitudes, is governed by the TDSE with Hamiltonian

$$\boldsymbol{H} = \hbar \begin{pmatrix} 0 & 0 & -(\Omega_P(t) + \bar{\Omega}_S(t)) \\ 0 & \omega_e & -(\bar{\Omega}_P(t) + \Omega_S(t)) \\ -(\Omega_P(t) + \bar{\Omega}_S(t)) & -(\bar{\Omega}_P(t) + \Omega_S(t)) & \omega_T \end{pmatrix}, \tag{4}$$

where $\Omega_{P,S}(t) = \Omega_{P0,S0}(t)\cos[\omega_{P,S}t + \phi_{P,S}(t)]$, $\bar{\Omega}_{P,S}(t) = \bar{\Omega}_{P0,S0}(t)\cos[\omega_{P,S}t + \phi_{P,S}(t)]$, $\Omega_{P0,S0}(t) = \mu_{0T,T1}E_{P,S}(t)/\hbar$, and $\bar{\Omega}_{P0,S0}(t) = \mu_{1T,T0}$

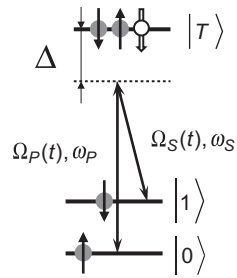

Fig. 3 Energy structure of the three-level system comprised of the two electron spin states and the trion state.

$E_{P,S}(t)/\hbar$ are the Rabi frequencies, $\mu_{0T,T1}$ are the dipole moments, $E_{P,S}(t)$ are the pulse envelopes, $\omega_{P,S}$ are the center frequencies, $\phi_{P,S}(t)$ are the time-dependent phases, and $\hbar\omega_T$ is the energy of the trion state. For the generality, in the present analysis we suppose a symmetrized excitation, with the pump and Stokes fields driving both transitions of the three-level system of Fig. 3. We are addressing here a case of linearly chirped pulses such that

$$\phi_{P,S}(t) = \phi_{P,S} + \alpha_{P,S}t^2/2, \tag{5}$$

where $\phi_{P,S}$ are the initial phases and $\alpha_{P,S}$ are the chirps of the pulses.

In the RWA, neglecting the rapidly oscillating terms with frequency $2\omega_S$, $2\omega_P$ and $\omega_S + \omega_P$, the Hamiltonian has the following form

$$\widetilde{\boldsymbol{H}} = -\frac{\hbar}{2}\begin{pmatrix} 0 & 0 & \Omega_{P+} + \bar{\Omega}_{S+}e^{-i\Delta\omega t} \\ 0 & 2(\Delta\omega - \omega_e) & \bar{\Omega}_{P+}(t)e^{i\Delta\omega t} + \Omega_{S+} \\ \Omega^*_{P+} + \bar{\Omega}^*_{S+}e^{i\Delta\omega t} & \bar{\Omega}^*_{P+}e^{-i\Delta\omega t} + \Omega^*_{S+} & -2\Delta_P \end{pmatrix}, \tag{6}$$

where $\Delta_P = \omega_T - \omega_P$, $\Delta\omega = \omega_P - \omega_S$, $\Omega_{P+} = \Omega_{P0}(t)e^{i\phi_P(t)}$, $\Omega_{S+} = \Omega_{S0}(t)e^{i\phi_S(t)}$, $\bar{\Omega}_{P+} = \bar{\Omega}_{P0}(t)e^{i\phi_P(t)}$, $\bar{\Omega}_{S+} = \bar{\Omega}_{S0}(t)e^{i\phi_S(t)}$ and the asterisk represents the complex conjugate.

Assuming large detunings of the pump and Stokes field frequencies from the transition frequencies to the trion state, we apply the adiabatic elimination of the trion state. After some algebra, taking into account the exact time dependence of the phases in Eq. (5), we obtain the following form for the Hamiltonian in the field interaction representation

$$\bar{\boldsymbol{H}} = -\frac{\hbar}{2}\begin{pmatrix} \delta(t) & \Omega_e(t)e^{i\Delta\phi} \\ \Omega^*_e(t)e^{-i\Delta\phi} & -\delta(t) \end{pmatrix}, \tag{7}$$

where $\delta(t) = \delta - \zeta t$, $\delta = \omega_e + \omega_S - \omega_P$, $\zeta = \alpha_P - \alpha_S$, $\Delta\phi = \phi_P - \phi_S$, and

$$\Omega_e(t) = \frac{\Omega_{P0}(t)\Omega_{S0}(t)}{2\Delta_P}\left(1 + \frac{\Omega_{P0}(t)\bar{\Omega}_{P0}(t) + \Omega_{S0}(t)\bar{\Omega}_{S0}(t)}{\Omega_{P0}(t)\Omega_{S0}(t)}e^{-i[\Delta\phi + \Delta\omega t + \zeta t^2/2]} + \frac{\bar{\Omega}_{P0}(t)\bar{\Omega}_{S0}(t)}{\Omega_{P0}(t)\Omega_{S0}(t)}e^{-2i[\Delta\phi + \Delta\omega t + \zeta t^2/2]}\right) \tag{8}$$

is the effective Rabi frequency. For simplicity, we use the two-photon resonance condition and $\mu_{0T} \approx \mu_{1T}$, so that the differential AC Stark shift can be neglected for completely overlapping pulses.

In some excitation schemes, due to selection rules that take into account the polarization of the external field, the pump and Stokes fields interact only with the corresponding transitions and the general Hamiltonian can be simplified further by replacing the expression for the effective Rabi frequency, Eq. (8), with $\Omega_e(t) = \Omega_{P0}(t)\Omega_{S0}(t)/(2\Delta_P)$. This is the so-called nonimpulsive excitation regime, which we address next.

3.1 Adiabatic Solution

The Hamiltonian in Eq. (7) controls the dynamics of the qubit wave function in the approximation of the adiabatic elimination of the trion state. Here we consider the adiabatic excitation of the qubit and find the solution of its corresponding TDSE.

Since the phase factor $e^{i\Delta\phi}$ of the coupling term in Eq. (7) is time independent, it is convenient to use the following transformation, $|\Phi(t)\rangle = \boldsymbol{A}|\Psi(t)\rangle$, where

$$\boldsymbol{A} = |0\rangle\langle 0| + e^{i\Delta\phi}|1\rangle\langle 1| = e^{i\Delta\phi/2}e^{-i\Delta\phi\boldsymbol{\sigma}_z/2}, \tag{9}$$

so that the new wave function is governed by the Hamiltonian

$$\bar{\boldsymbol{H}} = \boldsymbol{A}\breve{\boldsymbol{H}}\boldsymbol{A}^{-1} = -\frac{\hbar}{2}(\delta(t)\boldsymbol{\sigma}_z + \Omega_e(t)\boldsymbol{\sigma}_x). \tag{10}$$

To solve the TDSE in the adiabatic representation, we apply another transformation: $|\bar{\Phi}(t)\rangle = \boldsymbol{R}(t)|\Phi(t)\rangle$, where

$$\boldsymbol{R}(t) = \begin{pmatrix} \cos\theta(t) & \sin\theta(t) \\ -\sin\theta(t) & \cos\theta(t) \end{pmatrix} = e^{i\theta(t)\boldsymbol{\sigma}_y}, \tag{11}$$

and $\tan[2\theta(t)] = \Omega_e(t)/\delta(t)$. In the new basis the Hamiltonian, Eq. (10), takes the form

$$\widetilde{\boldsymbol{H}}(t) = \boldsymbol{R}(t)\bar{\boldsymbol{H}}(t)\boldsymbol{R}^{-1}(t) = -\hbar\lambda(t)\boldsymbol{\sigma}_z/2, \tag{12}$$

where $\lambda(t) = \sqrt{\delta^2(t) + \Omega_e^2(t)}$.

As we see, the Hamiltonian in Eq. (12) is diagonal in the adiabatic basis and we can readily write down the solution. However, since the transformation $\boldsymbol{R}(t)$ is time dependent, an additional nonadiabatic coupling term is present in the general Schrödinger equation

$$i\hbar|\dot{\bar{\Phi}}(t)\rangle = -\frac{1}{2}\hbar\lambda(t)\boldsymbol{\sigma}_z|\bar{\Phi}(t)\rangle - \hbar\dot{\theta}(t)\boldsymbol{\sigma}_y|\bar{\Phi}(t)\rangle, \tag{13}$$

where

$$\dot{\theta}(t) = -\frac{\Omega_e(t)\dot{\delta}(t) - \delta(t)\dot{\Omega}_e(t)}{2\left(\Omega_e^2(t) + \delta^2(t)\right)}. \tag{14}$$

Neglecting the nonadiabatic coupling term in Eq. (13), we readily obtain for the qubit wave function in the original basis,

$$|\Psi(t)\rangle = e^{i\frac{\Delta\phi}{2}\boldsymbol{\sigma}_z} e^{-i\theta(t)\boldsymbol{\sigma}_y} e^{i\frac{\Lambda(t)}{2}\boldsymbol{\sigma}_z} e^{i\theta(0)\boldsymbol{\sigma}_y} e^{-i\frac{\Delta\phi}{2}\boldsymbol{\sigma}_z} |\Psi(0)\rangle, \tag{15}$$

where $\Lambda(t) = \int_0^t dt'\lambda(t')$. Note that the general form of the evolution operator in Eq. (15) is well justified if the following condition $|\Omega_e(t)\dot{\delta}(t) - \dot{\Omega}_e(t)\delta(t)| \ll \lambda^3(t)$ is valid.

In the case of completely overlapping pulses, $\Omega_{P0}(t) = \Omega_{S0}(t)$, with identical chirp rates, $\alpha_P = \alpha_S$, for the resonant qubit, $\delta(t) = \delta = 0$, we have $\theta(t) = \theta(0) = \pi/4$ and the transformation matrix becomes $\boldsymbol{R}(t) = \boldsymbol{R}(0) = e^{i\pi\boldsymbol{\sigma}_y/4}$. Therefore, the unitary evolution operator for the wave function of the resonant qubit takes the form

$$\boldsymbol{U}(t) = \cos(S(t)/2)\boldsymbol{I} - i\sin(S(t)/2)(\boldsymbol{n}\cdot\boldsymbol{\sigma}) = e^{-iS(t)\boldsymbol{n}\cdot\boldsymbol{\sigma}/2}, \tag{16}$$

where $S(t) = \int_0^t dt'\Omega_e(t')$ is the effective pulse area, $\boldsymbol{n} = (-\cos\Delta\phi, \sin\Delta\phi, 0)$. Note also that the nonadiabatic coupling term, Eq. (14), is zero for the resonant qubit and the solution of the TDSE in the adiabatic approximation, Eq. (16), is the exact solution, identical to Eq. (2).

The density plots of the population and coherence ($|a_0(T)a_1^*(T)|$) at final time (after the pulse excitation) as a function of the effective pulse area, $S(T)$, and the dimensionless frequency chirp parameter, α'/τ_0^2, are depicted in Fig. 4. We use Gaussian pulses, assuming that the linear chirps are obtained by applying linear optics, so an initially transform-limited pulse of duration τ_0 is chirped, conserving the energy of the pulse (Malinovsky and Krause, 2001a,b). The temporal (α) and spectral (α') chirps are related as $\alpha = \alpha'\tau_0^{-4}/(1 + \alpha'^2/\tau_0^4)$ (Malinovsky and Krause, 2001a,b). We observe the Rabi oscillation regime, when the population of the qubit states is changing between 0 and 1 while the coherence is changing between 0 and 1/2. This behavior does not depend on the chirp rate, since the effective Rabi frequency $\Omega_e(t)$ is determined by the product of the pump and Stokes Rabi frequencies: $\Omega_{P0,S0}(t) = \Omega_0 \exp\{-t^2/(2\tau^2)\}/[1 + \alpha'^2/\tau_0^4]^{1/4}$ with the chirp-dependent pulse duration $\tau = \tau_0[1 + \alpha'^2/\tau_0^4]^{1/2}$ and the amplitude (Malinovsky and Krause, 2001a,b).

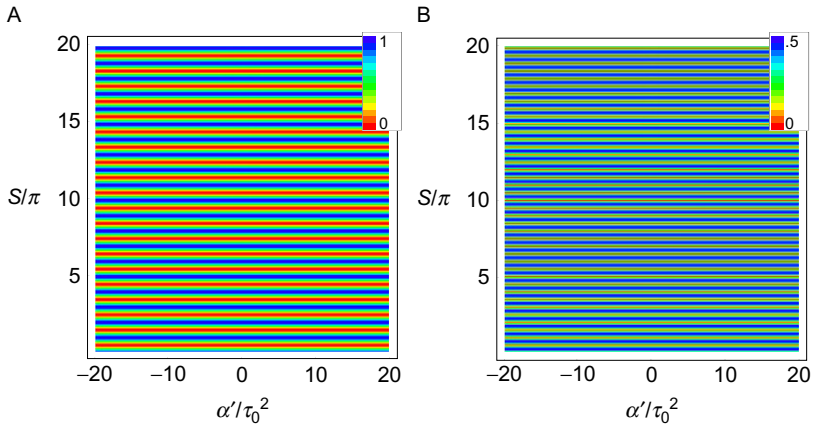

Fig. 4 The density plot of the state $|1\rangle$ population (A) and coherence (B) as a function of the effective pulse area and frequency chirp; $\alpha_P = \alpha_S$, $\delta = 0$. Initially, only the $|1\rangle$ state is populated. *Adapted from Malinovsky, V.S., Rudin, S., 2012b. Ultrafast control of electron spin in a quantum dot using geometric phase. Solid State Electron. 78, 28–33.*

In turn, for the off-resonant qubits, $\delta \neq 0$, the evolution operator in the adiabatic approximation takes the form

$$\boldsymbol{U}(t) = \begin{pmatrix} e^{i\xi(t)}\cos\theta(t) & -e^{-i\xi(t)}e^{i\Delta\phi}\sin\theta(t) \\ e^{i\xi(t)}e^{-i\Delta\phi}\sin\theta(t) & e^{-i\xi(t)}\cos\theta(t) \end{pmatrix}, \tag{17}$$

where

$$\cos\theta(t) = \frac{1}{\sqrt{2}}\sqrt{1+\frac{\delta}{\sqrt{\delta^2+\Omega_e^2(t)}}}, \tag{18a}$$

$$\sin\theta(t) = \frac{1}{\sqrt{2}}\sqrt{1-\frac{\delta}{\sqrt{\delta^2+\Omega_e^2(t)}}} \tag{18b}$$

and $\xi(t) = \frac{1}{2}\int_0^t \sqrt{\delta^2+\Omega_e^2(t')}dt'$ is the effective pulse area.

As expected, the population of the off-resonant qubit at final time is not changed by the external fields as long as the pulse excitation parameters are in the adiabatic regime, leading to adiabatic return. However, in Fig. 5 we also observe the Rabi oscillation for the value of the chirp $|\alpha'| \lesssim 5\tau_0^2$. This is the regime of nonadiabatic population transfer where the nonadiabatic coupling term cannot be neglected in Eq. (13).

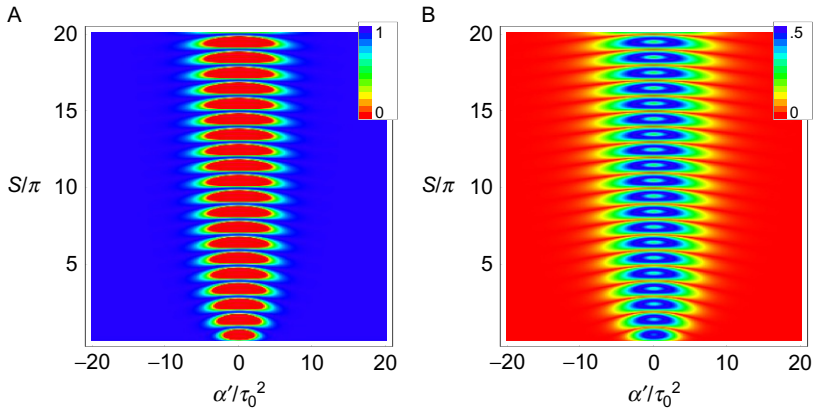

Fig. 5 The density plot of the state $|1\rangle$ population (A) and coherence (B) as a function of the effective pulse area and frequency chirp; $\alpha_P = \alpha_S$, $\delta\tau_0 = 0.75$. Initially, only the $|1\rangle$ state is populated. *Adapted from Malinovsky, V.S., Rudin, S., 2012b. Ultrafast control of electron spin in a quantum dot using geometric phase. Solid State Electron. 78, 28–33.*

3.2 Adiabatic Control of Raman Coherence

Modified adiabatic passage schemes using frequency chirped pulses can be successfully applied to create maximum coherence with applications in Coherent ant-Stokes Raman Scattering (CARS) spectroscopy (Malinovskaya and Malinovsky, 2007). The maximum coherence between the ground and excited vibrational states in a molecule optimizes the magnitude of the CARS signal generated upon propagation of an incident light through a molecular medium. CARS is a four-wave mixing process, Fig. 6A that involves the interaction of molecular vibrational modes with the pump and Stokes pulses resulting in a preparation of a molecular system in a coherent superposition of the ground and the excited vibrational states. This superposition is analyzed by the probe pulse that may be delayed with respect to the pump pulse and usually possesses the same frequency. It induces the anti-Stokes signal at frequency $\omega_A = 2\omega_P - \omega_S$.

We developed the adiabatic passage method to selectively maximize the Raman coherence between predetermined vibration states. We use two linearly chirped femtosecond pulses defined as $\epsilon_P(t) = E_{P0}(t)\cos(\omega_P(t-t_0)+\alpha(t-t_0)^2/2)$, and $\epsilon_S(t) = E_{S0}(t)\cos(\omega_S(t-t_0)+\beta(t-t_0)^2/2)$, where $E_{P0,S0}(t)$ are the Gaussian envelopes, with the chirp-dependent pulse duration τ. It implies β to be constant giving monotonous change of the Stokes pulse frequency, and α to have same magnitude and opposite sign for times before the central time t_0, (when the field amplitude reaches

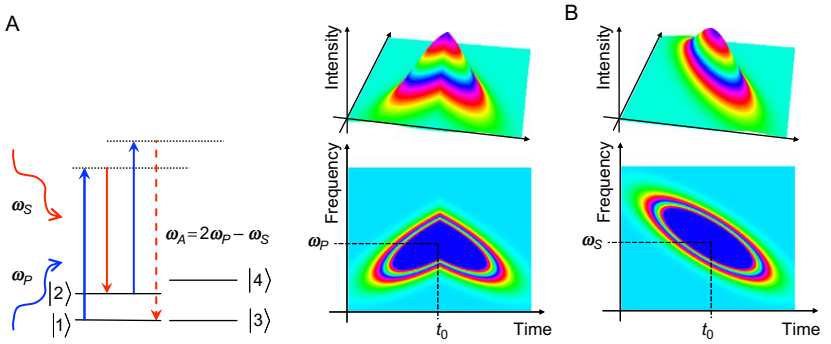

Fig. 6 (A) Schematic of the coherent anti-Stokes Raman scattering. The interaction of the two-level systems with the pump and Stokes femtosecond pulses induces coherence between the lower and upper levels. The coherence is analyzed by the probe pulse that stimulates anti-Stokes Raman transition. (B) Wigner plots of the pump (*left frame*) and Stokes (*right frame*) pulses.

maximum), and then to flip the sign (see Fig. 6B). At t_0 the frequency difference of the pump and Stokes pulse comes into resonance with the $|1\rangle-|2\rangle$ two-level system and remains in resonance for the rest the pulse duration. The method is called the roof method in accordance with the temporal shape of the pump pulse instantaneous frequency, Fig. 6B. Numerical studies show that coherence in the resonant and in the detuned two-level systems, formed by the two-photon adiabatic passage, demonstrates fundamentally different behavior. In the resonant $|1\rangle-|2\rangle$ two-level system, the maximum coherence is created in the broad range of field intensities, from 10^{11} to 10^{12} W/cm^2. The coherence as a function of the pulse area and the frequency chirp is shown in Fig. 7A. Meanwhile in the $|3\rangle-|4\rangle$ two-level system detuned by δ with respect to the $|1\rangle-|2\rangle$ system, the coherence is at minimum value for the same range of the pulse area and the frequency chirp, Fig. 7B. For the selectivity of excitations the condition $\delta\tau \geq 1$ must be satisfied.

The proposed method suggests the robust way to obtain noninvasive image of biological structure. For example, various biological tissue contain molecular groups, having CH vibrations which span from 2800 to 3100 cm^{-1} and may be selectively excited to provide noninvasive image with high chemical sensitivity. Besides, if to fix the pump field central frequency ω_p and to scan the Stokes pulse frequency ω_s, one can obtain the vibrational spectrum of unknown molecular species. For each instantaneous magnitude of the Stokes pulse central frequency, the maximum intense CARS signal and the efficient suppression of the background signal can be achieved. More details on optimization of the Raman coherence using adiabatic methods can be found in Malinovskaya and Malinovsky (2007) and Malinovskaya (2006, 2007, 2009).

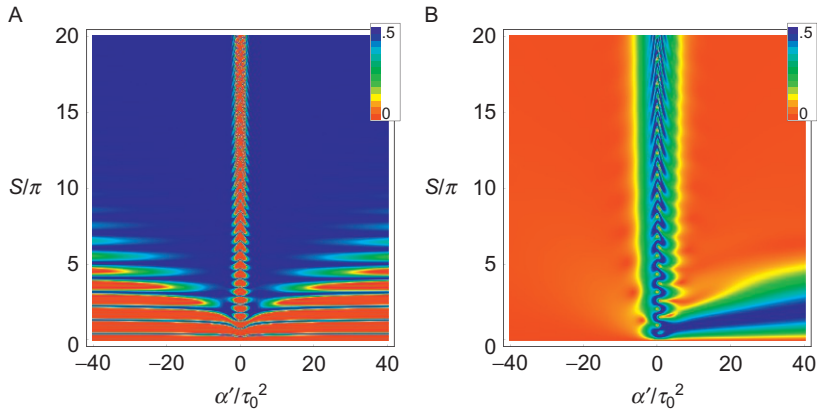

Fig. 7 The coherence density plot as a function of the effective pulse area and dimensionless frequency chirp parameter, calculated using the roof method and $\omega_{21}\tau_0 = 15$; (A) the resonant two-level system, (B) the detuned two-level system, $\delta/\omega_{21} = 0.1$. Adiabatic passage induced in both two-level systems leads to the maximum in one (*blue*) and minimum coherence (*red*) in another two-level system.

3.3 Bloch Vector Representation

The dynamics of the qubit wave function can be described equally well using the Bloch vector representation. The Bloch vector formalism provides a very nice and clear geometrical interpretation of the qubit dynamics (Berman and Malinovsky, 2011). In this section, we give a short overview of the Bloch picture.

A general state of a qubit can be described as

$$|\Psi\rangle = a_0(t)|0\rangle + a_1(t)|1\rangle = \cos(\beta/2)|0\rangle + e^{i\alpha}\sin(\beta/2)|1\rangle, \tag{19}$$

where α and β are the phase parameters. Up to an insignificant global phase, the wave function can be mapped into a unitary Bloch vector $\mathbf{B} = (u, v, w)$, as shown in Fig. 8. To use the Bloch vector representation, we construct the qubit density matrix

$$\varrho = |\Psi\rangle\langle\Psi| = \begin{pmatrix} \varrho_{00} & \varrho_{01} \\ \varrho_{10} & \varrho_{11} \end{pmatrix} = \frac{1}{2}\begin{pmatrix} 1+\cos\beta & e^{-i\alpha}\sin\beta \\ e^{i\alpha}\sin\beta & 1-\cos\beta \end{pmatrix}, \tag{20}$$

where $\varrho_{ij} = a_i(t)a_j^*(t)$, $i, j = 0, 1$. The density matrix can be decomposed using Pauli matrices as

$$\varrho = \frac{1}{2}\left(\boldsymbol{I} + \boldsymbol{B}\cdot\vec{\boldsymbol{\sigma}}\right). \tag{21}$$

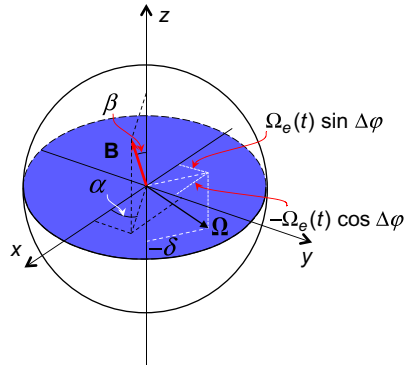

Fig. 8 The Bloch vector representation of the qubit state. Excitation of the qubit by an external field corresponds to the rotation of the **B** vector about the pseudo-field vector, **Ω**, with components determined by the effective Rabi frequency $\Omega_e(t)$, detuning δ, and the relative phase $\Delta\phi$.

It is easy to verify that

$$\boldsymbol{B} = Tr[\vec{\boldsymbol{\sigma}}\,\boldsymbol{\varrho}] = \left(Tr[\boldsymbol{\sigma}_x\boldsymbol{\varrho}], Tr[\boldsymbol{\sigma}_y\boldsymbol{\varrho}], Tr[\boldsymbol{\sigma}_z\boldsymbol{\varrho}]\right) = (u, v, w), \tag{22}$$

and identify the relation between the components of the qubit wave function, the qubit density matrix elements, and the Bloch vector components: $u = \varrho_{01} + \varrho_{10} = \cos\alpha \sin\beta$, $v = i(\varrho_{01} - \varrho_{10}) = \sin\alpha \sin\beta$, $w = \varrho_{00} - \varrho_{11} = \cos\beta$.

Using the Pauli matrix decomposition procedure $Tr[\vec{\boldsymbol{\sigma}}\,\boldsymbol{H}]$, we can rewrite the Hamiltonian in Eq. (7) in the form

$$\boldsymbol{H} = \frac{\hbar}{2}\left(\Omega \cdot \vec{\boldsymbol{\sigma}}\right), \tag{23}$$

where the components of the pseudo-field vector

$$\boldsymbol{\Omega} = (-\Omega_e(t)\cos\Delta\phi, \Omega_e(t)\sin\Delta\phi, -\delta(t)) \tag{24}$$

are determined by the effective Rabi frequency, the two-photon detuning, and the relative phase between the pump and Stokes pulses. Therefore, the equation of motion for the density matrix, $\dot{\boldsymbol{\varrho}} = i(\boldsymbol{\varrho H} - \boldsymbol{H\varrho})/\hbar$, can be rewritten as the Bloch equation

$$\dot{\boldsymbol{B}} = Tr[\vec{\boldsymbol{\sigma}}\,\dot{\boldsymbol{\varrho}}] = \frac{1}{2}Tr[\vec{\boldsymbol{\sigma}} \cdot \vec{\boldsymbol{\sigma}} \cdot (\boldsymbol{\Omega} \times \boldsymbol{B})] = \boldsymbol{\Omega} \times \boldsymbol{B}, \tag{25}$$

which describes a precession of the Bloch vector, $\boldsymbol{B}$, about the pseudo-field vector, $\boldsymbol{\Omega}$, and allows a clear, intuitive interpretation of the qubit dynamics.

Since we already know the evolution operator of the qubit, for example for the exact resonance case, Eq. (16), we can easily construct the evolution operator for the Bloch vector. Using the definition of the density matrix, $\boldsymbol{\varrho}(t) = \boldsymbol{U}(t)\boldsymbol{\varrho}(0)\boldsymbol{U}^{\dagger}(t)$, after some algebra we obtain for the Bloch vector evolution the following expression

$$\boldsymbol{B}(t) = \begin{pmatrix} \mathcal{C}^2 + \mathcal{S}^2\cos(2\Delta\phi) & -\mathcal{S}^2\sin(2\Delta\phi) & 2\,\mathcal{C}\cdot\mathcal{S}\sin(\Delta\phi) \\ -\mathcal{S}^2\sin(2\Delta\phi) & \mathcal{C}^2 - \mathcal{S}^2\cos(2\Delta\phi) & 2\,\mathcal{C}\cdot\mathcal{S}\cos(\Delta\phi) \\ -2\,\mathcal{C}\cdot\mathcal{S}\sin(\Delta\phi) & -2\,\mathcal{C}\cdot\mathcal{S}\cos(\Delta\phi) & \mathcal{C}^2 - \mathcal{S}^2 \end{pmatrix} \boldsymbol{B}(0), \tag{26}$$

where $\mathcal{C} = \cos(S(t)/2)$, $\mathcal{S} = \sin(S(t)/2)$, and $\boldsymbol{B}(0)$ is the initial Bloch vector.

3.4 Single Qubit Gates Using Geometrical Phase

At this point, we are ready to discuss implementation of the single-qubit gates since we have obtained the analytic solution for the qubit wave function and constructed the evolution operator in the Bloch vector representation. A universal set of quantum gates has been intensively discussed in the literature related to the universality in quantum computation (Deutsch et al., 1995; DiVincenzo, 2000; Lloyd, 1995; Nielsen and Chuang, 2006). To perform quantum computation, we must have two major building blocks at our disposal: arbitrary unitary operations on a single qubit and a controlled-NOT operation on two qubits. Here we address only the single-qubit manipulation.

To demonstrate arbitrary geometric operations on a single qubit, we use the Bloch vector representation discussed in the previous section. Since any unitary rotation of the Bloch vector can be decomposed, for example, as $\boldsymbol{U} = e^{i\alpha_0}\boldsymbol{R}_z(\alpha_1)\boldsymbol{R}_y(\alpha_2)\boldsymbol{R}_z(\alpha_3)$, where $\boldsymbol{R}_i = e^{i\alpha\boldsymbol{\sigma}_i}$ ($i = y, z$) are the rotation operators (Nakahara and Ohmi, 2008; Nielsen and Chuang, 2006), we need to demonstrate rotations of the qubit Bloch vector about the z- and y-axes by applying various sequences of external pulses. This decomposition plays an important role in circuit-based quantum computing, as it shows explicitly that two single-qubit operations allow us to prepare arbitrary qubit state. Here we show how this can be accomplished by controlling the parameters of the external pulses, which are defined by the explicit form of the evolution operator (see Eq. 16). There are two distinct implementations depending on which part of the total qubit phase we employ: dynamical or geometrical (Bohm et al., 2003). Quantum gates relying on geometrical

quantum phases are called holonomic gates and they are expected to be robust with respect to noise (Chiara and Palma, 2003; Lupo and Aniello, 2009; Zanardi and Rasetti, 1999).

To implement the rotation of the Bloch vector about the z-axis (the phase gate) based on the geometrical phase, we can use the evolution operator of the resonant qubit, Eq. (16). The product of two evolution operators corresponding to the sequence of two π-pulses with the relative phase $\Delta\phi = \varphi + \pi$, gives $\boldsymbol{R}_z(\varphi) = \boldsymbol{U}_{\pi;\varphi+\pi}\boldsymbol{U}_{\pi;0} = e^{i\varphi\boldsymbol{\sigma}_z}$, where the first subindex of $\boldsymbol{U}$ indicates the pulse area, and the second one indicates the phase.

Fig. 9 shows the Bloch vector trajectories of the qubit basis states $|0\rangle$ and $|1\rangle$, which correspond to the angles $\beta = 0$ and $\beta = \pi$ in Eq. (19) and the Bloch vector initially pointing in the z and $-z$ directions while the vector $\boldsymbol{\Omega}_1 = (-\Omega_e, 0, 0)$ is pointing in the $-x$ direction. For simplicity we chose $\Delta\phi = 0$ for the first π-pulse. The first π-pulse flips the population to the state $|1\rangle$ ($|0\rangle$); correspondingly, the Bloch vector turns about the effective field vector $\boldsymbol{\Omega}_1$ (about the x-axis), and it stays in the y, z plane all the time and points in the $-z$ (z) direction at the end of the pulse. Due to the second π-pulse, the population is transferred back to the initial state $|0\rangle$ ($|1\rangle$); therefore, the Bloch vector returns to its original position pointing along the z ($-z$) axis. However, since we chose $\Delta\phi = \varphi + \pi$ for the second π-pulse, the pseudo-field vector is rotated counterclockwise by the angle $\varphi + \pi$ in the x, y plane, $\boldsymbol{\Omega}_2 = (\Omega_e \cos\varphi, -\Omega_e \sin\varphi, 0)$, and the Bloch vector moves in the plane perpendicular to the x, y plane and has the angle $\pi/2 - \alpha$ ($-\pi/2 - \alpha$) with the x, z plane.

The Bloch vectors representing a pair of orthogonal basis states $|0\rangle$ and $|1\rangle$ follow a path enclosing solid angles of 2φ and -2φ. The geometrical phase is equal to one half of the solid angle, which means the basis states

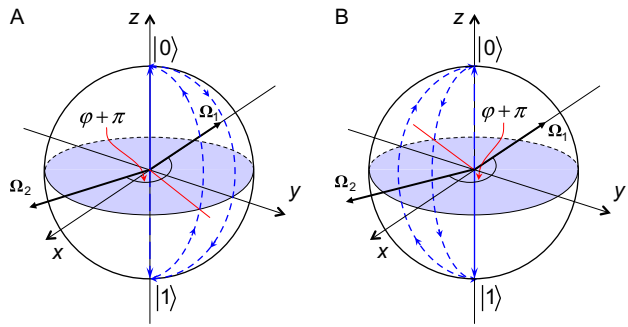

Fig. 9 The Bloch vector trajectory for the qubit state $|0\rangle$ in panel (A) and the qubit state $|1\rangle$ in panel (B) generated by the sequence of two π-pulses with the relative phase $\varphi + \pi$.

$|0\rangle$ and $|1\rangle$ gain phases φ and $-\varphi$ and the evolution operator takes the form of the phase gate, with the relative phase controlling the phase of the gate.

The rotation operator about the y-axis can be constructed using three pulses. The first and third pulse are $\pi/2$-pulses with $\Delta\phi = 0$, while the second pulse is a π-pulse with relative phase $\pi + \varphi$. It is easy to show, using Eq. (16), that this three-pulse sequence results in $\boldsymbol{R}_y(\varphi) = \boldsymbol{U}_{\frac{\pi}{2};0}\boldsymbol{U}_{\pi;\pi+\varphi}\boldsymbol{U}_{\frac{\pi}{2};0} = e^{i\varphi\boldsymbol{\sigma}_y}$. To demonstrate the geometrical nature of the $\boldsymbol{R}_y(\varphi)$ operation, we use the fact that it creates the relative phase between the qubit basis states $|\pm i\rangle = (|0\rangle \pm i|1\rangle)/\sqrt{2}$. In the Bloch representation, these states have the form $|\pm i\rangle = \cos(\pi/4)|0\rangle + e^{\pm i\pi/2}\sin(\pi/4)|1\rangle$, which are two vectors defined by the angles $\beta = \pi/2$ and $\alpha = \pm\pi/2$ and pointing in the y and $-y$ directions, as shown in Fig. 10. The trajectory of the Bloch vector representing the states $|\pm\, i\rangle$ is shown in Fig. 10. The pseudo-field vectors $\boldsymbol{\Omega}_1$ and $\boldsymbol{\Omega}_3$ are defined by the effective Rabi frequencies of the first and third pulses and are pointing in the $-x$ direction since $\Delta\phi = 0$. The second pseudo-field vector $\boldsymbol{\Omega}_2$ is rotated counterclockwise by the angle $\varphi + \pi$ in the x, y plane same as in the case above. The initial Bloch vector is pointing in the y ($-y$) direction. The first $\pi/2$-pulse rotates the Bloch vector about $\boldsymbol{\Omega}_1$ to the position of the state $|1\rangle$ ($|0\rangle$). The second pulse flips the direction of the Bloch vector. The third $\pi/2$-pulse returns the Bloch vector to its original position. The Bloch vector and the pseudo-field vector are orthogonal during the whole evolution. Similar to the previous case, we observe that the basis states $|i\rangle$ and $|-\, i\rangle$ follow a path enclosing solid angles of 2φ and -2φ. Therefore, they gain the relative phase 2φ, which is the

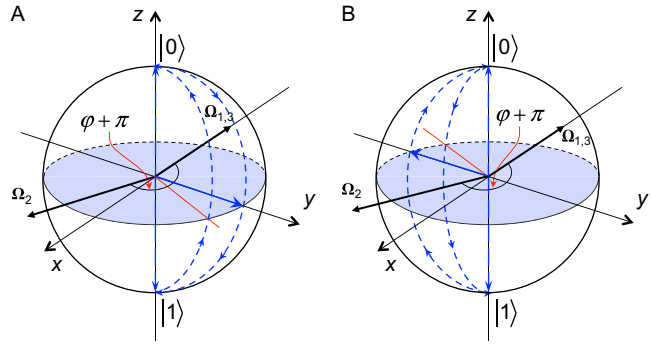

Fig. 10 The Bloch vector trajectory for the qubit state $|i\rangle$ in panel (A) and the qubit state $|-\, i\rangle$ in panel (B) generated by the sequence of two $\pi/2$-pulses and one π-pulse with the relative phase $\varphi + \pi$.

geometrical phase defined by the relative phase between the pulses. It is easy to show that the phase gate in the $|\pm i\rangle$ basis is equivalent to the $\boldsymbol{R}_y(\varphi)$ gate in the $|0\rangle$, $|1\rangle$ basis.

3.4.1 Single-Qubit Operation Using Bright-Dark Basis

In sections 3.1 and 3.2, we have considered several excitation schemes of the three-level system and discussed a possible implementation of single-qubit gates. It was shown that all possible qubit states can be created in a controllable fashion using a couple of completely overlapping laser pulses, $\Omega_P(t) = \Omega_S(t)$. In this section, we present a more general solution, which allows some additional flexibility in terms of the ratio of the pump and Stokes pulse amplitudes. Again, we address here the coherent Raman excitation in a three-level Λ-type system consisting of the two lowest states of electron spin $|0\rangle \equiv |- X\rangle$ and $|0\rangle \equiv |X\rangle$ coupled through an intermediate trion state $|T\rangle$ (see Fig. 3) and assume that the trion state is far off-resonance with the external fields. In addition, we restrict our consideration to the non-impulsive regime and can then put $\bar{\Omega}_{P+}(t) = \bar{\Omega}_{S+}(t) = 0$ in Eq. (6), so that the Hamiltonian takes the form

$$\widetilde{\boldsymbol{H}} = -\frac{\hbar}{2}\begin{pmatrix} 0 & 0 & \Omega_{P+} \\ 0 & 2(\Delta\omega - \omega_e) & \Omega_{S+} \\ \Omega_{P+}^* & \Omega_{S+}^* & -2\Delta_P \end{pmatrix}, \tag{27}$$

where $\Delta_P = \omega_T - \omega_P$, $\Delta\omega = \omega_P - \omega_S$, $\Omega_{P+} = \Omega_{P0}(t)e^{i\phi_P(t)}$, $\Omega_{S+} = \Omega_{S0}(t)e^{i\phi_S(t)}$, and $\phi_{P,\,S}(t) = \phi_{P,\,S} + \alpha_{P,\,S}t^2/2$.

Let us consider the case when $\Omega_{P0}(t) = \Omega_0(t)\cos\vartheta$ and $\Omega_{S0}(t) = \Omega_0(t)\sin\vartheta$; the pump and Stokes Rabi frequencies have the same envelope but different peak amplitudes, controlled by the mixing angle ϑ. Applying the transformation to the bright-dark basis, $|\overline{\Psi}\rangle = \left\{a_B(t), a_D(t), \widetilde{b}(t)\right\} = \mathcal{R}_{bd}|\widetilde{\Psi}\rangle$, where

$$\mathcal{R}_{bd} = \begin{pmatrix} e^{-i\phi_P}\cos\vartheta & e^{-i\phi_S}\sin\vartheta & 0 \\ -e^{i\phi_S}\sin\vartheta & e^{i\phi_P}\cos\vartheta & 0 \\ 0 & 0 & 1 \end{pmatrix}, \tag{28}$$

in the two-photon resonance ($\delta = 0$), equal chirp rates ($\alpha_P = \alpha_S$) case, we have

$$\bar{\boldsymbol{H}} = \mathcal{R}_{bd}\widetilde{\boldsymbol{H}}\mathcal{R}_{bd}^{-1} = \frac{\hbar}{2}\begin{pmatrix} 0 & 0 & -e^{i\alpha t^2/2}\Omega_0(t) \\ 0 & 0 & 0 \\ -e^{-i\alpha t^2/2}\Omega_0(t) & 0 & 2\Delta_P \end{pmatrix}. \tag{29}$$

After the adiabatic elimination of the excited state $|T\rangle$ (assuming that $\dot{\tilde{b}}(t) \approx 0$), we obtain the following expression for the evolution operator of the qubit states

$$\boldsymbol{U}(t) = e^{iS(t)/2} e^{-iS(t)\boldsymbol{n}\cdot\boldsymbol{\sigma}/2}, \tag{30}$$

where $S(t) = \int_0^t \Omega_0^2(t')dt'/(4\Delta_P)$ is the effective two-photon Rabi frequency, and

$$\boldsymbol{n} = (-\cos(\Delta\phi)\sin(2\vartheta), \sin(\Delta\phi)\sin(2\vartheta), -\cos(2\vartheta)). \tag{31}$$

For $\vartheta = \pi/4$, Eq. (30) is identical to the previously obtained solution, Eq. (16), and can be considered as a more general result, providing additional freedom to the single-qubit manipulation by adjusting the ratio between the pump and Stokes pulse amplitudes.

3.4.2 Electron Spin in a Quantum Dot as a Qubit

Above, we discussed several methods of an arbitrary manipulation of a qubit wave function using the geometric phase. The proposed scheme can be implemented on electron spin states in a charged quantum dot. Due to quantum confinement, the state of the electron can be expressed as a product of the Bloch function and an envelope function, which has the typical size of a quantum dot, a few nanometers. The energy level structure and optical selection rules have been studied extensively in the literature (Chen et al., 2004; Economou and Reinecke, 2007; Liu et al., 2010; Press et al., 2008). A commonly accepted energy level structure is comprised of four levels, the two electron spin states and two trion spin states, which allow for the optical control of the electron spin qubit. The electron spin control experiments are usually performed at low temperature ($\sim$1 K). An external magnetic field in the Voigt configuration (of order $2 \div 7$ T) is applied along the x-axis, perpendicular to the sample growth direction, the z-axis. Zeeman splittings of the electron and trion spin states are on the order of $\omega_e = 10$ meV and $\omega_h = 10$ μeV. In these conditions, taking into account the optical selection rules, the four-level system can be considered as a double Λ system (Chen et al., 2004; Economou and Reinecke, 2007; Greilich et al., 2006; Liu et al., 2010; Press et al., 2008). Using the two σ^+ or σ^- polarized fields, one can couple the electron spin states appropriately and the three-level model can be implemented. A more detailed discussion of the implementation and timescale of the quantum gates operation can be found in Hawkins et al. (2012) and Malinovsky and Rudin (2012a,b).

Note that using only the geometric phase for manipulation of a qubit has some advantages, since it reduces the requirements of perfect tuning of the control field parameters and it is significantly more robust against noise (Chiara and Palma, 2003; Lupo and Aniello, 2009; Zanardi and Rasetti, 1999).

4. STIRAP IN MULTILEVEL QUANTUM SYSTEMS

Coherent control of quantum systems has attracted a considerable interest in recent years. Efficient and robust population transfer between quantum states has been the ultimate goal of many theoretical and experimental studies. This problem is relevant to many applications, including spectroscopy, collision dynamics, optical control of chemical reactions, waveguide photonic system, and quantum gate implementation in various quantum computer architectures. A considerable number of studies have been devoted to the process of stimulated Raman adiabatic passage (STIRAP) in three-level and multilevel systems coupled by a number of external fields (see Fig. 11). Here we review some important features of STIRAP and its applications.

4.1 Three-Level System

The STIRAP mechanism of population transfer in a three-level system has been explored in details, both numerically and analytically. Many analytic studies have been performed in the adiabatic limit (Glushko and Kryzhanovsky, 1992; Kuklinski et al., 1989; Vitanov and Stenholm, 1997) although some nonadiabatic effects have been also considered as well (Sun and Metcalf, 2014; Vitanov and Stenholm, 1996). STIRAP has also been demonstrated experimentally for the Rydberg state preparation in Cubel et al. (2005). Recent reviews of the literature related to STIRAP in atomic

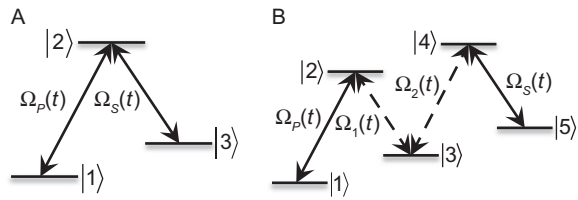

Fig. 11 Scheme of the three-level (A) and five-level (B) systems sequentially coupled by external fields.

and molecular systems can be found in Bergmann et al. (1998) and Vitanov et al. (2001, 2017).

In the RWA, considering two-photon resonance, the Hamiltonian has the form

$$\boldsymbol{H} = -\frac{\hbar}{2}\begin{pmatrix} 0 & e^{i\varphi_P}\Omega_P(t) & 0 \\ e^{-i\varphi_P}\Omega_P(t) & 2\Delta & e^{-i\varphi_S}\Omega_S(t) \\ 0 & e^{i\varphi_S}\Omega_S(t) & 0 \end{pmatrix}, \tag{32}$$

where $\boldsymbol{\Omega}_{P,S}(t)$ are the pump and Stokes Rabi frequencies, $\Delta = \Delta_P = \Delta_S$ is the single-photon detuning, and $\varphi_{P,S}$ are the initial phases. We address the Raman excitation of three-level system by external fields with a continuous pulse envelope, such as a Gaussian. For simplicity, we focus on a closed system, assuming long coherence or absence of dephasing and dissipation, that allows us to use the time-dependent Schrödinger equation to describe the population dynamics.

The mechanism of the population transfer in STIRAP can be understood using the dressed state picture. To do that, we find the eigenvalues and eigenvectors of the Hamiltonian in Eq. (32); for the single-photon resonance, $\Delta = 0$, the eigenvalues (energies) are

$$\lambda_0 = 0, \quad \lambda_\mp = \mp\frac{\hbar}{2}\sqrt{\Omega_P^2(t) + \Omega_S^2(t)}, \tag{33}$$

and the respective eigenvectors are

$$\begin{aligned} \boldsymbol{\Phi}_0 &= \left(-\frac{e^{i\varphi_P - i\varphi_S}\Omega_S(t)}{\sqrt{\Omega_P(t)^2 + \Omega_S(t)^2}}, 0, \frac{\Omega_P(t)}{\sqrt{\Omega_P(t)^2 + \Omega_S(t)^2}}\right), \\ \boldsymbol{\Phi}_- &= \left(\frac{e^{i\varphi_P - i\varphi_S}\Omega_P(t)}{\sqrt{2}\sqrt{\Omega_P(t)^2 + \Omega_S(t)^2}}, \frac{e^{-i\varphi_S}}{\sqrt{2}}, \frac{\Omega_S(t)}{\sqrt{2}\sqrt{\Omega_P(t)^2 + \Omega_S(t)^2}}\right), \\ \boldsymbol{\Phi}_+ &= \left(\frac{e^{i\varphi_P - i\varphi_S}\Omega_P(t)}{\sqrt{2}\sqrt{\Omega_P(t)^2 + \Omega_S(t)^2}}, -\frac{e^{-i\varphi_S}}{\sqrt{2}}, \frac{\Omega_S(t)}{\sqrt{2}\sqrt{\Omega_P(t)^2 + \Omega_S(t)^2}}\right). \end{aligned} \tag{34}$$

As we can see, the eigenstate $\boldsymbol{\Phi}_0$ with the eigenenergy $\lambda_0 = 0$ is the dark state since its projection to the state $|2\rangle$ is zero in the adiabatic limit. The adiabatic theorem guarantees that a quantum system will evolve in one adiabatic state if it is initially prepared in a single adiabatic state and the adiabaticity condition of the Hamiltonian change is satisfied. Analyzing the projections of the dressed state $\boldsymbol{\Phi}_0$ on the bare states $|1\rangle$ and $|3\rangle$, we observe that the counterintuitive pulse sequence, when the Stokes pulse

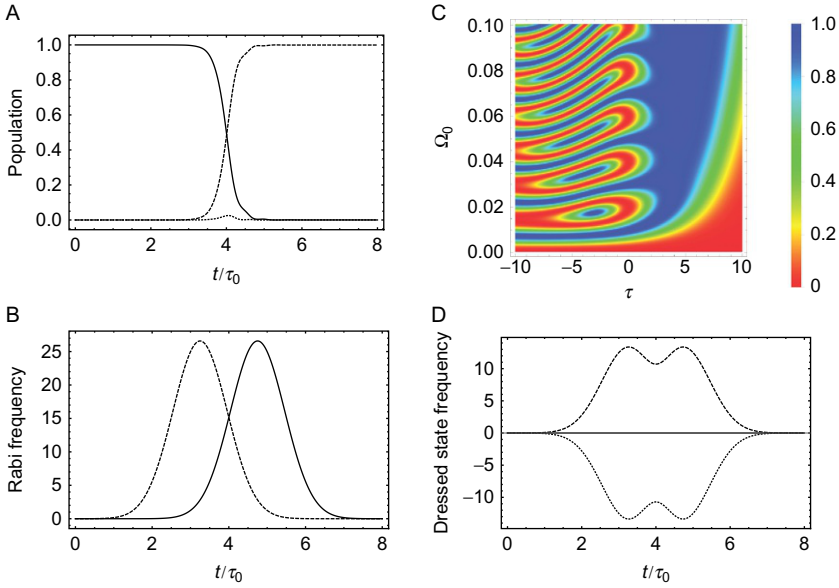

Fig. 12 (A) Population histories in STIRAP: $|a_1(t)|^2$—*solid line*, $|a_3(t)|^2$—*dashed line*, $|a_2(t)|^2$—*dotted line*. (B) Pump (*solid*) and Stokes (*dashed*) pulses. (C) Density plot of population transfer in a Λ three-level system as a function of maximum Rabi frequency, Ω_0, and time delay, τ, between the pump and Stokes pulses. Positive delay implies that the Stokes precedes the pump pulse. (D) Dressed states. The initially populated dressed state in STIRAP is the dark state shown by *solid line*.

$\Omega_S(t)$ precedes the pump pulse, provides a robust solution of population transfer from state $|1\rangle$ to state $|3\rangle$ without populating state $|2\rangle$.

Fig. 12 illustrates the STIRAP dynamics in a three-level system. The results are obtained by solving numerically the TDSE with the Hamiltonian in Eq. (32). The population dynamics is shown in Fig. 12A when the counterintuitive pulse sequence (Fig. 12B) excites the three-level system. The dressed states frequencies $\lambda_{0,\mp}/\hbar$ as a function of time are shown in Fig. 12D. Fig. 12B shows a density plot of the target state ($|3\rangle$) population at final time, as a function of the time delay between the Stokes and pump pulses and the peak Rabi frequency. The plot clearly reveals the remarkable robustness of population transfer in the wide area for positive time delays (the counterintuitive pulse sequence).

The intermediate level population is not exactly zero at the time when the pump and Stokes pulsed maximally overlap, Fig. 12A. This detrimental population in $|2\rangle$ is due to nonadiabatic coupling between the dressed states.

Since the Hamiltonian, Eq. (32), is time dependent, the Schrödinger equation in the dressed state basis has the form

$$i\hbar\dot{\Phi}(t) = \boldsymbol{D}(t)\Phi(t) - i\hbar\boldsymbol{R}_D(t)\dot{\boldsymbol{R}}_D^{-1}(t)\Phi(t), \tag{35}$$

where $\boldsymbol{D}(t)$ is the diagonal matrix with the eigenstate energies, Eq. (33), and $\boldsymbol{R}_D(t)$ is the transformation matrix, which can be constructed using the eigenvectors, Eq. (34). The general expression for the nonadiabatic coupling term can be written as

$$-i\hbar\boldsymbol{R}_D(t)\dot{\boldsymbol{R}}_D^{-1}(t) = -i\hbar\dot{\theta}(t)\frac{1}{\sqrt{2}}\begin{pmatrix} 0 & -e^{-i\phi_+} & 0 \\ e^{i\phi_+} & 0 & e^{i\phi_+} \\ 0 & -e^{-i\phi_+} & 0 \end{pmatrix}, \tag{36}$$

where $\phi_+ = \phi_P + \phi_S$, and

$$\dot{\theta}(t) = \frac{\dot{\Omega}_P(t)\Omega_S(t) - \Omega_P(t)\dot{\Omega}_S(t)}{\sqrt{2}\left[\Omega_P^2(t) + \Omega_S^2(t)\right]}. \tag{37}$$

Therefore, the adiabaticity condition for STIRAP can be presented in the form

$$\sqrt{\Omega_p^2(t) + \Omega_s^2(t)} \gg \frac{\left|\dot{\Omega}_P(t)\Omega_S(t) - \Omega_P(t)\dot{\Omega}_S(t)\right|}{\left[\Omega_P^2(t) + \Omega_S^2(t)\right]}, \tag{38}$$

which implies that the distance between the dressed states must be larger than the nonadiabatic coupling. In principle, the amount of population in $|2\rangle$ can be used as a measure of the transfer adiabaticity. Note that using frequency chirped pulses in STIRAP may help to improve the adiabaticity of the population transfer in quantum systems (Sola et al., 1999a).

Finally, we would like to point out that STIRAP solution has been found as an optimal solution of the global optimal control theory (Sola et al., 1999b) as well as a solution of the local control problem for population transfer in a three-level system, when the intermediate state population was penalized (Malinovsky and Tannor, 1997).

4.2 Generalization of STIRAP

Now we discuss generalized STIRAP schemes of population transfer in N-level system with sequential couplings (Fig. 11). There is a significant difference in the mechanisms of adiabatic transfer for even and odd number of levels. A detailed study of this difference can be found in Sola et al. (1999b)

and Vitanov et al. (1998). Here we describe the main features of the schemes in multilevel systems with odd number of levels, using the five-level system as an example. In the RWA, the five-level system Hamiltonian in the resonant case has the form

$$\boldsymbol{H} = -\frac{\hbar}{2}[\Omega_P(t)|1\rangle\langle 2| + \Omega_1(t)|2\rangle\langle 3| + \Omega_2(t)|3\rangle\langle 4| + \Omega_S(t)|4\rangle\langle 5| + c.c.]. \tag{39}$$

There are two possible versions of STIRAP for multilevel systems with odd number of levels: in one, the straddling STIRAP (S-STIRAP) scheme (Malinovsky and Tannor, 1997), the Stokes pulse again precedes the pump pulse, but all the pulses connecting intermediate levels "straddle" both the Stokes and the pump pulses ($\Omega_1(t) = \Omega_2(t) = \Omega_{ST}(t)$). In the other, the alternating STIRAP (A-STIRAP) scheme, all the pulses have the same shape and amplitude, but the pulses corresponding to all even transitions precede the pulses corresponding to all odd transitions ($\Omega_1(t) = \Omega_S(t)$ and $\Omega_2(t) = \Omega_P$) (Shore et al., 1991).

The eigenvalues of the Hamiltonian for the S-STIRAP, assuming $\Omega_{ST}(t) \gg \Omega_{P,\ S}(t)$ are

$$\lambda_0 = 0,\ \lambda_{1,2} = \mp\frac{\hbar}{2\sqrt{2}}\sqrt{\Omega_P^2(t) + \Omega_S^2(t)},\ \lambda_{3,4} = \mp\frac{\hbar}{\sqrt{2}}\Omega_{ST}(t), \tag{40}$$

while for the A-STIRAP we have

$$\lambda_0 = 0,\ \lambda_{1,2,3,4} = \mp\frac{\hbar}{2\sqrt{2}}\sqrt{\Omega_P^2(t) \mp \Omega_P(t)\Omega_S(t) + \Omega_S^2(t)}. \tag{41}$$

In both cases there is a dark state corresponding to the zero eigenvalue. The respective eigenvector is, in the S-STIRAP case,

$$\Phi_0 = (\Omega_S(t), 0, -\Omega_S(t)\Omega_P(t)/\Omega_{ST}(t), 0, \Omega_P(t))/\sqrt{\Omega_P(t)^2 + \Omega_S(t)^2}, \tag{42}$$

whereas in the A-STIRAP case we have

$$\Phi_0 = \left(\Omega_S^2(t), 0, -\Omega_S(t)\Omega_P(t), 0, \Omega_P^2(t)\right)/\sqrt{\Omega_P(t)^4 + \Omega_P(t)^2\Omega_S(t)^2 + \Omega_S(t)^4}. \tag{43}$$

The difference between the S-STIRAP and A-STIRAP arrangements resides in the probability amplitude of the level $|3\rangle$, Eqs. (42) and (43). The maximum population in $|3\rangle$ is 1/3 (when the pump and Stokes pulses maximally overlap) in A-STIRAP, while in S-STIRAP this population is given approximately by $\Omega_S(t)\Omega_P(t)/\Omega_{ST}^2(t)$ and can be substantially suppressed.

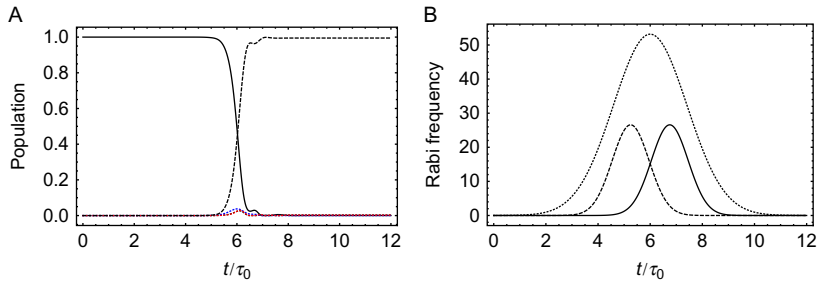

Fig. 13 Straddling STIRAP. (A) Population dynamics: $|a_1(t)|^2$—*solid line*, $|a_5(t)|^2$—*dashed line*, $|a_{2,3,4}(t)|^2$—*dotted lines*. (B) Pump (*solid*), Stokes (*dashed*), and straddling (*dotted*) pulses.

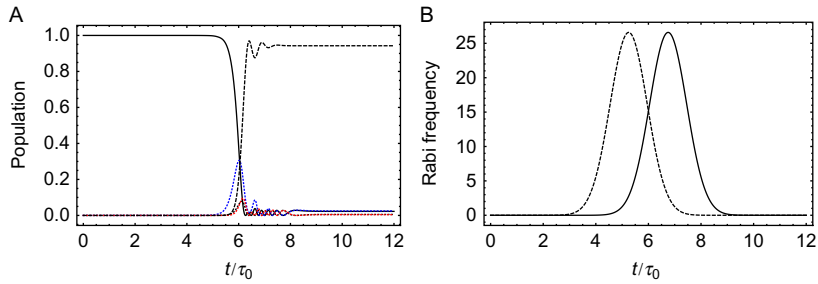

Fig. 14 Alternating STIRAP. (A) Population dynamics: $|a_1(t)|^2$—*solid line*, $|a_5(t)|^2$—*dashed line*, $|a_{2,3,4}(t)|^2$—*dotted lines*. (B) Pump (*solid*) and Stokes (*dashed*) pulses.

Figs. 13 and 14 show the population dynamics in the five-level system, respectively for the S-STIRAP and A-STIRAP pulse sequences. Comparison of the intermediate level population in Figs. 13A and 14A suggests a greater efficiency and robustness of the S-STIRAP scheme for the case where level $|3\rangle$ is not stable.

Note that the S-STIRAP pulse sequence has been discovered using local optimal control theory penalizing the intermediate state population (Malinovsky and Tannor, 1997) and its performance has been successfully verified in ultracold experiments to prepare rovibronic states of Cs_2 (Nägerl et al., 2011).

5. PHASE-CONTROLLED TWO-QUBIT QUANTUM GATES

In this section we consider the dynamics of a quantum system with closed-loop configuration. Control of such systems is possible due to the relative phase adjustment of two (or more) pathways from an initial to the target state (Shapiro and Brumer, 2003). A two-qubit system will be

considered as an example, where we address the role of the relative phase between external fields to control entanglement and to design two-qubit quantum gates.

In the last years, several methods have been proposed to create entanglement in quantum systems involving a small number of particles as well as multiparticle entanglement (Ladd et al., 2010; Leibfried et al., 2003; Schmidt-Kaler et al., 2003). One promising system to build a quantum computer is based on trapped ions, different schemes of coherent manipulation by quantum states of trapped ions have been developed. The excitation can proceed in two ways, by individually addressing each ion or through simultaneous indistinguishable excitations. Both cases have been considered in the literature and were shown to be very promising since even hot ions could be used for quantum computations, contrary to most protocols for quantum manipulations. The reason for this is that the effective couplings between the different states of the ions do not depend on the vibrational quantum number in the Lamb–Dicke limit. Here we reexamine both excitation schemes and demonstrate that the relative phase is a fundamentally important factor, which has remarkable influence on the trapped-ion state manipulation. We show that the state population and entanglement dynamics of the trapped ions depend strongly on the relative phase between the external fields. For properly chosen relative phases one can observe either Rabi oscillations according to the Mølmer–Sørensen (M-S) scheme (Mølmer and Sørensen, 1999; Sørensen and Mølmer, 1999, 2000) or collapse and revival phenomena, similar to the well-known Jaynes–Cummings model in quantum optics (Jaynes and Cummings, 1963; Shore and Knight, 1993; Tavis and Cummings, 1968).

5.1 Individual Qubit Addressing: Collapse and Revival of Entanglement

Let us consider the dynamics of two distinguishable qubits in a one-dimensional harmonic trap. Assuming that the other degrees of freedom are suppressed and decoherence effects can be neglected, the collective motion of the ions is defined by an effective harmonic trap potential, with the Hamiltonian

$$\boldsymbol{H} = \hbar\nu\left(a^{\dagger}a + \frac{1}{2}\right) + \sum_{i}\frac{E_1^{(i)}}{2}(\boldsymbol{I} - \boldsymbol{\sigma}_{zi}) + J\boldsymbol{\sigma}_{z1}\boldsymbol{\sigma}_{z2}, \tag{44}$$

where ν is the frequency of the vibrational motion, $E_1^{(i)}$ is the transition energy in the i qubit, $\boldsymbol{\sigma}_{zi}$ are Pauli matrices and $a^{\dagger}$, a are the vibrational ladder

operators. The interaction between the qubits can be treated as an effective spin–spin coupling Hamiltonian, where J is the coupling constant. The qubit interaction with the external fields can be described as

$$\boldsymbol{V}_i = -\hbar \sum_{j,i} \Omega_j(t) \cos\left[\omega_j t + \phi_j - \eta_j(a^\dagger + a)\right] \boldsymbol{\sigma}_{xi} + h.c. \tag{45}$$

where ω_j, ϕ_j are the laser frequency and phase, $\Omega_j(t)$ are the Rabi frequencies, $\eta_j = k_j\sqrt{\hbar/4m\omega_t}$ the Lamb–Dicke parameters, and ω_t is the trap frequency.

In general, due to the interaction between the qubits, the transition frequencies of the four-level system (Fig. 15) are different, depending on the specific system realization. This interaction between qubits is the main reason of blockade effects known as dipole blockade in atomic systems (Jaksch et al., 2000; Lukin et al., 2001) and in semiconductor quantum dots (Li et al., 2003). Here, we consider a general scheme of excitation by four off-resonant fields driving the following transitions: $|00n\rangle \Leftrightarrow |01n-1\rangle \Leftrightarrow |11n\rangle$ and $|00n\rangle \Leftrightarrow |01n+1\rangle \Leftrightarrow |11n\rangle$ (see Fig. 15), where "0"("1") denotes the qubit state and n is the vibrational quantum number. In the RWA and field interaction representation, the Hamiltonian has the form

$$\boldsymbol{H} = -\frac{\hbar}{2}\begin{pmatrix} 0 & \Omega_{1,n} & \Omega_{2,n+1} & 0 \\ \Omega^*_{1,n} & -2\delta_1 & 0 & \Omega_{3,n} \\ \Omega^*_{2,n+1} & 0 & -2\delta_2 & \Omega_{4,n+1} \\ 0 & \Omega^*_{3,n} & \Omega^*_{4,n+1} & 0 \end{pmatrix}, \tag{46}$$

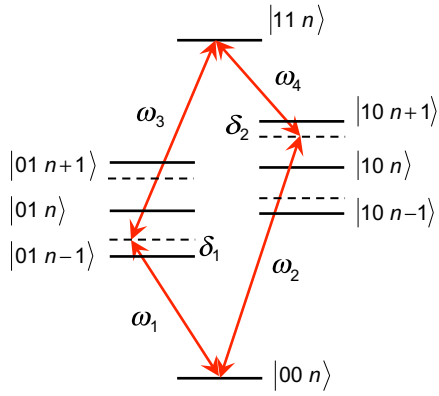

Fig. 15 Scheme of a four-level system for two qubits with distinguishable interactions in a linear ion trap.

where $\Omega_{i,n} = \eta_i \Omega_{i,0}(t) e^{i\phi_i} \sqrt{n}$, $\Omega_{i,0}(t)$ are the Rabi frequency envelopes, and $\delta_{1,2}$ the detunings including energy level shifts due to the spin–spin coupling. The total wave function of the system is represented as $|\psi\rangle = a_1|00n\rangle + a_2|11n\rangle + b_1|01n-1\rangle + b_2|10n+1\rangle$.

Choosing the detunings as $\delta_2 = -\delta_1 = \delta_0$, after the adiabatic elimination of the b_i amplitudes (off-resonant excitation) in the case of fully overlapping pulses, $\Omega_{i,0}(t) = \Omega_0(t)$, we obtain

$$\boldsymbol{H} = -\frac{\eta^2 \Omega_0^2(t)}{4\delta_0} \begin{pmatrix} 1 & i\alpha^* \\ -i\alpha & 1 \end{pmatrix}, \tag{47}$$

where $\alpha = [(2n+1)\sin(\phi/2) + i\cos(\phi/2)]$, $\phi = \phi_4 + \phi_2 - \phi_1 - \phi_3$ is the effective phase difference between the two distinct two-photon couplings, and we use $\eta_1 = \eta_2 = \eta$.

As we see, the coupling between states $|00n\rangle$ and $|11n\rangle$ in Eq. (47) depends on the relative phase, ϕ, and the vibrational quantum number, n. Only at $\phi = 0$ the coupling between the internal states does not depend on the motional states, and Eq. (47) reproduces the well-known M-S Hamiltonian of trapped ions (Mølmer and Sørensen, 1999; Sørensen and Mølmer, 1999, 2000). In this case one observes Rabi oscillations between the ground and excited electronic states even if the motional state is not a single Fock state.

The solution of the Schrödinger equation with the Hamiltonian of Eq. (47) for arbitrary phase is $a_1 = \cos[\varepsilon_n S(t)]$ and $a_2 = \alpha \sin[\varepsilon_n S(t)]/\varepsilon_n$, where $S(t) = \frac{\eta^2}{4\delta_0}\int_0^t \Omega_0^2(t')dt'$, $\varepsilon_n = [1 + 4n(n+1)\sin^2(\phi/2)]^{1/2}$ (Malinovsky and Sola, 2006). To demonstrate the effect of the relative phase we now consider the *cw* regime, $\Omega_0(t) = \Omega_0$. When the initial state of the phonons is not a single Fock state, we average the results over the corresponding state distribution. Averaging using the coherent state distribution, $P_c(n) = e^{-\bar{n}}\,\bar{n}^n/n!$, where $\bar{n}$ is the average number of phonons, we obtain for the population inversion, $W = \sum_{n=0}^{\infty} P_c(n)(|a_1|^2 - |a_2|^2) = \sum_{n=0}^{\infty} P_c(n)\cos[2gt\varepsilon_n]$, where $g = \eta^2\Omega_0^2/4\delta_0$.

Fig. 16A shows the population inversion dynamics for different values of the relative phase after averaging over the coherent state distribution. At $\phi = 0$ the dynamics of the system does not depend on the vibrational quantum number, as it was shown in Mølmer and Sørensen (1999) and Sørensen and Mølmer (1999, 2000), and we observe simple Rabi oscillations with frequency defined by $2g$. However, in general the Rabi frequencies depend on the vibrational quantum number n, $G_n = 2g\varepsilon_n$. In the limit of

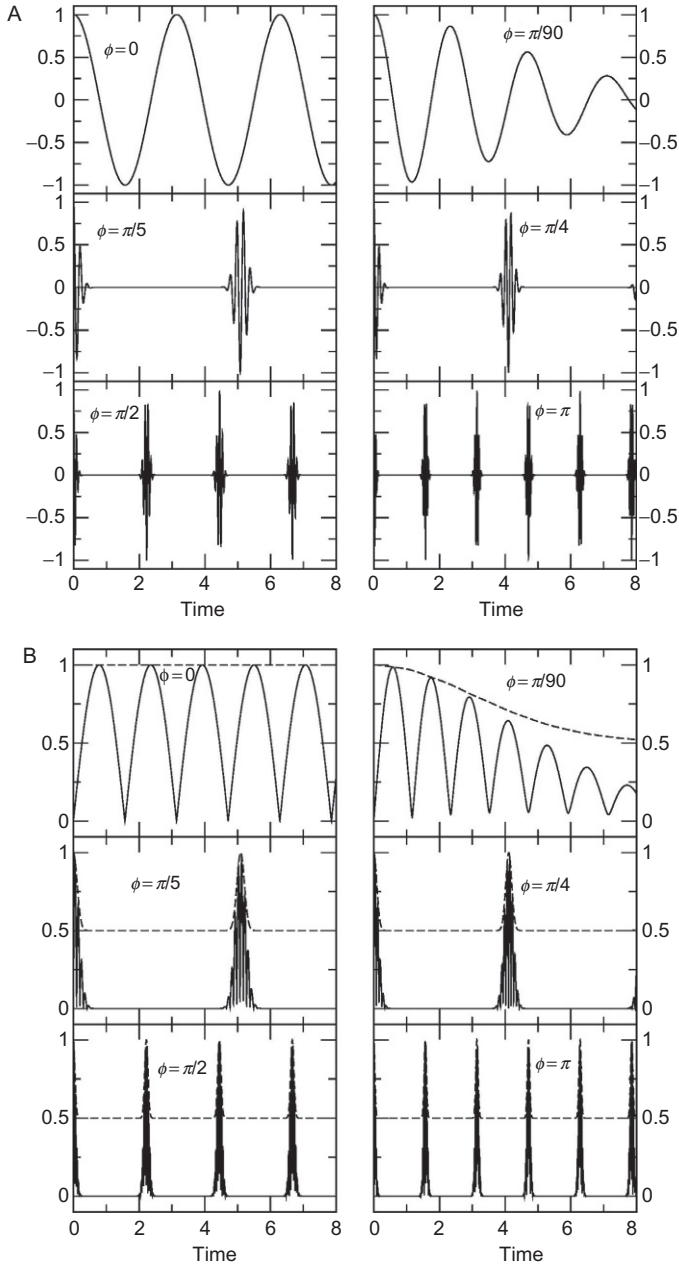

Fig. 16 Population inversion dynamics [$W(t)$] (A), concurrence (*solid line*) and Renyi entropy (*dashed line*) (B) in a system of two trapped qubits as a function of time at various relative phases, ϕ for a initial coherent state of phonons with average number $\bar{n} = 25$. *Adapted from Malinovsky, V.S., Sola, I.R., 2006. Phase-controlled collapse and revival of entanglement of two interacting qubits. Phys. Rev. Lett. 96, 050502.*

$\bar{n} \gg 1$ we obtain the analytic expression for the population inversion, $W(t) = e^{-2\bar{n}\sin^2(\tau/2)}\cos(\bar{n}\sin\tau)$, where $\tau = 4gt\sin(\phi/2)$. The envelope function, $e^{-2\bar{n}\sin^2(\tau/2)}$, shows that all revivals in this model are full revivals. Using the analytic expressions for the probability amplitudes, we estimate the following characteristic times for the dynamics: the period of the Rabi oscillations, $t_R \approx 1/4g\bar{n}\sin(\phi/2)$, the collapse time, $t_c = [8g\sqrt{\bar{n}}\sin(\phi/2)]^{-1}$, and the interval between revivals, $t_r \approx \pi m/[2g\sin(\phi/2)]$, where $m = 1, 2, \ldots$. The results in Fig. 16A are in a perfect agreement with our estimates.

Since the state $|00n\rangle + |11n\rangle$ is the entangled state, we quantify the degree of entanglement by constructing the density matrix ρ and calculating the concurrence $C(\rho)$ (Hill and Wootters, 1997; Rungta et al., 2001; Wootters, 1998; Yu and Eberly, 2002, 2003). Fig. 16B shows the dynamics of entanglement in the two-qubit system at various values of the relative phase. We observe that for the coherent state distribution of phonons the concurrence fully revives at any value of the relative phase, which controls the revival time and the width of the reviving comb. The dependence of the Renyi entropy, $P(\rho) = Tr[\rho^2]$, which can be used as a measure of the system purity, on the relative phase, is also presented in Fig. 16B. More details about the phase-induced collapse and revival of entanglement can be found in Malinovsky and Sola (2006).

5.2 Indistinguishable Qubit Addressing: Two-Qubit Gates

Now we consider the dynamics of two distinguishable qubits in a one-dimensional harmonic trap when both qubits are excited by external fields. The Hamiltonian of the system and the interaction part of Eqs. (44) and (45) are still valid. However, the number of the states involved in the dynamics changes, as well as the coupling between states is changed, as shown in Fig. 17. The total two-qubit wave function has the form

$$\begin{aligned}|\Psi(t)\rangle = {} & a_1(t)|00n\rangle + a_2(t)|10n\rangle + a_3(t)|01n\rangle + a_4(t)|11n\rangle \\ & + b_1(t)|01n-1\rangle + b_2(t)|10n+1\rangle + b_3(t)|01n+1\rangle \\ & + b_4(t)|10n-1\rangle + c_1(t)|00n-1\rangle + c_2(t)|00n+1\rangle \\ & + c_3(t)|11n-1\rangle + c_4(t)|11n+1\rangle,\end{aligned} \tag{48}$$

which contains the computational subspace ($|00n\rangle$, $|10n\rangle$, $|01n\rangle$, $|11n\rangle$) and additional ancillary states ($|00n \pm 1\rangle$, $|10n \pm 1\rangle$, $|01n \pm 1\rangle$, $|11n \pm 1\rangle$). As in Sørensen and Mølmer (1999, 2000) and Mølmer and Sørensen (1999), here we address the excitation of the trapped ion by

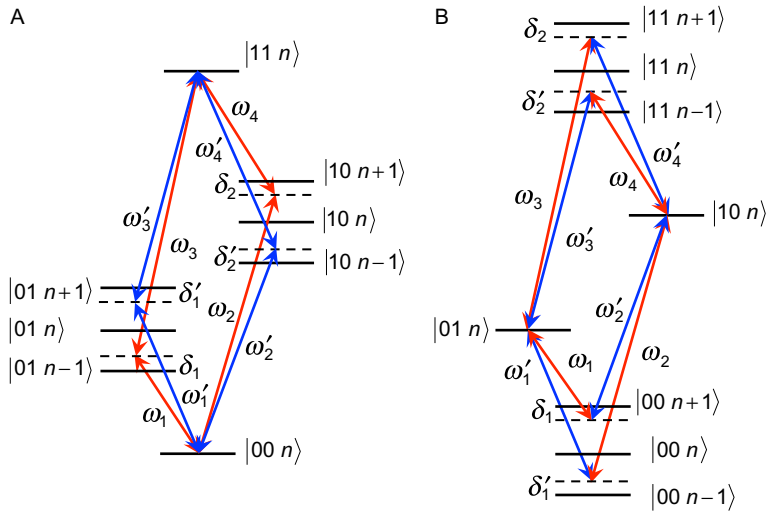

Fig. 17 Energy level structure of the two-ion system and their couplings induced by external fields. To simplify the figure, we show the couplings between the $|00n\rangle$, $|11n\rangle$ states, and between the $|01n\rangle$, $|10n\rangle$ states in two frames, (A) and (B), respectively.

using off-resonant laser fields. In the general case, we have eight different couplings with frequencies arranged in pairwise way to accomplish two-photon resonance between the computational states while all ancillary states are not excited.

Assuming that all single-photon detunings, $\delta_{1,2}$ and $\delta'_{1,2}$, are sufficiently large, we make the adiabatic elimination of the ancillary vibrational states (Berman and Malinovsky, 2011) and obtain the Schrödinger equation for the probability amplitudes of the computational states, a_i. The general system of four differential equations splits in two uncoupled two-level systems, shown in Fig. 17A and B. For simplicity, we consider here only the case when all the external fields are fully overlapping, $\Omega_j(t) = \Omega_0(t)$ and symmetric detunings, $\delta_1 = \delta'_2$, $\delta_2 = \delta'_1$.

The effective Hamiltonian for states $|00n\rangle$ and $|11n\rangle$ (see Fig. 17A) and for states $|01n\rangle$ and $|10n\rangle$ (see Fig. 17B) has the form

$$\boldsymbol{H}_e = -\hbar \begin{pmatrix} \Omega_{ac}(t) & \Omega_e(t) \\ \Omega_e^*(t) & \Omega_{ac}(t) \end{pmatrix}, \tag{49}$$

where $\Omega_{ac}(t)$ is the ac Stark shift, and $\Omega_e(t)$ is the effective two-photon Rabi frequency. Both the ac Stark shift and the effective two-photon Rabi

frequency depend on the vibrational quantum number and the relative phase of the fields (Malinovsky et al., 2014).

To address the case of two indistinguishable ions excited by only two external fields we need to impose the following relations for the phases $\phi_1 \equiv \phi_2' \equiv \phi_4 \equiv \phi_3'$ and $\phi_2 \equiv \phi_1' \equiv \phi_3 \equiv \phi_4'$ and symmetrize the detunings by taking $\delta_2 = -\delta_1 = \delta_0$. Under these conditions the ac shifts for all computational states are identical, $\Omega_{ac}(t) = \eta^2\Omega_0^2(t)/(2\delta_0)$, while the Rabi frequencies are

$$\Omega_{14}(t) = \eta^2\Omega_0^2(t)e^{i(\phi_1+\phi_2)}/(2\delta_0), \quad \Omega_{23}(t) = \eta^2\Omega_0^2(t)/(2\delta_0). \tag{50}$$

Note that the Rabi frequency $\Omega_{14}(t)$ couples the states $|00n\rangle$ and $|11n\rangle$, while the Rabi frequency $\Omega_{23}(t)$ couples states $|01n\rangle$ and $|10n\rangle$. The independence of the Rabi frequencies on the vibrational quantum number indicates that the excitation scheme does not require laser cooling to the motional ground state (Mølmer and Sørensen, 1999).

The ac Stark shift is irrelevant here, since it produces only a dynamic global phase. Therefore, the final form of the total Hamiltonian in the limit of adiabatic elimination of the ancillary states is

$$\boldsymbol{H}(t) = -2\hbar g(t)[\cos(\phi_+/2)\boldsymbol{\sigma}_x - \sin(\phi_+/2)\boldsymbol{\sigma}_y]\otimes[\cos(\phi_+/2)\boldsymbol{\sigma}_x - \sin(\phi_+/2)\boldsymbol{\sigma}_y], \tag{51}$$

where $\phi_+ = \phi_1 + \phi_2$, $g(t) = \eta^2\Omega_0^2(t)/(4\delta_0)$. Solving the Schrödinger equation with the Hamiltonian in Eq. (51), the complete evolution operator in the computational basis $\{|00\rangle, |01\rangle, |10\rangle, |11\rangle\}$ can be written in the general canonical form

$$U_t(\xi) \ = C_1\otimes C_2 e^{i\xi(t)\boldsymbol{\sigma}_x\otimes\boldsymbol{\sigma}_x} C_1^{-1}\otimes C_2^{-1}, \tag{52}$$

where $\xi(t) = 2\int_0^t dt' g(t')$ is the effective pulse area, and $C_{1,2} = e^{i\phi_+\boldsymbol{\sigma}_z/4}$.

The canonical form of $U_t(\xi)$ in Eq. (52) is equivalent to the Cartan decomposition (Zhang et al., 2003) of an element of the group $SU(4)$. This is of the form $U = k_1 U_A k_2$, where k_1 and k_2 represent single-qubit operations from the $SU(2) \otimes SU(2)$ subgroup of $SU(4)$. In our case, the Cartan decomposition of $U_t(\xi)$ is given as $U_t(\xi) = k_1(\phi_+)U_{xx}(\xi)k_2(\phi_+)$, which explicitly demonstrates that the entangling capabilities of $U_t(\xi)$, contained in $U_{xx}(\xi)$, are invariant to any variations of the phase ϕ_+ including phase errors. This makes the gate naturally more robust to phase errors and allows to correct these errors by single-qubit operations that are usually easier to implement. The exact CNOT gate decomposition, which can facilitate further advances

in the practical implementation of the circuit-based quantum computation, is explicitly derived in (Malinovsky et al., 2014).

6. MOLECULAR WAVE PACKETS: ELECTRONIC TRANSITIONS IN MOLECULES

Previously, in this chapter, we have studied laser driven processes with pulses long enough to resolve the dynamics in the energy eigenstates of the system. In the RWA such dynamics is characterized by the lack of (or the very slow) dynamic dephasing. The basic requirement is the use of lasers with spectral bandwidth smaller than the energy spacing of the system that induce effective interactions (that is, with Rabi frequencies) smaller than the energy spacing. In the presence of short or intense pulses, coherent superpositions or nearby levels are formed, inducing dynamics controlled by the field-free Hamiltonian, H_0. Although in principle the situation can be more difficult to be analyzed, three limiting cases have natural analytic solutions which can be used as starting points to understand the dynamics and to extend strategies previously proposed for N-level systems. These are the sudden (or impulsive) limit, the adiabatic limit, and the strong-field limit. The last one will be the subject of Section 7.

The main disadvantage of using short pulses is the loss of energy-resolved state selectivity. The advantages, however, are many. From the experimental side it is far simpler to work with stable coherent laser sources in the femtosecond regime to induce coherent molecular dynamics, precisely because most decoherent processes (e.g., collisions, spontaneous decay) act on longer timescales. In addition, shorter pulses can often be stronger, allowing to access highly excited states via multiphoton transitions or to affect the system in other nonlinear ways (Stark shifts) that provide new control knobs in the dynamics. And then, even if the pulses are stronger, the energy flow may remain low enough as to avoid damaging the sample. Finally, any technique involving phase modulation of the pulses is simpler to implement using shorter rather than longer pulses.

But if state selectivity can not be achieved in principle, what are going to be the controlled observables in the dynamics of wave packets? Although obviously subject to Heisenberg's uncertainty principle and to natural spreading, molecular wave packets typically involve spatial (in some molecular coordinates) localization during timescales that may correspond to that of the controlled motion. It is therefore natural to observe, manipulate, and control the spatial distribution of the wave packet using short pulses, as evidenced in

the development of Femtochemistry (Rosker et al., 1988; Zewail, 1988, 2000) and of one of the first QC schemes, the Tannor–Kosloff–Rice control of chemical reaction by time-delaying pulses (Tannor and Rice, 1985; Tannor et al., 1986).

Additionally, because of the hierarchical energy structure of most quantum systems with different reduced masses, in particular molecules, the pulse can be chosen so that its spectral width is larger than the energy spacing of only some degrees of freedom, inducing a wave packet in that coordinate, but selectively addressing the others. Hence, picosecond pulses can generate rotational wave packets, called pendular states (Friedrich and Herschbach, 1995; Ortigoso et al., 1999), but address selectively a vibrational mode; and similarly femtosecond pulses can create vibrational wave packets within an electronic state. Hence, one can control population flow in this degree or degrees of freedom. But also, there is no principle that disallows the selective control in the degree of freedom where the wave packet is formed. As in the Coherent Control scheme where several routes can select a single state from a set of degenerate levels by quantum interference, we will show in Section 8 that state selectivity is finally also possible, albeit it typically requires laser pulse modulation or the previous preparation of the initial state.

In this section we will concentrate on the dynamics of vibrational wave packets and the control of electronic transitions. There has been a wealth of ideas and schemes devised to control rotational wave packets, for which we refer the reader to the relevant literature (Seideman and Hamilton, 2005; Stapelfeldt and Seideman, 2003; Townsend et al., 2011). To simplify the analysis we start by considering diatomic molecules oriented with respect to a single external field $\epsilon(t)$. We use the rotating wave approximation (RWA), such that $\epsilon(t) \approx E(t)e^{\pm i\varphi(t)}/2$, where $E(t)$ is a slowly varying envelope function, compared to the rate of change of the dynamical phase $\varphi(t)$. The negative sign is used to describe absorption, while the positive sign is used for the stimulated emission. In general, for chirped pulses, $\varphi(t) = \int \omega(t')dt'$, where $\omega(t)$ is the time-varying frequency. If only two electronic states participate in the dynamics, the following very general TDSE can be used to describe the dynamics of the nuclear wave packets, particularly if the pulses are not very intense,

$$i\hbar\frac{\partial}{\partial t}\begin{pmatrix}\psi_1(R,t)\\ \psi_2(R,t)\end{pmatrix} = \begin{pmatrix}\mathbf{T}+V_1(R) & \mathbf{K}-\frac{1}{2}\mu_{12}(R)E(t)\\ \mathbf{K}-\frac{1}{2}\mu_{12}(R)E(t) & \mathbf{T}+V_2(R)-\hbar\omega(t)\end{pmatrix}\begin{pmatrix}\psi_1(R,t)\\ \psi_2(R,t)\end{pmatrix}, \tag{53}$$

where $\psi_j(R, t)$ are the nuclear wave packets moving in the $V_j(R)$ electronic potentials, $\mathbf{T} = -\frac{\hbar^2}{2m}\frac{\partial^2}{\partial R^2}$ is the kinetic energy operator (m the reduced mass) and $\mathbf{K}$ takes into account nonadiabatic couplings that break the Born–Oppenheimer approximation, either of kinetic origin or due to spin–orbit couplings (Worth and Richings, 2013).

Our first concern is how to control the electronic transition of the wave packets between the two electronic states, for which we show the limiting solutions and comment on how they can be used in more complex scenarios or for other goals.

6.1 The Impulsive Limit: Making Molecular π-Pulses

Consider a molecule in the vibrational ground state of its electronic ground state. How can we maximize the electronic absorption to an excited electronic state, to which it is coupled by a laser? The simplest control model that we know of is the population transfer by π-pulses. If the pulse is very short we can assume that during the excitation the packet does not move, such that the kinetic energy can be regarded constant (which can be taken away from the Hamiltonian).

How short that must be? We follow here the argument of Garraway and Suominen (1995). Typically the shortest timescale is related to the motion of the wave packet promoted to the excited state, since in the most common situations, the bond equilibrium distance in the ground state, R_0, lies in the repulsive barrier of the excited state, so the excited packet will experience a strong gradient. To estimate the timescale of motion we linearly expand the excited potential around R_0, $V_2 \approx -\alpha(R - R_0)$. The excited packet suffers an acceleration $a \approx \frac{1}{m}\frac{\partial V_2}{\partial R} \approx \alpha/m$ and the time that it takes to move a distance equal to its standard deviation, σ, is

$$\tau_e \sim \sqrt{\frac{2m\sigma}{\alpha}}. \tag{54}$$

Hence, we need the time duration of the pulse, τ, to be shorter than τ_e.

However, if the potentials differ, the resonance condition can only be achieved at a certain internuclear distance, as Fig. 18 shows. We define a coordinate-dependent detuning, $\Delta(R) = V_2(R) - V_1(R) - \hbar\omega$. Assuming that the transition dipole remains fairly constant around the packet and omitting the nonadiabatic coupling terms, the TDSE of Eq. (53) can be simplified to

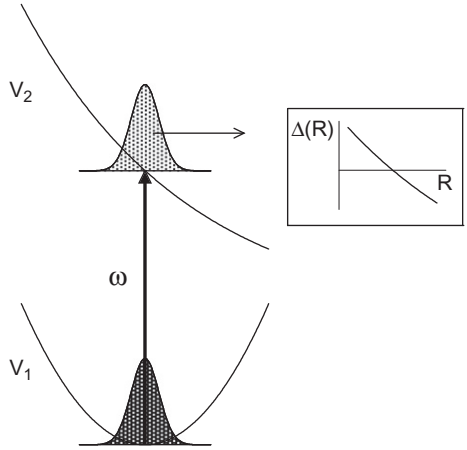

Fig. 18 Sketch of the Franck–Condon transition as a set of two-level systems with different detunings for each value of *R*.

$$i\hbar\frac{\partial}{\partial t}\begin{pmatrix}\psi_1(R)\\ \psi_2(R)\end{pmatrix}=\begin{pmatrix}0 & -\hbar\Omega(t)/2\\ -\hbar\Omega(t)/2 & \Delta(R)\end{pmatrix}\begin{pmatrix}\psi_1(R)\\ \psi_2(R)\end{pmatrix}. \tag{55}$$

For each value of R we have the Hamiltonian of a two-level system, with detuning $\Delta(R)$. General analytical solutions are not known although there are fair guesses (Robiscoe, 1983). For a pulse of the form $E(t) = E_0\mathrm{sech}(t/T)$, the Rosen-Zener solution gives, at final time T, the excitation probability (Rosen and Zener, 1932)

$$P(V_1(R)\rightarrow V_2(R)) = \sin^2(S/2)\,\mathrm{sech}^2[\pi\Delta(R)T], \tag{56}$$

where S is the pulse area. The excited population at time T can be obtained integrating over R,

$$P_2 = \int dR'|\psi_1(R',0)|^2\,P(V_1(R')\rightarrow V_2(R')). \tag{57}$$

This depends on the pulse area, as the Rabi solution, but takes into account the detuning. Defining Δ_{FC} as the range that $\Delta(R)$ takes within the confines of the wave packet, the so-called Franck–Condon region, we find that if $T \ll 1/\Delta_{FC}$, $\mathrm{sech}^2(\pi\Delta(R)T) \approx 1$ and the π-pulses lead to better than 95% population in the excited state (for a Franck–Condon region extended 2σ around R_0). This implies the obvious condition that in order to transfer all the wave packet to the excited state we need the pulse bandwidth to extend over all the absorption band, a condition much harder to meet than

that imposed by τ_e. We call Franck–Condon transitions (FCT) to these "vertical" excitations. A delta pulse, with all frequency components *in phase* with equal magnitude, guarantees full electronic population inversion, but femtosecond pulses often provide good approximations for not very light molecules. Some rough numbers for the $X^1\Sigma_g$ to $A^1\Sigma_u$ transition or A band in Na_2 give $\tau_e \sim 50$ fs and $\Delta_{FC}^{-1} = 5$ fs, showing that molecular π-pulses are within actual capabilities.

The control of the electronic transition is a first step to most control scenarios in molecules. The excited electronic potential provides gradients that move the promoted wave packet away from the equilibrium configuration, inducing vibrations or (depending on the nature of the excited state) photodissociation. Another properly time-delayed molecular π-pulse can be used to move the packet back to the ground state, inducing high vibrational excitation, isomerization, or photodissociation, as in the original pump–dump scheme of Tannor et al. (1986). However, in polyatomic molecules it is often necessary to add a certain momentum to the wave function before it is promoted to the excited state. This can be achieved by using an infrared pulse before the molecular π-pulse hits the molecule (Amstrup and Henriksen, 1992; Elghobashi and González, 2004; Meyer and Engel, 1997). As the wave packet moves, the time duration of the pump or dump pulses must be adjusted so that their spectral widths overlap the absorption or emission bands.

In addition to controlling the position of the packet by cleverly using the gradients of the excited and ground potentials at the right time, molecular π-pulses can be used for molecular squeezing, that is, the control of the width of the wave function or the dispersion of the position of the particle. When the potentials have different harmonic frequencies, the dynamics implies *breathing*, where the packet stretches in the excited state and squeezes in the ground state as long as it remains Gaussian. A succession of properly time-delayed π-pulses can lead to a high level of dynamic squeezing by iterative pump–dump control. This is the principle under the iterative stretching–squeezing scheme, ISS (Chang and Sola, 2005; Chang et al., 2006a). For harmonic oscillators, the process can be continued forever, with the only limitation that, in each iteration the π-pulse bandwidth must increase. Chang and Sola (2005) have developed analytical formulas in the harmonic approximation regarding the maximum degree of squeezing that can be achieved given a fixed (limited) maximum pulse bandwidth and have applied these formulas to study squeezing in two electronic transitions in Rb_2: $X\ ^1\Sigma_g \rightarrow 1\ ^1\Pi_u$ and $1\ ^1\Sigma_u \rightarrow 3\ ^1\Pi_g$ (Chang et al., 2006a).

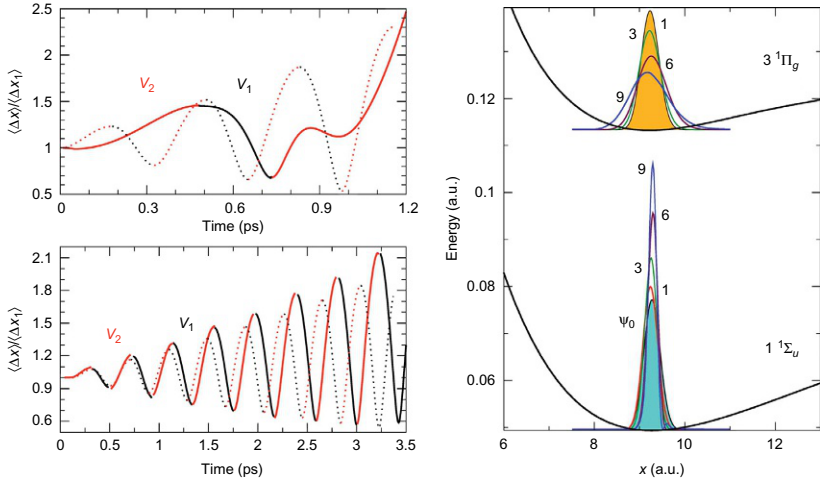

Fig. 19 Wave packet breathing dynamics of the ISS in Rb_2 for the $X\ ^1\Sigma_g \rightarrow 1\ ^1\Pi_u$ transition (*upper left frame*) and for the $1\ ^1\Sigma_u \rightarrow 3\ ^1\Pi_g$ (*lower left frame*). *Dotted lines* represent the analytical results in the HO approximation and *solid lines* give the numerical solution of the TDSE; *red lines* refer to the excited state and *black* to the ground state. The *right frame* shows the maximally stretched and squeezed wave packets in the ISS scheme for the transitions from $1\ ^1\Pi_u$ and $1\ ^1\Sigma_u$ to $3\ ^1\Pi_g$. The *numbers* in the wave packets label the iteration in the stretching–squeezing process. *Adapted from Chang, B.Y., Lee, S., Sola, I.R., Santamaria, J., 2006. Adiabatic and diabatic transformations as physical resources for wave packet squeezing. Phys. Rev. A 73 (1), 013404. https://doi.org/10.1103/PhysRevA.73.013404 with permission.*

Fig. 19 shows the evolution of the width of the wave packet relative to its initial width. In the first transition, the potentials are very different, leading to fast squeezing (in less iterations) but also fast spreading of the packet, limiting the maximum squeezing that can be achieved. However, the $1\ ^1\Sigma_u$ and $3\ ^1\Pi_g$ potentials have very similar shapes, providing an excellent example of the capabilities of population inversion by molecular π-pulses. The process is almost a perfect FCT where the wave packets simply breath in each potential, leading to successively maximum stretch (in the excited state) and maximum squeeze (in the ground state) at each iteration. Using 25 fs FWHM pulses of 300 GW/cm^2 peak intensity, one can achieve a maximum squeezing of nearly 50% of the original width (Chang et al., 2005, 2006a).

The physical origin of the squeezing is caused by the phase accumulation generated by the mismatch in the electronic forces exerted in the different molecular potentials at different iterations. Alternatively, the squeezing can be induced by interference between two wave packets if the pulses imposes two different pathways, using the principles of coherent control

(Abrashkevich et al., 1994; Averbukh and Shapiro, 1993) or it can proceed adiabatically, by the combined Stark shift pressure of at least two pulses with slowly increasing intensity (Chang et al., 2005), as we comment in Section 7.2.

6.2 The Adiabatic Limit: Necessary Conditions for AP

We know that the π-pulse method, while effective in certain cases, is not in general a robust method for population transfer. Can we apply the previous approximations to study adiabatic passage for wave packets in molecules?

In analyzing the conditions required to reach AP, one must take into account that under linear optics, the laser amplitudes and durations depend on the chirp rates. In Section 8.6 we refer to the most common processes of pulse modulation. Assuming an initial Gaussian transformed-limited pulse (TLP) of duration τ_0 and spectral width $\Gamma_0 = 1/\tau_0$, the spectrum is modified by quadratic phase dispersion

$$\epsilon(\omega) = E_0' \exp\left[-\frac{(\omega-\omega_0)^2}{2\Gamma^2} + i\alpha'\frac{(\omega-\omega_0)^2}{2}\right]. \tag{58}$$

The transformed pulse in the time domain then remains Gaussian,

$$\epsilon(t) = E_0 \exp\left[-\frac{t^2}{2\tau^2} - i\omega_0 t - i\alpha\frac{t^2}{2}\right], \tag{59}$$

and α and α' are the linear temporal and spectral chirps, which are related. Whereas the temporal duration depends on the chirp

$$\tau^2 = \frac{1}{\Gamma^2}(1+\alpha'\Gamma^4), \tag{60}$$

the spectral width is fixed, $\Gamma = \Gamma_0$. In addition, assuming no losses, the chirped pulse intensity I decreases with the chirp, so that the relation between the pulse areas of the chirped pulse S, and its parent TLP S_0, is

$$\frac{S}{S_0} \sim \frac{\Omega\,\tau}{\Omega_0\tau_0} = \sqrt{\frac{\tau}{\tau_0}}, \tag{61}$$

where $\Omega_0 = \mu E_0/\hbar$ is the peak Rabi frequency of the TLP. In a two-level system, application of the Landau–Zener model (assuming a constant field Ω_0) gives as adiabatic criteria for AP the condition $\Omega_0^2 > 4\alpha$. Interestingly,

the relation between the different parameters makes the AP basically independent of the chirp (Malinovsky and Krause, 2001a),

$$P_2 \approx 1 - \exp\left(-\pi\frac{\Omega_0^2}{2\alpha}\right) = 1 - \exp\left(-\frac{\pi}{2}\Omega_0^2\tau_0^2\right). \tag{62}$$

However, taking into account that the pulse duration is finite, and that at initial time the two states must be separated at least by Ω_0 to start the dynamics in a single dressed state, gives the additional condition $\tau \geq \Omega_0/\alpha$. The main difficulty to achieve electronic population inversion remains the same as with the π-pulses: the bandwidth of the parent transformed-limited pulse must overlap the entire band of the absorption spectra. Because τ_0 must be very short, following Eq. (62), Ω_0 must be very large, although sometimes strong-field effects can be neglected. Population inversion by chirped pulses has been observed experimentally in I_2 and other molecules (Melinger et al., 1991; Yakovlev et al., 1998).

In principle, to obtain analytic formulas one could use the same TDSE as previously (Eq. 55). Now the detuning $\Delta(R,t) = V_2(R) - V_1(R) - \hbar\omega(t)$ is both position dependent and time dependent. Modeling the frequency with a tangent hyperbolic function (with a nearly linear chirp), one obtains the Demkov–Kunike model (Garraway and Suominen, 1995). Solving the two-level system for each R, and later integrating over R as before, Paloviita et al. (1995) showed that the yields of population transfer correspond well with the exact results obtained from the numerical integration of the TDSE. Surprisingly, one can obtain population inversion with large α and short pulses, with pulse areas not much larger than π (Cao et al., 1998). Although the conditions are not exactly those of AP, the motion of the wave packet actually favors the passage, even in the absence of chirping, since as the wave packet leaves the Franck–Condon region, it decouples the stimulated emission, so that there is no Rabi cycling for even π-pulses unless $\tau_0 \sim \tau_e$. By chirping, however, one has other interesting control effects on the shape of the packet that depend on the sign of the chirp. For instance, using red-to-blue chirp, the low energy components of the packet, with lower momentum, are excited first, and the higher energy components, with larger momentum, later. Although during the excitation the packet spreads, the components recombine and the packet refocuses at a later time. The opposite occurs when one chooses a blue-to-red chirp. This so-called molecular reflectron or molecular cannon effects can be used to control the shape of the wave function at a later time

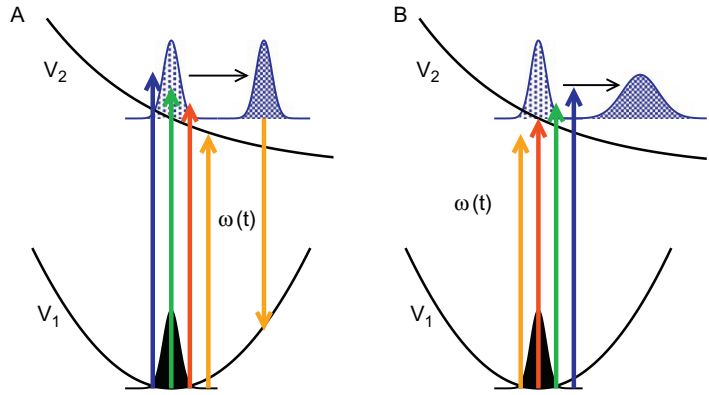

Fig. 20 Sketch of an adiabatic electronic transition with (A) *blue*-to-*red* chirp; (B) *red*-to-*blue* chirp, leading to spreading or focusing of the wave packet, and intrapulse stimulated Raman scattering.

(Cao and Wilson, 1997; Guhr et al., 2004; Krause et al., 1993). In addition, the blue-to-red chirp can induce stimulated emission. As the wave packet propagates in the excited potential, the red components of the same field can overlap the emission spectrum inducing intrapulse stimulated Raman scattering, ISRS (Ruhman and Kosloff, 1990) that vibrationally heats the molecule in the ground potential (Malinovsky and Tannor, 1997). Both situations are sketched in Fig. 20. On the other hand, one can operate in the opposite limit. If the bandwidth of the TLP is smaller than the energy spacing, then the excitation can be state-selective (Malinovsky and Krause, 2001a). But even if that condition does not hold, depending on the sign of the chirp one can select the highest/lowest vibrational level of the manifold (Chang et al., 2003a).

Although we have considered here only electronic population transfer by AP, chirped pulses have been proposed and used for many other purposes in molecules. In particular, a single infrared pulse can be used to induce vibrational ladder climbing (Chelkowski et al., 1990; Falvo et al., 2013; Guérin, 1997; Hess et al., 2000; Maas et al., 1998; Witte et al., 2003) and a pair of optical pulses can extend the ladder climbing by a Raman process (Chang et al., 2001a,b; Chelkowski and Bandrauk, 1997; Chelkowski and Gibson, 1995; Davis and Warren, 1999). Using two or more pulses it is possible to achieve AP with a sequence of transformed-limited pulses, as in the STIRAP scheme and its extensions. We reviewed some results of STIRAP in level systems in Section 4. Its applications to molecules with strong fields are the subject of the following section.

7. STRONG FIELD SOLUTIONS: DYNAMICS IN LIGHT-INDUCED POTENTIALS

In N-level Hamiltonians, when adiabatic conditions apply (for long and strong pulses) it is usually simpler to follow the dynamics in the dressed states. The same idea can be extended to wave packet dynamics, where now the instantaneous adiabatic potentials are called light-induced potentials or LIPs (Bandrauk and Sink, 1981; Yuan and George, 1978).

To explain the different features of strong-field dynamics we use the Hamiltonian of Eq. (53) but add polarizability terms to account for nonlinear laser effects, such that the effective Hamiltonian is

$$\mathbf{H}=\begin{pmatrix}\mathbf{T} & \mathbf{K}\\ \mathbf{K} & \mathbf{T}\end{pmatrix}+\begin{pmatrix}V_1(R)-\frac{1}{4}\alpha_{11}(R)E^2(t) & -\frac{1}{2}\mu_{12}(R)E(t)\\ -\frac{1}{2}\mu_{12}(R)E(t) & V_2(R)-\hbar\omega(t)-\frac{1}{4}\alpha_{22}(R)E^2(t)\end{pmatrix}. \tag{63}$$

In Eq. (63) we have assumed that the field may be resonant or quasi-resonant between the two electronic states, coupled via the dipole moment μ_{12}, and nonresonant with respect to the remaining states of the molecule. The effect of the remaining states on the two selected states is described in terms of the quasi-polarizabilities (α_{11} and α_{22}) up to the next leading order in the field, E^2.

The description of the strong-field effects is based on clarifying the relation between certain topological features of the LIPs and the quantum processes they conveyed in the molecular potentials. We consider two different regimes depending on whether the effect of the laser on the potentials renders a "soft" or "hard" shaping. The first one is characterized by the lack of a resonant or quasi-resonant excitation so that the off-diagonal terms are negligible. Then the initially populated LIP can be written as

$$V_1^a(R,E)\approx V_1(R)-\frac{1}{4}\alpha_{11}(R)E^2(t),$$

in which α is the dynamic polarizability. In some cases the polarizability is dominated by a single electronic state, closer in energy to $V_1(R)+\hbar\omega$. In other cases, the frequency is much smaller (e.g., an infrared laser or an electric pulse) and the static polarizability can be used instead. Unless $\alpha_{11}(R)$ changes drastically around the equilibrium geometry of $V_1(R)$, the

topological changes in $V_1(R)$ induced by the field will be small, hence the "soft" character of the shaping. The control is mainly exerted by $E(t)$, inducing energy variations (Stark shifts) of the potential. It is often the case that the ground LIP is very similar to the ground molecular potential, except at long internuclear distances, where the energies of $V_1(R)+\hbar\omega$ and $V_2(R)$ lie closer, inducing bond softening in $V_1^a(R)$ (Allendorf and Szöke, 1991; Bucksbaum et al., 1990; Giusti-Suzor et al., 1995; Jolicard and Atabek, 1992; Yang et al., 1991; Zavriyev et al., 1990). The corresponding effect in the excited state is more dramatic, specially if V_2 is dissociative or weakly bound. Then the coupling induces bond hardening or vibrational stabilization (Aubanel et al., 1993a,b; Giusti-Suzor and Mies, 1992; Yao and Chu, 1992; Zavriyev et al., 1993).

On the other hand, when the interaction is quasi-resonant, as a first approximation one can neglect the polarizability and concentrate on the two crossing potentials. The LIPs are obtained by diagonalizing the potential energy operator, including the field coupling. They are the instantaneous eingenstates of the electronic Hamiltonian. Applying the rotation matrix

$$\begin{pmatrix} \cos\theta(R;E) & \sin\theta(R;E) \\ -\sin\theta(R;E) & \cos\theta(R;E) \end{pmatrix},$$

where $\theta(R;E)$ is the rotation or mixing angle that diagonalizes the matrix, we obtain

$$\mathbf{H}^{\mathrm{DS}} = \begin{pmatrix} \mathbf{T} & \mathbf{K}' \\ \mathbf{K}' & \mathbf{T} \end{pmatrix} + \begin{pmatrix} V_1^a(R;E) & i\dot{\theta}\cos 2\theta \\ -i\dot{\theta}\cos 2\theta & V_2^a(R;E) \end{pmatrix}. \tag{64}$$

The off-diagonal terms in the kinetic operator, $\mathbf{K}'$, are often referred to as *spatial* nonadiabatic terms, while those in the potential operator are *dynamical* nonadiabatic terms. They depend on the time-derivative in the mixing angle, $\dot{\theta}$, which reflects the time-variation of the field, $\dot{E}(t)$ (Chang et al., 2001c). When the pulses are strong and their time evolution is slow (compared to the motion of the nuclear wave functions) the off-diagonal terms can be neglected. Then, if initially $V_1(R)$ correlates to a single LIP, $V_1^a(R;E(0))$, all the dynamics will occur in this LIP and the final electronic state as well as all the properties of the system during all times will solely depend on $V_1^a(R;E(t))$. In order to characterize the LIP we need to know the structure of the strongly coupled electronic potentials, V_1 and V_2. It is most important to localize the light-induced avoided crossing (LIAC) R_c, defined by the condition

$$\Delta(R_c, t) = V_2(R_c) - V_1(R_c) - \hbar\omega(t) = 0. \tag{65}$$

The populated LIP can be expressed as a function of the original molecular potentials, as

$$V_1^a(R, E) = \cos\theta(R, E)\, V_1(R) + \sin\theta(R, E)\, V_2(R), \tag{66}$$

where the mixing angle θ changes from 0 to $\pi/2$ at both sides of R_c. The LIAC changes the character of the electronic states: $V_1^a(R)$ looks like $V_1(R < R_c)$ before the crossing and $V_2(R > R_c)$ after it. Through the LIAC, the nuclear wave packet can transfer part of the population. It operates in analogous way to a molecular (beyond Born–Oppenheimer-like) internal conversion, induced by **K**. In the adiabatic limit, which requires a large energy gap between the LIPs around the LIAC and slow changes in the pulse envelope $E(t)$, the population in the initial electronic state is given by $\cos^2\theta(R, E)$, while the population in the other coupled electronic state is given by $\sin^2\theta(R, E)$. Therefore, the motion of a nuclear wave packet across R_c in $V_1^a(R, E)$ represents full population transfer from V_1 to V_2.

7.1 Population Transfer

We will now briefly mention some features of population transfer analyzed from the perspective of LIPs. As noticed, one of the most important steps in the design of laser control schemes is to localize the LIAC of the LIP, as this topological point is an indication of possible population inversion. In order to fully transfer the population from V_1 to V_2 one needs to modulate θ via the control field $E(t)$. However, depending on the structure of the LIP and the initial kinetic energy, the nuclear wave function will be able or not to cross the region of the potential that correlates with V_2. In the most simple cases, as e.g., in population transfer from a bound to a dissociating electronic state, a chirped pulse where the pulse frequency $\omega(t)$ sweeps through the Franck–Condon region is often enough to allow the mixing angle $\theta(R, E)$ to change from 0 to $\pi/2$ for all values of R where the wave packet is located. In other cases, one needs to find a more difficult adiabatic path that connects V_1 to V_2 via the LIP, requiring a more elaborate trajectory of $\theta(R, E)$. Typically, when the equilibrium geometries of V_1 and V_2 are very separated and the energy gap between the LIPs at the LIAC is large, one needs to find additional electronic states that allow to modulate the LIP from V_1 to V_2 adiabatically. Garraway and Suominen (1998) proposed the first scheme of adiabatic passage by light-induced potentials or APLIP.

In APLIP, the AP is possible by using two control pulses: $E_1(t)$ that couples V_1 to an intermediate electronic state V_b, and $E_2(t)$ that couples

V_b to V_2. For instance, consider that we want to invert the population in Na_2 from the ground $X^1\Sigma_g^+$ state (V_1) to a second excited $2^1\Pi_g$ state (V_2), using a resonant two-photon transition through the intermediate $A^1\Sigma_u^+$ state (V_b), whose equilibrium geometry lies in between that of the initial and the final state (although this is not an essential requirement for the intermediate state, it typically reduces the pulse intensities needed for the APLIP scheme). Garraway and Suominen (1998) showed that a counterintuitive pulse sequence with $E_S(t)$ preceding $E_p(t)$ could lead to full population inversion without populating the intermediate state at all. This is possible because such pulse sequence prepares a LIP, $V_d^a(R,t) = \cos\theta V_1(R) - \sin\theta V_2(R)$, that has no contribution from V_b. If the population transfer is fully adiabatic, there is no internal barrier in the adiabatic pathway at the bottom of the LIP connecting the initial equilibrium geometry corresponding to V_1 to the final equilibrium geometry corresponding to V_2, as shown in the LIP of Fig. 21.

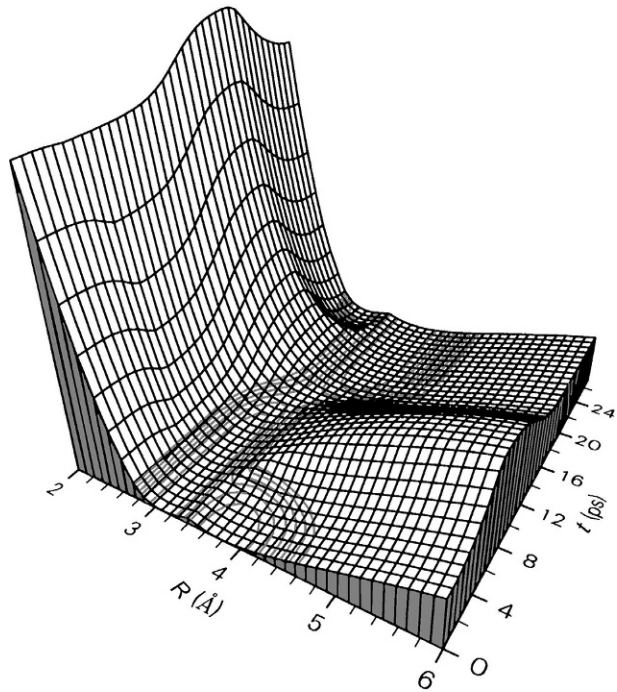

Fig. 21 Light-induced potential responsible for the APLIP process. *Adapted from Garraway, B.M., Suominen, K.A., 1998. Adiabatic passage by light-induced potentials in molecules. Phys. Rev. Lett. 80 (5), 932–935. https://doi.org/10.1103/PhysRevLett.80.932 with permission.*

Under these circumstances the transfer preserves the form of the nuclear wave function. In particular, the dynamics conserves the vibrational quanta. The dynamics in APLIP holds several similarities with that of STIRAP but using stronger fields. The advantage of APLIP is its universality and "apparent" robustness (or robustness under ideal conditions).

The application of STIRAP to molecular system poses problems derived from the need to privilege a single dressed state from the multiply allowed couplings between the vibrational states of V_1 and V_b and those of V_b and V_2. One needs to find a proper "bridge vibrational state," $\phi_\nu^{(B)}$, with strong and relatively similar couplings with the initial $\phi_0^{(1)}$ and target $\phi_t^{(2)}$ vibrational states. Depending on the geometry of the potentials, this may pose a problem. Malinovsky et al. (2003) illustrated this point comparing how STIRAP and APLIP perform for selecting the ground vibrational state of two different final electronic states in Na_2, the B $^1\Pi_g$ state (in short V_B) and the C $^1\Sigma_g$ state (V_C), from the initial state X $^1\Sigma_g$ (V_X) and through an intermediate A $^1\Sigma_u$ potential, V_A, that allows the two-photon process. We call these the XAB and XAC systems, as depicted in Fig. 22. In the XAB system, the equilibrium bond distance is more relaxed in V_B than in V_A, so one can find a good bridge state ($\nu = 10$) with comparatively large Franck–Condon factors

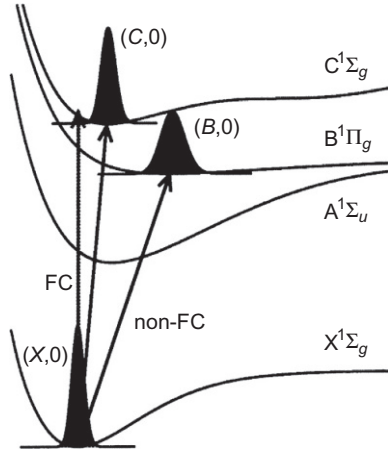

Fig. 22 Na_2 potentials considered for population transfer from the initial to two possible target wave functions, defining the so-called XAB and XAC systems. *Adapted from Malinovsky, V.S., Santamaria, J., Sola, I.R., 2003. Controlling nonfranckcondon transitions: counterintuitive schemes of population transfer in the adiabatic and strong adiabatic regimes. J. Phys. Chem. A 107 (40), 8259–8270. ISSN 1089-5639. https://doi.org/10.1021/jp0226477 with permission.*

(FCC) for both vibrationally selective electronic transitions, $\phi_0^{(X)} \rightarrow \phi_{10}^{(A)}$ and $\phi_{10}^{(A)} \rightarrow \phi_0^{(B)}$.

On the other hand, because V_C is similar to V_A while the equilibrium geometry of V_A is displaced to larger bond distances than in V_X, the FCC from $\phi_0^{(X)}$ favor large v for the bridge state, while the FCC from $\phi_0^{(C)}$ favor small $v \approx 0$ for the bridge state. The best compromise is to choose $v = 2$, with comparatively small FCC for both transitions. Worse, the FCC with adjacent vibrational levels (with smaller v for the first electronic transition, and larger v for the second) are larger and typically have different *signs*. This induces destructive interference of possible parallel adiabatic transitions through different bridge states (Sola and Malinovsky, 2003), so that STIRAP is only possible with very long (and hence weaker) pulses, as Fig. 23 shows.

In contrast, working in nonresonant conditions, APLIP constructively uses all possible adiabatic routes linking all bridge states (Sola and Malinovsky, 2003) so that the adiabatic passage is possible for any intermediate and final electronic state, as shown in Fig. 23. As the wave packet moves from V_X to V_B or V_C the system uses the most convenient set of bridge states, so in the vibrational basis one first observes Raman Stokes transitions in V_1 and anti-Stokes Raman transitions in V_2 before the target vibrational state is selected. In addition, the target state is chosen even in nonresonant two-photon conditions, by adiabatic following, as shown in Fig. 24.

One problem of APLIP is the need of very strong laser pulses, such that the RWA assumptions breakdown. Both nonresonant adiabatic passage routes, $V_1 \rightarrow^{\omega_1} V_b \rightarrow^{\omega_2} V_2$ implying blue-shift from the A band and $V_1 \rightarrow^{\omega_2} V_b \rightarrow^{\omega_1} V_2$ implying red-shift from the A band, contribute to the passage, but while the first one leads to V_2, the second one implies population return to V_1 (Sola et al., 2000a). Fig. 24 reveals how without the RWA the robustness of the results is weakened.

With different properties, other APLIP pulse sequences allow full adiabatic passage (Malinovsky et al., 2003; Sola et al., 2000a) and the scheme can be extended to multiphoton passage involving an even number of pulses (Suominen, 2014) or can be aided by chirping the pulses (Band and Magnes, 1994; Chang et al., 2000; Kallush and Band, 2000). Shorter pulses with durations of the order of 100 fs can be used as well, at the expense of giving up on the selection of a single vibrational state. However, by starting the dynamics on an optimized wave packet in the ground state, one can

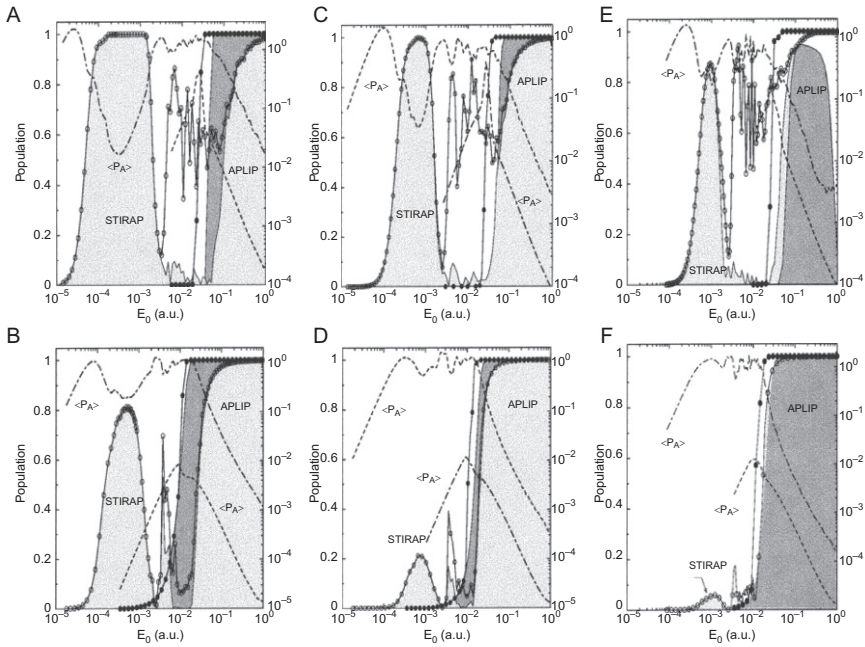

Fig. 23 Efficiency and selectivity of the two-photon transfer as a function of the field amplitude, for different pulse time widths and different target states. The curve with *open circles* represents the population at final time on the target electronic state for the resonant STIRAP transition, the *light gray shaded curve* gives the population on the target vibrational state. The time-averaged population on the intermediate electronic state, $\langle P_A \rangle$, is given by the *dot-dashed curve* in logarithmic scale at the right side of the plot. In the *top row* we show the results for the XAB system, and in the *bottom row* the results for the XAC system. From *left* to *right* the time widths of the pulses change as $\sigma = 6$ (A,B panels), 1.5 (C,D panels), and 0.6 ps (E,F panels). *Adapted from Malinovsky, V.S., Santamaria, J., Sola, I.R., 2003. Controlling nonfranckcondon transitions: counterintuitive schemes of population transfer in the adiabatic and strong adiabatic regimes. J. Phys. Chem. A 107 (40), 8259–8270. ISSN 1089-5639. https://doi.org/10.1021/jp0226477 with permission.*

regain the selectivity and achieve higher yields with weaker pulses (Sampedro et al., 2016b). However, the main problem remains in avoiding other multiphoton transitions to higher excited states and ionization. These problems have not allowed yet the experimental verification of APLIP. To break through, it is important to design simpler APLIP protocols.

Recently, Sampedro et al. (2016a) proposed an APLIP process that can be achieved using a single nonresonant pulse, called the nonresonant electronic transition through light-induced potentials or NETLIP scheme. In this case the electric field must create a different Stark effect on two different parts of the potential energy surface, generating an effective LIP that will

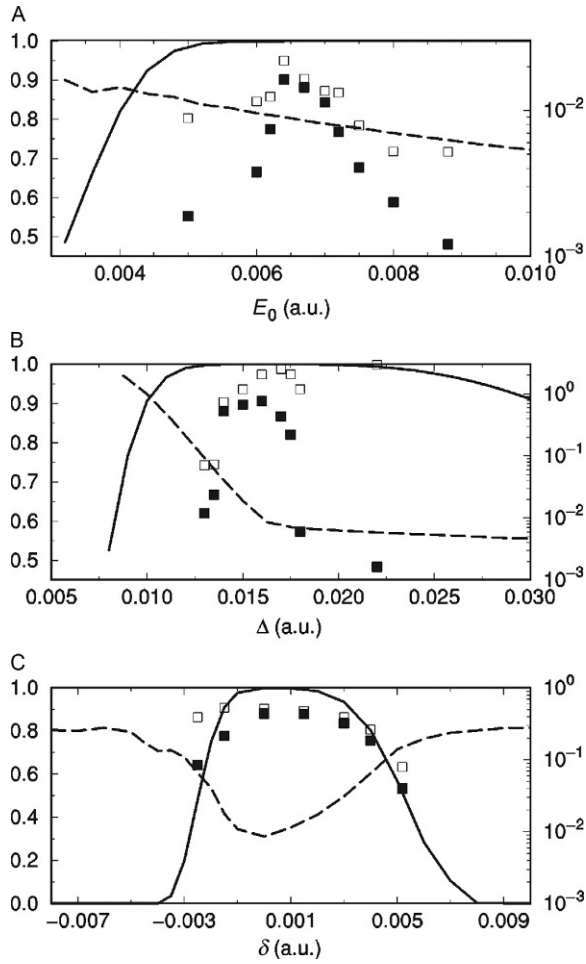

Fig. 24 Final populations in the target electronic state and in its ground vibrational level, as a function of the pulse amplitude E_0 (A), the one-photon detuning $\Delta = V_X(R_0) + \hbar\omega - V_A(R_0$ (B) and the two-photon detuning $\delta = V_C - V_X - \hbar(\omega_1 + \omega_2)$ (C). The *solid line* is the final electronic population in the target electronic state and the *dashed line* the time-averaged population in the intermediate electronic state (scale at the right side), calculated using the RWA. *Empty* and *solid squares* give the final populations in the electronic state and its ground vibrational level, respectively, for a calculation without the RWA. *Adapted from Sola, I.R., Santamaria, J., Malinovsky, V.S., 2000b. Efficiency and robustness of adiabatic passage by light-induced potentials. Phys. Rev. A 61 (4), 043413. https://doi.org/10.1103/PhysRevA.61.043413 with permission.*

allow the system to oscillate between the two coupled states. The necessary asymmetry can also be induced by an antisymmetric transition dipole. However, the transition cannot be adiabatic in the nuclear motion. If the pulse is switched on slowly the wave packet will adiabatically shift from the

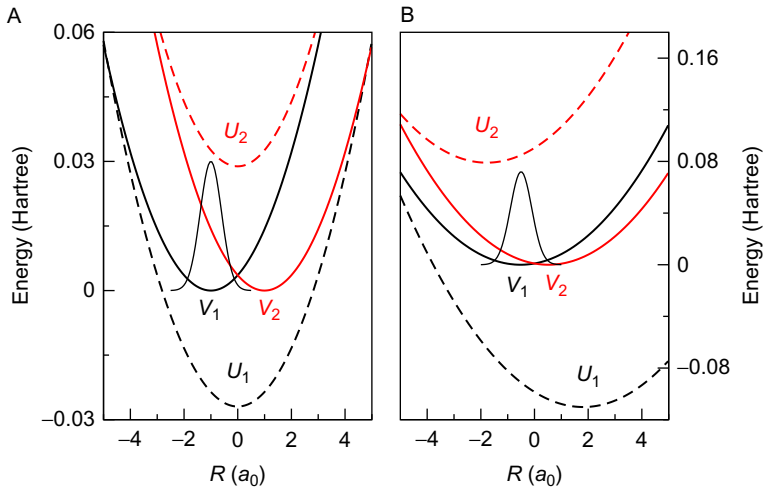

Fig. 25 Electronic potentials and LIPs generated by a strong-field slightly off-resonant from the absorption band. In (A) the equilibrium geometries are more separated than in (B), so that the ground state wave function (shown) overlaps excited state configurations in the latter case. In (B) the LIPs are calculated when the transition dipole depends linearly with R. *Adapted from Sampedro, P., Chang, B.Y., Sola, I.R., 2016a. Nonresonant electronic transitions induced by vibrational motion in light-induced potentials. Phys. Chem. Chem. Phys. 18 (36), 25265–25270. ISSN 1463-9076. https://doi.org/10.1039/C6CP04761K with permission.*

equilibrium geometry of V_1 to that of V_2, only to revert the transition when the pulse is switched off.

Fig. 25 reveals such effect for the simplest system formed by two harmonic oscillators, V_1 and V_2, coupled by a field. In the first case (Fig. 25A) the excited state was chosen exactly as the ground state but shifted to a new equilibrium geometry, $R_1 - R_0 = \delta$, where $\delta = 2a_0$ (approximately the displacement of the equilibrium geometries of the ground and first excited electronic states of Na_2). and the transition dipole was assumed constant. As we are not exciting at the Franck–Condon region, the transition from V_1 to V_2 is hindered by an energy barrier V_b that the nuclear wave packet, initially in V_1, must overcome. For sufficiently strong fields this barrier is absent in the LIPs, U_1 and U_2, so the packet can move from small values of R, correlating with the V_1 state, to large values or R, correlating with V_2.

The NETLIP scheme works as long as the equilibrium geometries of the electronic potentials are separated. On the other hand, if δ is smaller than the characteristic extension of the initial nuclear wave function (that is, the

region where the probability density cannot be neglected), then part of this wave function correlates with U_1 in the adiabatic representation (for $R < 0$), and part of it with U_2 (for $R > 0$). Under a strong field we generate a wave packet in two LIPs with no internal barriers, leading to interference and electronic beatings, but a coordinate-dependent transition dipole can compensate this effect. In Fig. 25B the LIPs for $\delta = 1a_0$ and linear dipole, $\mu = a + bR$ ($a = 3.79$ a.u.; $b = 0.257$ a.u., the parameters chosen to approximate the true dipole in Na_2), are shown. The effect of the dipole is to separate the equilibrium geometries of the LIPs, allowing to prepare the initial wave function in a single LIP. The gradient of the dipole decides the shape of the LIPs. If b is positive, then the interaction energy due to the coupling with the field, bRE, is larger in $V_2(\delta)$ than in $V_1(-\delta)$ and grows with the internuclear distance. Hence the Stark shift is larger in the former and the LIP U_1 will move the packet toward V_2. On the other hand, if the gradient of the dipole has opposite sign, $\mu' = a - bR$, then the interaction energy would be larger in $V_1(-\delta)$ than in $V_2(\delta)$ and the equilibrium geometry of U_1 would sit near V_1. In this case the wave packet remains relatively trapped at the ground electronic state, the trapping increasing with the pulse intensity.

Fig. 26 shows the application of the NETLIP scheme to adiabatic passage of the molecular wave packet from the ground state $X\ ^1\Sigma_g$ to the first excited state $A\ ^1\Sigma_u$ in Na_2 using 689 nm pulses (slightly below the A band peak). The absorption yield is shown as a function of the pulse duration τ (FWHM), for different pulse intensities. The dependence of the yield with τ follows from the vibrational motion of the wave packet in the LIP. The right panels show

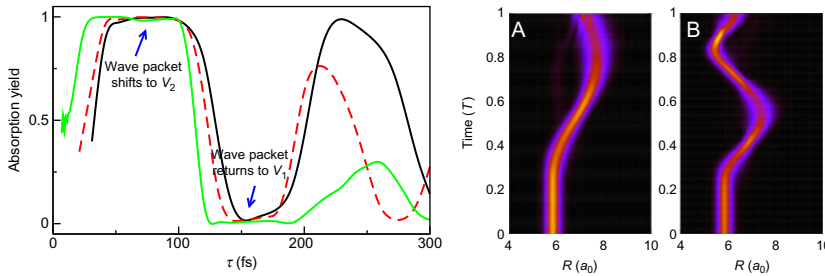

Fig. 26 *Left panel*: Absorption yield for the *A* band of Na_2 using 25 MV/cm (*black*), 50 MV/cm (*red*, *dashed*) and 250 MV/cm (*green*) peak amplitudes. *Right panels*: Wave packet dynamics in Na_2 when the pulse duration leads to population inversion (A) or population return (B). *Adapted from Sampedro, P., Chang, B.Y., Sola, I.R., 2016a. Non-resonant electronic transitions induced by vibrational motion in light-induced potentials. Phys. Chem. Chem. Phys. 18 (36), 25265–25270. ISSN 1463-9076. https://doi.org/10.1039/C6CP04761K with permission.*

the time evolution of the square of the wave packet for two pulse durations: 75 fs (within the maximum absorption band) and 150 fs (within the population return conditions, with no net photon absorption) using a pulse of 0.27 GV/m peak amplitude. In principle, the NETLIP process can be extended to any multiphoton process with *odd* number of pulses and the ionization can be used to monitor the dynamics in the LIP.

The control of population transfer with strong pulses is the doorway of most strategies to control many observables or quantum processes in excited states, as shown in sections 7.2 and 7.3

7.2 Controlling Geometries and Charges

It is well known that intense off-resonant lasers can induce important changes in the geometry of the molecule, which can be most straightforwardly explained in terms of LIPs. By coupling the ground potential V_1 to a dissociative (or loosely bound) excited electronic state V_2 with a strong field, the ground state attains some character of the continuum, exhibiting bond softening, while the continuum attains some character of the bond state, exhibiting bond hardening or vibrational trapping. The molecular geometry is fully characterized by the LIP. Typically, the rearrangement of charges and changes in the geometry are small in the ground state (and even smaller near its equilibrium bond length), and have been characterized using analytical models by Thomas and Henriksen (2016). A large control over the bond distance can only be attained in the excited state, particularly if V_2 is dissociative. The laser adiabatic manipulation of the bond or LAMB process is the laser protocol that must be found to adiabatically transfer the wave function from the ground potential to the desired LIP, while the laser that creates the LIP remains switched on.

A slightly modified APLIP procedure (where the second pulse, $E_2(t)$, must remain switched on at the end of the dynamics) can be used for LAMB (Chang et al., 2003a). Simpler LAMB implementations are possible when V_2 is coupled directly to the initial state and V_b (now called V_3) is used to dress V_2 (Chang et al., 2003b, 2004). Then it is even possible to use a single pulse responsible both for the transfer and the dressing of the final potentials (Chang et al., 2010).

Fig. 27 outlines both two-pulse as well as one-pulse scenarios. In the first case the LAMB process implies the following mechanism: Initially $E_2(t)$ is switched on, with an off-resonant frequency that prepares V_2^a with an LIAC between V_3 and V_2 at the desired bond length. Then, while $E_2(t) = E_0$

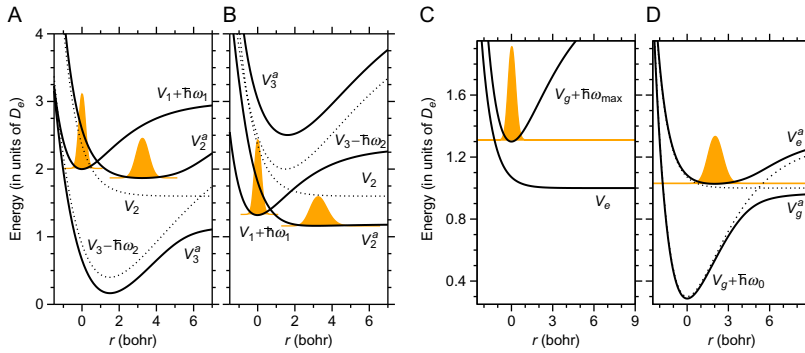

Fig. 27 Different scenarios of the LAMB scheme using one and two pulses. *Dotted lines* are the molecular potentials and *solid lines* are the potentials in the presence of the field (the LIPs plus the uncoupled V_1 potential). In (A) and (B) we show LAMB schemes using a chirped and a transform-limited pulse, blue-shifted or red-shifted with respect to the $V_2 \rightarrow V_3$ transition, respectively. In (C) and (D) the mechanism of LAMB with a single chirped pulse is represented. At initial times the pulse frequency must be blue-shifted from the photodissociation band, while at later times, the red-shifted frequency, after sweeping all the photodissociation band, sets the new "equilibrium" bond distance. *Adapted from Chang, B.Y., Shin, S., Santamaria, J., Sola, I.R., 2011. Laser adiabatic manipulation of the bond length of diatomic molecules with a single chirped pulse. J. Chem. Phys. 134 (14), 144303. https://doi.org/10.1063/1.3574837 with permission.*

remains constant, another pulse, $E_1(t)$, moves all the population from V_1 to V_2, which in the presence of E_0 is V_2^a. This electronic absorption can proceed rapidly, using an ultrashort transform-limited pulse that generates a nuclear wave packet moving in the LIP, as in a Franck–Condon transition (Chang et al., 2013). Or it can be quasi-static, using a chirped pulse, in which we talk of an adiabatic transfer (Chang et al., 2010). In both cases full population inversion requires pulse bandwidths $\Delta\omega_1$, at least as large as the absorption band, Δ_{FC}. In fact, in the quasi-static case, the chirp typically needs to span an even larger bandwidth. Fig. 27A and B shows how the shape of V_2^a is influenced by the choice of ω_2, blue-shifted or red-shifted with respect to the $V_2 \rightarrow V_3$ transition. In the first case there is properly an LIAC and the bond length in V_2^a is better defined. In the second case there is no proper LIAC and the control is mostly done by Stark effect. Then the LIP is much flatter and it is more difficult to achieve adiabatic population transfer.

On the other hand, it is possible to use a single chirped pulse, $E(t)$, responsible for both roles: the adiabatic transfer and the formation of the LIP. The basic mechanism is explained in Fig. 27C and D. At initial times $\omega(0)$ must be blue-shifted from the absorption spectrum to the dissociative

state V_e. Slowly sweeping through the photodissociation band the population is transferred in a quasi-static way, with the wave packet always located at the bottom of the LIP. Then the chirp must sweep through all the emission spectra. The final value of the frequency, ω_0, defines the LIAC and the bond length (Chang et al., 2010).

In comparison with an FCT process a typical LAMB process requires 10–100 more energy (integrated pulse amplitude or peak amplitude times duration) from the pulses. The extra energy is mainly used to deform the potential. This pays off in the fact that the molecular properties associated to the wave packet dynamics are entirely governed by the field parameters. In particular, any *trajectory* in the "chirp function" $\omega(t)$ entails different excursions of the average internuclear distance or bond length (Chang et al., 2017b). Then any time-symmetric function $\omega(t)$ induces fully reversible bond elongations that mimic a single period of a classical molecular vibration, with both the amplitude and frequency of the vibration being externally controlled (Chang et al., 2010, 2011). If $\omega(t)$ is periodic, the inverse of its period will be the "frequency" of this LIP-supported vibration (Sola et al., 2011). Relaxing the adiabaticity of the transfer gives some kinetic energy to the vibrational wave packet, which ends vibrating around the equilibrium distance of the LIP (Chang et al., 2012, 2013). Sometimes some laser protocols can be proposed to "absorb" the kinetic energy excess and stop the packet using asymmetric pulses (Sola, 2004).

Although most LIPs are wider than the ground electronic state (as they add the character of weakly bounded excited potentials) it is possible to create LIPs that lead to molecular squeezing, when at least three electronic states are coupled. Then, a LIP is formed between the attractive barrier of the excited potential and the repulsive barrier of the ground potential (Chang et al., 2005). As Fig. 28A shows, even when the LIP is formed by two wider electronic states (and in the example of Fig. 28 the excited $1\ ^1\Pi_g$ potential of Na_2 is very flat) the resulting LIP, U_s, has a narrower well. By adiabatically moving the wave packet to U_s by a slightly modified APLIP procedure (Chang et al., 2006b) one can achieve ~10% squeezing comparing the width of the packet with that of the ground vibrational state.

Instead of adiabatically squeezing the wave packet in a narrower LIP, one can more easily stretch it on a wider LIP, and then transfer it back to V_1 where it will dynamically squeeze, as shown in Fig. 28B. This is possible using asymmetric pulses, with slowly increasing heads leading to the adiabatic part of the transformation, and sudden trails, that release the packet

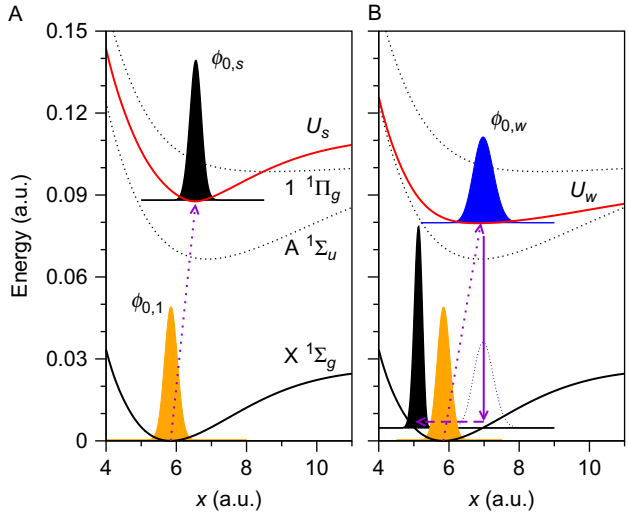

Fig. 28 Sketches of the adiabatic squeezing scheme formed at a narrower LIP, U_s (A) and of the asymmetric adiabatic–diabatic squeezing scheme (B) formed by preparing a wave packet in the wider U_w LIP and suddenly releasing the packet back to the ground state, showing the wave packets calculated by solving the TDSE in Na_2. *Adapted from Chang, B.Y., Lee, S., Sola, I.R., Santamaria, J., 2006b. Squeezing the ground vibrational state of diatomic molecules. J. Photochem. Photobio. A: Chem. 180 (3), 241–247. ISSN 1010-6030. https://doi.org/10.1016/j.jphotochem.2006.02.006. http://www.sciencedirect.com/science/article/pii/S1010603006000463 with permission.*

to its original potential diabatically, without reshaping the packet. Using such a procedure (Chang et al., 2006a,b) nearly ∼40% squeezing can be achieved. The advantage of the adiabatic squeezing is that the packet is frozen while the pulses act, and one has some degree of control over both the position and width of the packet at the desired time.

The main problem in using strong nonresonant pulses is ionization. Short wavelength pulses induce molecular ionization by multiphoton absorption, but the hurdle is not solved using long wavelength pulses because of tunneling ionization (Lewenstein et al., 1994). The external field $\epsilon(t)$ times the dipole breaks the local symmetry of the Coulomb potential V_C, and $V_C \pm qz\epsilon(t)$ (where q is the electron charge and z the coordinate along the field's polarization) induces the motion of the electron along the field. For strong enough fields the electron can ionize both above or below the internal barrier, particularly at large internuclear distances (Seideman et al., 1995). However, in molecules with large ionization potentials

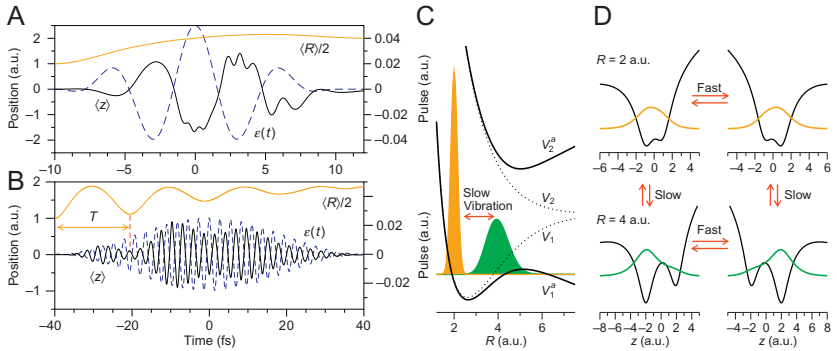

Fig. 29 (A) Average electron position $\langle z \rangle$ and internuclear distance $\langle R \rangle$ using (A) an ultrashort 800 nm pulse and (B) a longer 400 nm pulse. The electron position is anticorrelated with the amplitude of the electric field of the Gaussian pulse, shown in the *dashed line* (*right side*). The additional slower modulation in $\langle z \rangle$ is due to the vibrational motion. *Right panel*: Sketch of the mechanism for the creation of the dipole using a strong nonresonant pulse starting in the ground state. In (C) we show the LIPs. The vibrational motion of the nuclear wave packet in the ground LIP is mostly constrained. In (D) we show snapshots of the electronic wave function, periodically oscillating with the field. At short internuclear distances the wave function lies in between both protons, while at larger internuclear distances it is mainly localized in one proton, leading to a small modulation of the dipole amplitude with the vibrational motion.

(or, e.g., molecular cations) one can still use strong fields to guide the charges avoiding tunneling ionization. As Fig. 29 shows for a model of the Hydrogen molecular cation H_2^+ using soft-core Coulomb potentials (Chang et al., 2015a), the electron follows the field ($\langle z(t) \rangle$ is anticorrelated with the pulse amplitude) generating an oscillating dipole (a molecular antenna) as it shifts from one proton to the other. The effect of the vibrational motion of the molecule is a small modulation on the amplitude of the dipole. When the molecule is stretched the amplitude of the electron's motion is wider. Since the (slow) nuclear motion is constrained in the ground LIP the charge is barely displaced.

In order to create large dipoles, it is first necessary to move the wave packet to the excited LIP, where the bond is quite stretched, and in addition, it is necessary to correlate the electronic and nuclear motions. In a LAMB process, the total wave function of the system is a coherent superposition of both nuclear and electronic wave functions (Chang et al., 2010),

$$\Psi(R,q,t) = \phi_g(R,t)\Xi_g(q;R) + \phi_e(R,t)\Xi_e(q;R). \tag{67}$$

However, in adiabatic conditions, the nuclear wave packet in V_g and V_e have the same shape, $\phi_g(R,t) \propto \phi_e(R,t) \propto \phi^a(R,t)$, so one can write

$$\Psi(R,q,t) = \phi^a(R,t)\left[a_g(t)\Xi_g(q;R) + a_e(t)\Xi_e(q;R)\right] = \phi^a(R,t)\,\Xi^a(q,t;R), \quad (68)$$

where $\Xi^a(q, t; R)$ is the dressed electronic wave function (from which one calculates the LIP). The total wave function is thus separable and not an entangled state of nuclear and electronic states. Since the total wave function in the LIP is a single Born–Oppenheimer product, there is perfect correlation between the electronic and nuclear motion. Notice that the changes of the electronic wave function are externally controlled: they do not rely on dynamical phases as in superpositions of different electronic states. Adiabaticity is required for the single product wave function to faithfully represent the dynamics, so the changes in the LIP must be slower than the typical timescale of the nuclear dynamics. The perfect correlation of electronic and nuclear motion in the LIP is only possible when the electron dynamics occurs in the timescale of the nuclear dynamics.

Fig. 30 shows the results of the dynamics using DC fields (i.e., in the limit of zero frequency). The LIPs are in this case more properly named FIPs, from field-induced potentials. Now the electron motion is clearly correlated to the nuclear motion in the excited FIP, which shows bond hardening. In the excited state, the electron moves with the proton against the gradient of the field. The transient dipole increases with distance and it is possible to stabilize the molecule at very large bond lengths, up to ~40 a.u., creating huge molecular dipoles that oscillate in the far infrared, from 3 to 40 THz approximately.

It is possible to use low frequency laser pulses instead of constant fields, but then the pulses must meet very specific conditions (Chang et al., 2015a). In particular, the frequency must be approximately equal to the frequency of the vibrational motion in the LIP. Otherwise, the correlation between the motion of the electron driven by the field, and that of the protons, oscillating in the potential, is not perfect. The electron must move with one proton as the bond stretches, and hop to the other proton as the bond compresses and the phase of the field changes. It is crucial that the bond is maximally compressed when the amplitude of the oscillating electric field is zero as otherwise the electron cannot hop from one proton to the other, leading to dissociation (Chang et al., 2015a).

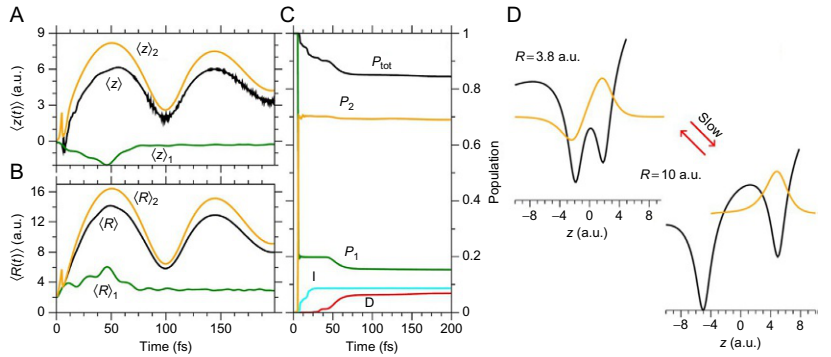

Fig. 30 (A) Average electron position and (B) average internuclear distance as functions of time. (C) Probability as a function of time for dissociation (D), ionization (I), and the population remaining in the U_1 and U_2 FIPs, P_1, and P_2, respectively. (D) Mechanism of the electron–nuclear correlation. Initially, the electron is mainly localized on the right atomic well. As the protons separate, as long as the energy of the wave function is below the ionization barrier, the electron remains with the right proton and moves in the timescale of the vibrational motion. *Adapted from Chang, B.Y., Shin, S., Palacios, A., Martín, F., Sola, I.R., 2013. Ultrafast coherent control of giant oscillating molecular dipoles in the presence of static electric fields. J. Chem. Phys. 139 (8), 084306. https://doi.org/10.1063/1.4818878 with permission.*

7.3 Control of Photophysical and Photochemical Processes

The LIPs are excited potential energy surfaces externally manipulated, offering ample possibilities to control chemical reactions that follow different energy landscapes. Recently, several experiments using strong nonresonant fields have revitalized the field of quantum control (Corrales et al., 2014, 2017; Kim et al., 2012; Sussman et al., 2006). However, the excited state dynamics of polyatomic molecules is dominated by nonadiabatic crossings and intramolecular couplings, with no dipole-allowed transitions, that open many deactivation pathways by internal conversion or intersystem crossing. There is empirical evidence that even in this scenario, the strong pulses are able to optimally drive the dynamics to the desired target or doorways states. Therefore, it is of great interest to design schemes from first principles that can be used to manipulate and control the nonadiabatic transitions and which may allow to interpret current experiments or implement new control strategies of chemical reactions on LIPs.

Focusing again in the effective Hamiltonian of Eq. (63), we consider the case where V_1 and V_2 are close enough in energy (at least for certain geometries that the wave function visits) that the nonadiabatic coupling $\mathbf{K}$ induces

unwanted transitions. Our goal is to use an external field to decouples such transition. González-Vázquez and coworkers developed a scheme that allows the control over the spin–orbit transition (Gonzalez-Vazquez et al., 2006b,c, 2007; Sola et al., 2006). They first considered the case where V_1 is a singlet state (typically the first excited one), S_1, and V_2 a nearby triplet state, T_1, and $\mathbf{K} = V_{SO}$ is strong enough that the singlet–triplet transition is on the timescale of the vibrational motion, as in Rb_2.

Fig. 31 shows the potential energy curves around the first excited singlet and lowest triplet in Rb_2, calculated in the diabatic representation, not including the singlet–triplet coupling V_{SO}. S_1 crosses with T_1 and the

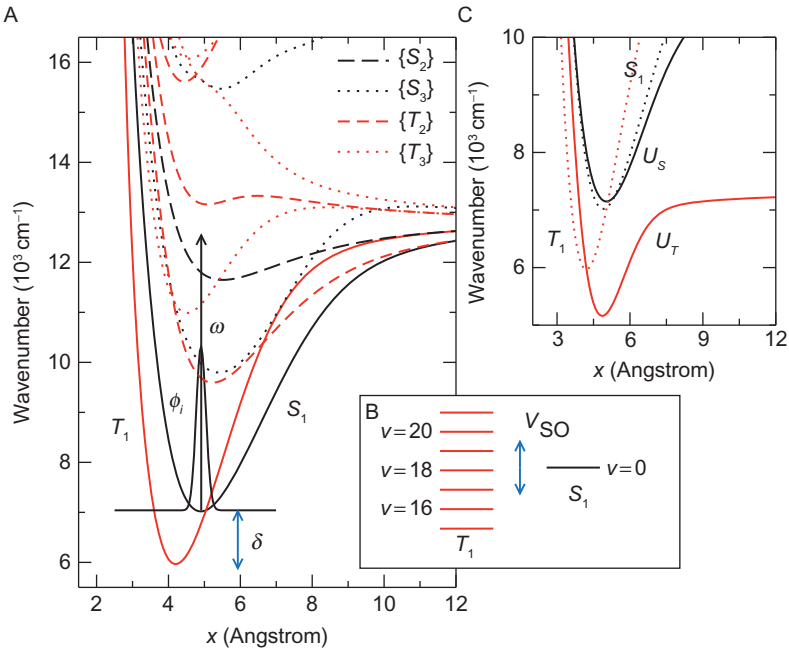

Fig. 31 (A) Singlet and triplet potential energy curves in Rb_2 close to the first excited singlet and triplet potentials, S_1 and T_1. S_2 and T_2 are the potentials directly coupled to S_1 and T_1 respectively, while S_3 and T_3 are those potentials that can only be coupled by multiphoton transitions. (B) Detailed view showing the vibrational energy structure in S_1 and T_1 around the crossing. The coupling, V_{SO}, is large enough to involve several vibrational levels in T_1. (C) Effect of a strong 1.7 TW/cm^2, 5500 cm^{-1} nonresonant field on the potentials, generating the U_S and U_T LIPs that do not cross. *Adapted from Gonzalez-Vazquez, J., Sola, I.R., Santamaria, J., Malinovsky, V.S., 2006c. Quantum control of spin-orbit coupling by dynamic Starkshifts induced by laser fields. Chem. Phys. Lett. 431 (4), 231–235. ISSN 0009-2614. https://doi.org/10.1016/j.cplett.2006.09.085. http://www.sciencedirect.com/science/article/pii/S0009261406014473 with permission.*

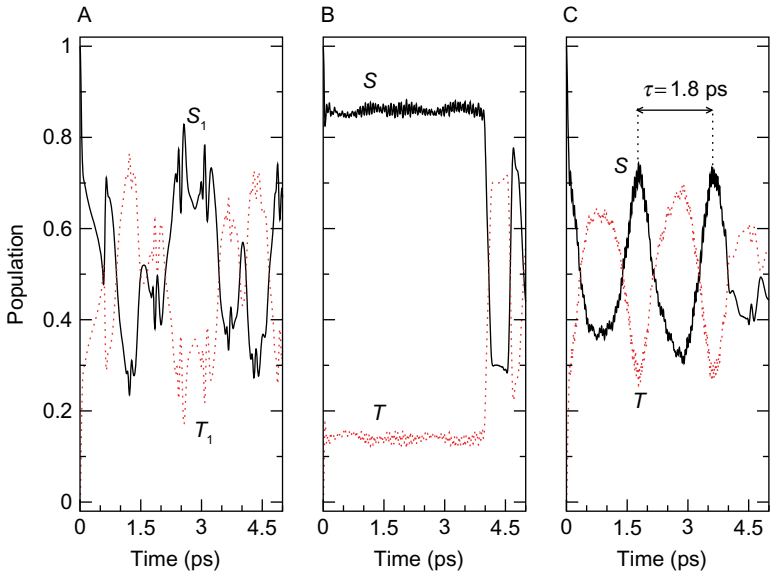

Fig. 32 (A) Laser-free singlet–triplet dynamics starting in the ground vibrational state of S_1. (B) Dynamics under a 5500 cm^{-1}1.7 TW/cm^2 laser, turned off at 4 ps. The singlet–triplet transition is effectively decoupled. (C) Dynamics under the same laser with wavelength 6150 cm^{-1}. A spin switch between the singlet and triplet is prepared by the laser. *Adapted from Gonzalez-Vazquez, J., Sola, I.R., Santamaria, J., Malinovsky, V.S., 2006c. Quantum control of spin-orbit coupling by dynamic Starkshifts induced by laser fields. Chem. Phys. Lett. 431 (4), 231–235. ISSN 0009-2614. https://doi.org/10.1016/j.cplett.2006.09.085. http://www.sciencedirect.com/science/article/pii/S0009261406014473 with permission.*

coupling is strong enough that involves several vibrational levels. The dynamics in the absence of any control field, shown in Fig. 32A involves spin switching between the singlet and triplet states. Can one stop such transition and remain in pure spin states, such as S_1? Because singlet–triplet transitions are dipole forbidden, the control can only be exerted indirectly, through the Stark shifts. Hence we are in a situation where Eq. (63) simplifies to

$$\mathbf{H} = \begin{pmatrix} \mathbf{T} + V_{S_1} - \frac{1}{4}\alpha_S(R)E^2(t) & V_{SO} \\ V_{SO} & \mathbf{T} + V_{T_1} - \frac{1}{4}\alpha_T(R)E^2(t) \end{pmatrix}, \tag{69}$$

where α_S and α_T are the polarizabilities of the singlet and triplet states, respectively. When they differ, the energy difference between the dressed

potentials at a certain R (where the packet is located), can be controlled by the field

$$\delta(E) = \delta(0) + \frac{1}{4}(\alpha_S - \alpha_T)E^2. \tag{70}$$

Making $\delta(E) > V_{SO}$ one can effectively decouple the transition. The dynamical polarizabilities are usually different because the structure of the singlets and triplets is not symmetric. In particular, in most closed-shell molecules there is always a ground singlet below S_1 and no triplet below T_1 so that the Stark effects will never be the same, even if the frequency of the pulse is not fine-tuned (and we can even used the static polarizabilities). Following the previous nomenclature this is a case of soft-shaping of the LIPs. Fig. 31C shows the resulting LIPs using an infrared pulse of 5500 cm^{-1} wave numbers and 1.7 TW/cm^2 intensity. While the pulse is on, the populations (and spin state) remain locked, as shown in Fig. 32B. The results depend on the choice of frequency and are sensitive to the model employed to calculate the spin–orbit coupling (Gonzalez-Vazquez et al., 2006b). Even more interestingly, one can use Eq. (70) to remove a detuning when the potentials are separated, inducing a vibrational-state selective spin switch (Gonzalez-Vazquez et al., 2007; Sola et al., 2006). Or, as shown in Fig. 32C the field can be used to smooth out the nonadiabatic transitions between the potentials. The main problem remains to avoid the ionization. It turns out that the control is most effective when the spin–orbit coupling is weak (Falge et al., 2012b, 2014).

A similar strategy can be used to control other photophysical processes, as internal conversion. Gonzalez-Vazquez et al. (2009) studied a one-dimensional model of 1,1-difluoroethylene, $H_2C{=}CF_2$. In the ground state (the N state) the equilibrium geometry is planar and the double bond hinders the molecular torsion τ, so the potential energy surface has a high internal barrier. However, in the first electronic state (the V state) the double bond has antibonding character, so the torsion is allowed and the most stable form has the two Hydrogens perpendicular to the $C{=}CF_2$ plane. Hence, under torsion in the excited state the N and V states are degenerate, allowing the fast de-excitation from V by internal conversion. In a one-dimensional model, beyond the Born–Oppenheimer approximation, the effect of the nuclear momentum in the torsional mode lifts the energies generating the avoided crossing (AC), but as a wave packet in V originally at the Franck–Condon region (the planar geometry, $\tau = 0$) moves to the perpendicular configuration some population decays to the ground state, as shown in Fig. 33.

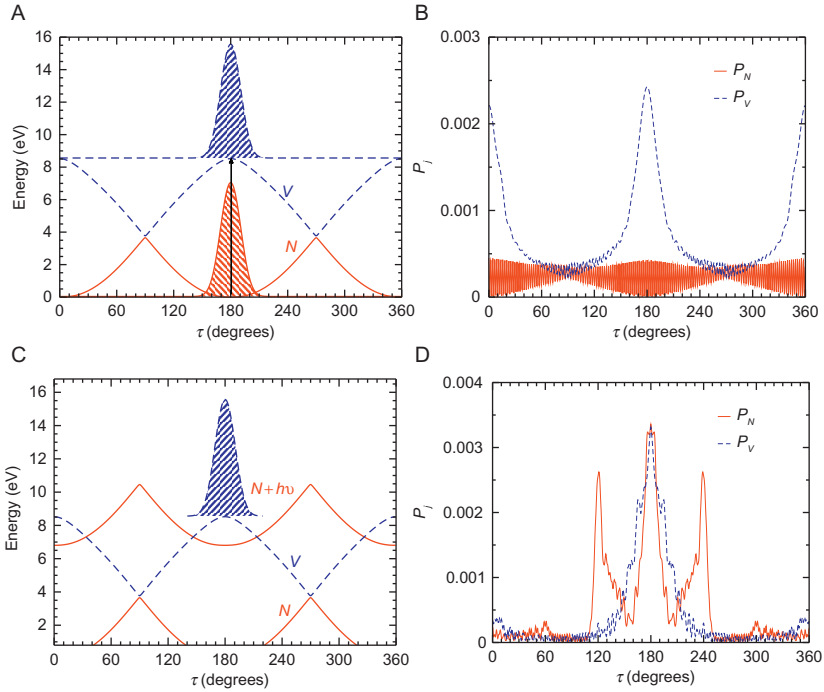

Fig. 33 Schematic representation of the control strategies (*left column*) and time-averaged population densities (*right column*) in the potentials *N* (*solid*) and *V* (*dashed*) for laser-free (*upper row*) and decoupling conditions (*lower row*). P_N (*solid*) and P_V (*dashed*) are the time-averaged populations in the *N* and *V* states. In (A) and (B) the wave packet in *N* is excited to *V* with a delta pulse which then evolves under field-free conditions. In (C) and (D) a decoupling mechanism operates by trapping the wave packet in *V* at the FC window, which then evolves on a small segment of available angles. *Adapted from Gonzalez-Vazquez, J., González, L., Sola, I.R., Santamaria, J., 2009. Laser control of conical intersections: quantum model simulations for the averaged loss-gain strategies of fast electronic deactivation in 1,1-difluoroethylene. J. Chem. Phys. 131 (10), 104302. https://doi.org/10.1063/1.3223998 with permission.*

Considering all nuclear degrees of freedom there is no single degeneracy point in the full-dimensional potential energy surface, but a funnel (a surface in the $N-1$ dimensions) that remains when we include the effect of the nuclear momentum. These are quite generic effects in complex molecules.

An interesting difference with respect to other nonadiabatic couplings (like the spin–orbit) is that the transition between the two electronic states can be dipole allowed, except at the geometry of the AC. This opens new strategies to control the population transfer by hard shaping of the LIPs, instead of soft-shaping. In particular, by using a slightly off-resonant

laser at the Franck–Condon region one can create an excited LIP that presents a strong LIAC that hinders the torsional relaxation. As the wave packet cannot move to the AC, even in the excited state (or rather the coherent superposition formed by the N and V configurations) the molecule remains in the planar geometry, effectively decoupling the internal conversion.

Interestingly, taking into account the vectorial properties of the laser (the orientation with respect to the molecular's dipole) an LIAC has the properties of a light-induced conical intersection or LICI, that is, the coupling is zero for some orientations. Therefore, even in the presence of a strong field all control mechanisms based on hard shaping have some deactivation processes unless the molecules are first aligned with the laser polarization. There has been great interest recently in characterizing the properties of LICIs (Csehi et al., 2017; Demekhin and Cederbaum, 2013; Halász et al., 2012a,b, 2013a,b, 2014, 2015; Moiseyev et al., 2008; Sindelka et al., 2011), in particular, if it presents a true geometrical phase, as a CI. Other mechanisms to control the wave packet motion around conical intersections have been proposed, some based on interference processes involving vibronic states (Sukharev and Seideman, 2004) or using optimal control theory (Abe et al., 2005; Geppert and de Vivie-Riedle, 2005). The opposite goal of using strong lasers to accelerate the internal conversion, acting on the wave packet's momentum, was also developed (Gonzalez-Vazquez et al., 2009; Tamura et al., 2006), so full control over internal conversion is in principle possible, paving the way to the control of isomerization reactions mediated through conical intersections or LICIs. Bucksbaum and coworkers (Kim et al., 2012) recently reported the first experimental evidence in the control of the photoisomerization of 1,3-cyclohexadiene by creating LICIs that manipulate the ring opening of the molecule.

Strong nonresonant fields can also be used to control photodissociation reactions using the nonresonant dynamic stark effect (NRDSE) scheme of Sussman et al. (2006). The apparent universality of the scheme prompted a resurgence of experiments controlling chemical reactions. The nonresonant field can be used to control (i) the photodissociation spectra, (ii) the lifetime of the transition state, (iii) the yield of competing reaction products, and (iv) the kinetic energy distribution of the fragments (KED) or the photofragment angular distributions (PAD).

The control of the photodissociation spectra is a direct consequence of the Stark effect and can be achieved by soft-shaping. Assuming that the control nonresonant pulse $E_c(t)$ is much more intense than the pump pulse

$E_p(t)$, the resonance at the Franck–Condon region, $D_{j0} = V_j(R_0) - V_0(R_0)$, is modified as

$$D^p_{j0}(E_c) = V^a_j(R_0) - V^a_0(R_0) \approx D_{j0} - \frac{1}{4}\left(\alpha_{jj} - \alpha_{00}\right)E_c^2, \tag{71}$$

where α_{jj} are the dynamic polarizabilities. The position of the photodissociation bands corresponding to different electronic channels can therefore be controlled. The control is most effective when the polarizabilities α_{jj} have different signs for different electronic states, such that E_c can both blue-shift and red-shift the different bands of the spectra.

The landscape of the photodissociative LIP $V^a_j(R)$ can be different than that of the laser-free molecule, changing the transients of the transition state. This is particularly the case when the LIP shows some hard shaping for the presence of nearby electronic channels, for instance when there is some predissociative (metastable) state V_i that only decays through the crossing with a dissociative state, V_d. By Stark shifting the potentials, the position of the crossing can be moved away from the Franck–Condon geometry, manipulating the lifetime of the species and the rate of the photodissociation reaction.

Since the LIPs imply superposition states of mixed electronic character, the control via NRDSE effectively changes the relative yields of the products. If $E_c(t)$ couples two dissociative potentials that lead to asymptotically different product channels, P_1 and P_2, the relative yield is approximately given by

$$\chi = \frac{P_2}{P_1} \sim \left(\frac{\mu_{12}E_c}{2\Delta}\right)^2, \tag{72}$$

where μ_{12} is the dipole coupling between the channels and Δ their energy gap, $V_2(\infty) - V_1(\infty) - \hbar\omega_c$. One of the exit channels can be the ground state, above dissociation energies. However, if $E_c(t)$ is switched off slowly or the dipole $\mu_{12}(R)$ decays slowly through the reaction coordinate, as the wave packet propagates through V^a_1 (or V^a_2) it will adiabatically revert to V_1 (or V_2). In order to control the yield one must abruptly switch off the pulse using an asymmetric pulses or a short pulse, playing with the pulse sequence.

We consider two cases: A PC sequence, when the control pulse is delayed with respect to the pump pulse, and a CP sequence, when the control pulse arrives earlier, such that the pump pulse overlaps the trail of $E_c(t)$. In the CP sequence the Franck–Condon excitation proceeds between V_0 and the

spectrally chosen (by ω_p) excited molecular state V_e ($e = 1, 2$) but the dissociation occurs in the asymptotic region of the molecular potential, leading to selective dissociation. If the chosen potential V_e^a is, e.g., V_2^a, then one collects all the fragments in the molecular state that correlates with that potential, that is, V_2,

$$\psi_0(R,t) \xrightarrow{E_c} \psi_2^a(R,t) \xrightarrow{E_p} \psi_2(R,t), \tag{73}$$

where ψ_j^a is the wave function initially in state j of mixed electronic character by virtue of the control pulse.

Conversely, in the PC sequence the Franck–Condon excitation occurs mainly in the excited molecular state e, selected by ω_p, but the dissociation occurs in the asymptotic region of V_j^a, leading to mixed dissociation. For instance, if we initially excite V_1,

$$\psi_0(R,t) \xrightarrow{E_p} \psi_1(R,t) \xrightarrow{E_c} \psi_1^a(R,t) \propto \sqrt{\chi(E_c)}\psi_1(R,t) + \psi_2(R,t), \tag{74}$$

where χ is roughly given by Eq. (72).

The timing of the control pulse with respect to the pump pulse affects the yield of the photodissociation reaction, but also the kinetic energies of the fragments. The situation is even more interesting when the LIPs have LIACs that allow to invert the electronic populations to have full control over the branching ratios.

Fig. 34 shows a sketch of the control mechanism over the yield of the products and the kinetic energy distribution of the fragments in the photodissociation of the A band of CH_3I, that can yield two channels, $I^*(^2P_{1/2})$, the adiabatic channel, and $I(^2P_{3/2})$, that can be reach through a CI at R_c. In the absence of the control pulse most population ends asymptotically in the adiabatic channel. However, the creation of a LIP and the manipulation of its LICI (its position depending on the frequency of ω_c) can be used to control the yield and kinetic energy of its fragments. For instance, choosing a particular time delay of 60 fs between the pump and control pulses, the fastest momentum components of the wave packet reach R_c before the control pulse acts, to naturally yield $I^*(^2P_{1/2})$. In contrast, the slowest momentum components cross R_c when the control pulse is at its maximum intensity, so they follow the LIP V_g^a, dissociating in V_g and therefore yielding ground state $I(^2P_{3/2})$. Under these conditions, the pulse sequence acts as a momentum filter that discriminates the velocity components of the dissociating wave packet on the different reaction channels.

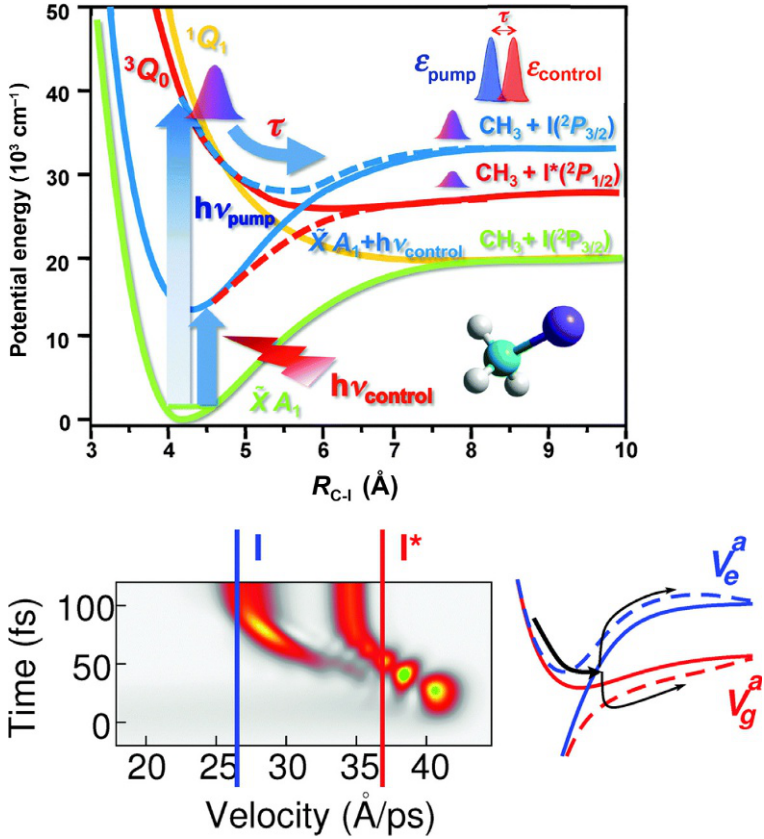

Fig. 34 (*Upper panel*) Potential energy curves of the relevant electronic states involved in the photodissociation of CH_3I in the *A*-band along the R_{CI} coordinate: the $^3Q_0$ (*red line*) and the $^1Q_1$ (*yellow line*). A pump pulse at 268 nm was used to prepare a wave packet in the $^3Q_0$ state and an intense ultrashort 804 nm control pulse was time delayed (τ) with respect to the pump pulse, to create the LIPs (*dashed lines*) and manipulate the LICI, shown at the intersection between the *red* and *blue lines*. (*Lower panel*) Calculations showing the relative velocity distribution of the fragments at different times, to control the KED using a strong (85 TW/cm^2) and short (50 fs) control pulse, 60 fs time delayed with respect to the pump pulse. The *arrows* sketch the main contributing processes along with the shifts in the velocities that lead to the observed broadening and shifting of the asymptotic distributions. *Adapted from Sola, I.R., Gonzalez-Vazquez, J., de Nalda, R., Bañares, L., 2015. Strong field laser control of photochemistry. Phys. Chem. Chem. Phys. 17 (20), 13183–13200. ISSN 1463-9076. https://doi.org/10.1039/C5CP00627A with permission.*

The energy distribution filtering (narrowing of the KED) is not the sole effect of the application of these short control pulses. From the velocity distribution of Fig. 34 (lower panel) it is clear that there is a significant red-shift of the KED in the main dissociation channel. This is a typical signature of

nonadiabatic effects. Indeed, as the crossing is created, there is an abrupt ramp up from a low to a high control field intensity, and thus the wave packet initially evolving on V_e is mainly transferred to V_g^a. Since the shape of V_g^a after the LICI is attractive, the momentum of the dissociating packet becomes smaller as it evolves, causing the red-shift of the KED. Similarly, the transient evolution of the photofragment angular distributions (PAD) shows how the NRDSE can also change the stereodynamics of the reaction in subtle ways (Corrales et al., 2017). A more direct control over the velocities can be effected by using the dipole force (Niikura et al., 2004).

8. TOWARD AUTOMATION: QUANTUM OPTIMAL CONTROL THEORY

The ultimate tool that distinguishes quantum control from the study of the quantum dynamics of the system is the development of optimization techniques from the theoretical side, and closed loops of pulse shaping experiments and learning algorithms, from the laboratory side. Tannor and Rice (1985) proposed the first variational formulation of the control of a chemical reaction following the maximization of its related Spectroscopic signal using time-dependent perturbation theory, while Peirce et al. (1988) and later Kosloff et al. (1989) realized that the problem could be expressed using the cost functionals of Optimal Control Theory. Soon the technique was fully developed and applied to many different systems and physical objectives, including all type of reactions. For an overview of applications the interested reader should inspect some books and reviews on Quantum Optimal Control Theory (Balint-Kurti et al., 2008; Brif et al., 2012; Brixner and Gerber, 2003; Brumer and Shapiro, 1992; Gordon and Rice, 1997; Goswami, 2003; Ho et al., 2014; Nuernberger et al., 2007; Rabitz et al., 2000; Rice and Zhao, 2000; Shapiro and Brumer, 2003). In this section we will explain the theoretical basis of Quantum Optimal Control Theory and develop some of the main ideas, barely mentioning the applications.

8.1 The Quantum Control Problem

As in Sections 6 and 7, our starting model will consist of a quantum system (e.g., a molecule), with Hamiltonian H_0, aligned with a laser pulse $\epsilon(t)$, thus disregarding the vectorial nature of the coupling. More importantly, we do not consider dissipation effects, allowing then to tackle the problem using the TDSE.

Essentially, the quantum control problem can be framed as follows: We know the initial wave function $\psi(0) \equiv \psi_i$ and we want to drive the system toward state ψ_f at time $t = T$; so we must find the function $\epsilon(t)$ that brings ψ_i as close as possible to ψ_f. This is an inversion problem and hence it is computationally more costly than a dynamical problem (solving the TDSE). It can be formulated as an optimization problem.

Theoretically, there are three big questions related to the control problem

1. If it exists a field $\epsilon(t)$ that brings ψ_i exactly (or as close as we want) to ψ_f. In control terminology this is called the *Controllability* problem (Ramakrishna et al., 1995).
2. How to find an "acceptable" $\epsilon(t)$. This is normally achieved designing a cost functional of the field from which one obtains the optimal field $\epsilon_{oc}(t)$ imposing extremalization conditions. The cost functional that we are mostly interested in is the transition probability

$$P_{if} = |\langle \psi_f | \mathbf{U}(T, 0; \epsilon_{oc}) | \psi_i \rangle|^2$$

   (where $\mathbf{U}$ is the time-evolution operator) that we want to maximize. This problem is called the *Quantum Optimal Control* problem and the algorithms necessary to solve the problem are called optimal control algorithms.
3. What are the properties of the space of all possible solutions, that is, how many different solutions are and how sensitive the probability P_{if} is to changes in the optimal fields $\epsilon_{oc}(t)$. Determining the most important field parameters and the mechanism of the control, etc. are questions very dependent on the Hamiltonian and the optimal field. More generally, one can try to find the global features of P_{if} or of the cost functional, for any initial and target states. This is called the *Landscape* or Optimal Landscape problem (Rabitz et al., 2004).

Controllability is a set of mathematical theorems (D'Alessandro, 2007; Ramakrishna et al., 1995) that proof the existence of solutions, but usually they are not constructive except in some special systems (Khaneja and Glaser, 2001; Khaneja et al., 2001; Schirmer et al., 2002), offering no guidance on how to find the optimal pulses. The first theorems treated piecewise constant pulses (Huang et al., 1983) but a breakthrough was achieved using the Lie-algebraic approach (Ramakrishna et al., 1995; Rangan et al., 2004; Schirmer et al., 2001; Turinici and Rabitz, 2001) A simpler theorem, based on connectivity, analyzes the basic set of couplings between the states that are necessary to allow population transfer (Turinici and Herschel, 2003; Wu et al., 2004).

On the other hand, the quantum control landscapes address the wider picture of the properties of the set of all solutions explaining how difficult it is to find them. In particular, the topology of the landscapes (i.e., the character of its critical points) determines the robustness of the solutions, providing hints whether local search algorithms will converge to global maxima. Among the most interesting findings is the general result (independent of the Hamiltonian) that if we maximize transition probabilities in controllable systems, and the functional is unconstrained, then there are no local traps; except for the global maxima ($P_{if} = 1$) and minima ($P_{if} = 1$) all other regular extrema are saddle points (Ho and Rabitz, 2006; Moore and Rabitz, 2011; Rabitz et al., 2004, 2005, 2006; Shen et al., 2006). This is not so surprising, as controllability in a sense guarantees free navigation on the Hilbert space (one can reach any state from a different one in finite time) and the matrix elements of the unitary evolution operator are, by definition, constrained between 0 and 1. For such operators, all local maxima are therefore artifacts of the constrains in the functional or the penalization in the laser fluence that affect the gradient. Theoretical analysis has shown that in controllable systems one can move continuously through a level set of the landscape, for which homotopy trajectory control algorithms (D-MORPH) can be designed (Rothman et al., 2005, 2006).

Here we will only focus on how to find the optimal pulses. There are several ways to address this problem:

1. We call an *open-loop design*[a] to an approximate maximization of $P_{if} = |\langle \varphi_t | \mathbf{U}(T, 0; \epsilon_{ap}) | \psi(0) \rangle|^2$ based on a motivated guess of a first-order solution, $\epsilon_0(t)$ (chosen from analytic knowledge of the dynamics under a Hamiltonian $\mathbf{H}_{ap}(t)$ that looks similar to $\mathbf{H}(t)$ under certain limits) whose parameters are fitted, typically by trial and error, until P_{if} is large enough. These are the families of control schemes that were previously presented in this chapter.
2. We call *local control theory* (LCT) to the procedure by which one finds (Engel et al., 2009) $\epsilon_{lc}(t)$ such that

$$\frac{dP_{if}}{dt} = \frac{d}{dt} |\langle \psi_f | \mathbf{U}(T, 0; \epsilon_{lc}) | \psi(0) \rangle|^2 \geq 0, \qquad \forall t.$$

[a] This nomenclature is not used for instance in the Engineering or Mathematical Control Theory or in Quantum Optics, but it is most often encounter in Molecular Physics. Perhaps more appropriate would be to consider it as a constrained search, or a few parameters search approach

3. We call *optical control* (OCT) to the variational procedure by which one finds (Werschnik and Gross, 2007) $\epsilon_{oc}(t)$ such that P_{if} is a local maximum under variations of $\epsilon_{oc}(t)$, that is

$$\frac{\delta P_{if}}{\delta \epsilon_{oc}(t)} = \frac{\delta |\langle \psi_f | \mathbf{U}(T, 0; \epsilon_{oc}) | \psi(0) \rangle|^2}{\delta \epsilon_{oc}(t)} = 0.$$

Below we derive the equations that $\epsilon_{lc}(t)$ and $\epsilon_{oc}(t)$ must obey. But before getting to this point, it is worth mentioning other QC problems related, but different, to the one that was stated above (Joe-Wong et al., 2016). For instance one may ask for less detailed control objectives where instead of ψ_f, the target is to maximize or minimize some expectation value, e.g., $\langle x \rangle$, $\langle H \rangle$, at a certain time (Shi and Rabitz, 1990; Sola et al., 1998b). They involve less detailed target states for which sometimes one can use simpler methodologies, as *local control theory* (Bartana et al., 1993; Kosloff et al., 1992; Tang et al., 1996), *tracking* (Gross et al., 1993; Nguyen-Dang et al., 1995; Ohtsuki et al., 1998; Sugawara et al., 2001), or semiclassical approaches (Botina et al., 1995, 1996; Chen et al., 1995; Shi et al., 1988). But in fact, maximization of P_{if} can be rewritten as the maximization of the expectation value of the projector operator $\mathbf{P} = |\psi_f\rangle\langle\psi_f|$. We will use this notation as the control formalism is then expressed in a more general way, and one can easily move from the expectation value of $\mathbf{P}$ to the expectation value of another quantum operator $\mathbf{A}$.

In principle, the operator $\mathbf{A}$ can be as complex as needed. In particular, it can imply a tradeoff between different goals. In addition, one can include time-dependent target states, where one maximizes the expectation value of the operator over some interval of time (Kaiser and May, 2004; Ohtsuki et al., 2004; Serban et al., 2005). This leads to more complex inhomogeneous TDSE that certain wave functions must satisfy.

Finally, one may ask for more complex control problems where instead of maximizing a single target state, P_{if}, the goal is to maximize different target states conditioned to the initial state. That is, one seeks to reconstruct an entire unitary operator $\mathbf{U}_f$ with the control $\epsilon(t)$, minimizing the difference between $||\mathbf{U}_f - \mathbf{U}(T, 0; \epsilon)||$, where the double vertical bar $||$ indicates some measure of distance or difference in the unitary matrices. This type of control problem is essential to the use of quantum control for Quantum Information or Quantum Computing. In QC, this is termed a multiobjective quantum control problem (Palao and Kosloff, 2002, 2003; Tesch and de Vivie-Riedle, 2002; Troppmann et al., 2006).

8.2 Local Control and Tracking

In LCT we set for a less ambitious goal. We want to find the field $\epsilon_{lc}(t)$ that forces the monotonic increase or decrease in time of the expectation value of a given observable of interest in the dynamics, $\langle \mathbf{A} \rangle$, be it a transfer probability P_{if} or a property such as the energy of the system $\langle \mathbf{H}_0 \rangle$.

Therefore, we must find the field so the derivative

$$\frac{d}{dt}\langle \psi(t)|\mathbf{A}|\psi(t)\rangle = -\frac{i}{\hbar}\langle \psi(t)|[\mathbf{A},\mathbf{H}]|\psi(t)\rangle \tag{75}$$

is always positive (or negative, depending on the goal), where we use the commutator $[\mathbf{A},\mathbf{H}] = \mathbf{AH} - \mathbf{HA}$. It is sometimes convenient to write Eq. (75) in the equivalent way

$$\frac{d}{dt}\langle \psi(t)|\mathbf{A}|\psi(t)\rangle = -\frac{2}{\hbar}\mathrm{Re}(i\langle \psi(t)|\mathbf{AH}|\psi(t)\rangle) = \frac{2}{\hbar}\mathrm{Im}(\langle \psi(t)|\mathbf{AH}|\psi(t)\rangle) \tag{76}$$

to remind us that the expectation value is a real number despite the presence of the imaginary unit in Eq. (75). Here, Re and Im denote the real and imaginary parts of a complex number.

Since $\mathbf{H}(t) = \mathbf{H}_0 - \mu\epsilon(t)$, separating the contributions of the two parts of the Hamiltonian in Eq. (75) we obtain

$$\frac{d}{dt}\langle \psi(t)|\mathbf{A}|\psi(t)\rangle = -\frac{i}{\hbar}\langle \psi(t)|[\mathbf{A},\mathbf{H}_0]|\psi(t)\rangle + \frac{i}{\hbar}\epsilon(t)\langle \psi(t)|[\mathbf{A},\mu]|\psi(t)\rangle, \tag{77}$$

to be rewritten as

$$\frac{d}{dt}\langle \psi(t)|\mathbf{A}|\psi(t)\rangle = h(t) + \epsilon(t)g(t). \tag{78}$$

Clearly, if $[\mathbf{A},\mu] = 0$ no control is possible (or at least we will not obtain any explicit dependence of our objective with the local control field). On the other hand, if $[\mathbf{A},\mathbf{H}_0] = 0$ the control is simple, since then, from Eq. (77) it is easy to impose $d\langle A(t)\rangle/dt \geq 0$ (or ≤ 0). It suffices to make $\epsilon(t)g(t) \geq 0$, or

$$\epsilon_{lc}(t) = f(t)g(t) = \frac{i}{\hbar}f(t)\langle \psi(t)|[\mathbf{A},\mu]|\psi(t)\rangle = -\frac{2}{\hbar}f(t)\mathrm{Im}(\langle \psi(t)|\mathbf{A}\mu|\psi(t)\rangle) \tag{79}$$

with $f(t) \geq 0$, since then $d\langle A(t)\rangle/dt = f(t)g(t)^2$. (For $d\langle A(t)\rangle/dt \leq 0$ we only need to choose $f(t) \leq 0$.) At the times when $g(t) = [\mathbf{A},\mu] = 0$ (or the

imaginary part of $\langle\psi(t)|\mathbf{A}\mu|\psi(t)\rangle$ is zero) the rate of change will be zero as well, provided $h(t) = 0$. If the last condition is not met, there is no easy way to know if that term will not cause a drop in $\langle A(t)\rangle$. This is why local control procedures are commonly used only for operators $\mathbf{A}$ such that $[\mathbf{A},\mathbf{H}_0] = 0$. This is the case when $\mathbf{A}$ is a projection operator on an eigenstate of the system, $\mathbf{P}$ or is proportional to the molecular Hamiltonian, $\mathbf{H}_0$.

Local control is a *local-in-time* procedure. One just needs to adjust the pulse instantaneously to the value of the integral that depends on the wave function evaluated at the same time, which forces the use of very short time steps in the numerical integration of the TDSE. On the other hand, as we will show later, OCT requires knowledge of all the dynamics to adjust the value of the pulse at each time.

In the closely related tracking approach, one forces $\langle\psi(t)|\mathbf{A}|\psi(t)\rangle$ to follow a preset trajectory $a(t)$. From Eq. (77) this is equivalent to demand

$$\epsilon(t)g(t) = \frac{da(t)}{dt} \tag{80}$$

again assuming $h(t) = 0$. Because Eq. (80) is ill-defined whenever $g(t) = 0$ and $da(t)/dt \neq 0$, and there is no way to know a priori (without previously knowing the field and solving the TDSE) what trajectories $a(t)$ are possible, in order to impose tracking one often needs to develop algorithms with regularization techniques, which soften the requirements of tracking (Salomon and Turinici, 2006; Zhu and Rabitz, 2003; Zhu et al., 1999).

There have been numerous applications of LCT and tracking, including molecular cooling and heating (Kosloff et al., 1992; Tang et al., 1996), and optical paralysis (Malinovsky et al., 1997), photodissociation (Gräfe et al., 2004), predissociation (Marquetand and Engel, 2005), photoassociation (Marquetand and Engel, 2007), and electron transfer (Vindel-Zandbergen et al., 2016). In Section 8.3 we will compare the equations for the LCT and OCT fields when $\hat{\boldsymbol{A}}$ is a projection operator, $\hat{\boldsymbol{P}}$. Here we consider two simple examples that show the physics behind the mathematical formalism of LCT.

First consider a field that stops or slows down a free electron, moving under $\mathbf{H}_0 = \mathbf{p}^2/2m$. Since $[\mathbf{p}^2,\mathbf{H}_0] = 0$ and $[\mathbf{p}^2,\mu] = 2ei\mathbf{p}/\hbar$, $(\mu = -ez)$, the required condition

$$\frac{d\langle\mathbf{p}^2\rangle}{dt} \leq 0$$

can be met making

$$\epsilon_{lc}(t) = -2f(t)\langle\psi(t)|\mathbf{p}|\psi(t)\rangle. \tag{81}$$

This equation just expresses the physically intuitive condition that the field must oppose the momentum of the electron, with an amplitude proportional to its value, in order to stop its flow. The same will be valid for any particle provided it is coupled to the field. The simple field given by Eq. (81) can be used to push the particle in one or the other direction.

Secondly, we use LCT to show how it elegantly generalizes the theory of population transfer by molecular π-pulses (Section 6.1). Let us consider again electronic excitation in molecules by ultrashort pulses,

$$i\hbar\frac{\partial}{\partial t}\begin{pmatrix}\psi_1\\ \psi_2\end{pmatrix} = \begin{pmatrix}\mathbf{T}+V_1 & \mu E_{lc}(t)/2\\ \mu E_{lc}^*(t)/2 & \mathbf{T}+V_2\end{pmatrix}\begin{pmatrix}\psi_1\\ \psi_2\end{pmatrix}, \tag{82}$$

where, using the RWA, $\epsilon_{lc}(t) = (E_{lc}(t)e^{-i\omega t} + E_{lc}^*(t)e^{i\omega t})/2$ (ω is the center frequency of the pulse) and $E_{lc}(t)$ must be complex, in general.[b] Our goal is to control the flow of population between the different electronic states, $P_j(t) = \langle\psi_j(t)|\psi_j(t)\rangle$. In LCT we demand monotonic increase or decrease of

$$\frac{d}{dt}P_2(t) = \frac{1}{\hbar}\mathrm{Im}[\langle\psi_1(t)|\mu|\psi_2(t)\rangle\epsilon_{lc}(t)]. \tag{83}$$

Hence, making $\epsilon_{lc}(t) = -i\,\langle\psi_2(t)|\mu|\psi_1(t)\rangle\, f(t)$, the sign of $f(t)$ forces the sign of the flux, increasing (or decreasing) the population in the excited electronic state for positive (or negative) functions. The amplitude of $f(t)$ only determines the rate of the transfer. This expression shows that adjusting the phase of the laser to that of the instantaneous dipole, $\langle\psi_2(t)|\mu|\psi_1(t)\rangle$, one can select whether there is absorption or spontaneous emission under the field, if the dipole is not zero. Eq. (83) generalizes the conditions for electronic population transfer under molecular π-pulses with moving wave packets, lifting the too restrictive conditions imposed in Section 6. Rather than requiring the transfer to finish before the packets move, it is just necessary that $\psi_1(t)$ and $\psi_2(t)$ overlap.

Alternatively, choosing $\epsilon_{lc}(t) = \langle\psi_1(t)|\mu|\psi_2(t)\rangle\, f(t)$, one locks the populations. Since additional conditions can be applied (for instance, that the pulse heats or cools the wave packets in one potential) one can set up

[b] Since forcing the field to be transformed-limited amounts to eliminate all control based on phase modulation, in general we need to work with complex fields in LCT.

conditions for laser-catalysis, where the laser acts without net flow of photons (Kosloff et al., 1992; Malinovsky and Tannor, 1997; Tang et al., 1996). In many occasions the obtained control fields violate the assumed RWA approximation, leading to some losses in the yields when the dynamics is solved without the RWA.

8.3 The Variational Approach: Deriving the Quantum Optimal Control Equations

We return to our fundamental control problem, defined in terms of projection operators. We want to find the field that maximizes $J = \langle \psi(T)|\mathbf{P}|\psi(T)\rangle$, where $\mathbf{P} = |\psi_f\rangle\langle\psi_f|$, such that $J = P_{if}$ is the transition probability to go from $\psi(0) = \psi_i$ at initial time to ψ_f at final time. The same derivation will be valid if $\mathbf{P}$ is any positive semidefinite operator. At the same time we want to penalize the use of very strong laser pulses, for two reasons: (i) strong pulses break the validity of most approximate Hamiltonian descriptions, and (ii) we need an explicit dependence on the field in our equations. As shown below, we need to include the field (at least) up to power two in J in order to find equations for the fields.

To start up, we set up a variational method to find the extremes of the cost functional

$$J = \langle \psi(T)|\mathbf{P}|\psi(T)\rangle - \frac{1}{T}\int \frac{\epsilon^2(t)}{f^2(t)}dt, \tag{84}$$

where $f(t)$ is a predetermined function that makes the functional dimensional free. The second term penalizes solutions that use strong fields: When $f(t)$ is large the penalty is small and the amplitude of the optimal field is not constrained. The opposite occurs when $f(t)$ is small. Hence, the envelope of $f(t)$ works as a general envelope of the optimal field (Manz et al., 1998). In particular, it forces the optimal field to zero, as we will show, when $f(t) = 0$, suppressing static field components. The peak amplitude of $f(t)$ sets a trade off between the two goals, maximizing the projection on the target at final time, and minimizing the pulse fluence. Taking variations in $\psi(T)$ and $\epsilon(t)$ we write

$$J + \delta J = \langle \psi(T) + \delta\psi(T)|\mathbf{P}|\psi(T) + \delta\psi(T)\rangle - \frac{1}{T}\int \frac{[\epsilon(t) + \delta\epsilon(t)]^2}{f^2(t)}dt. \tag{85}$$

Keeping only variations in first order of $\psi(T)$ and $\epsilon(t)$ we obtain

$$\delta J = 2\mathrm{Re}[\langle \psi(T)|\mathbf{P}|\delta\psi(T)\rangle] - \frac{2}{T}\int \frac{\epsilon(t)}{f^2(t)}\delta\epsilon(t)dt. \tag{86}$$

In order to find a maximum (or rather an extreme) of $\delta J/\delta\epsilon(t)$ we need to find how $\delta\psi(T)$ depends on $\delta\epsilon(t)$. In most derivations of the quantum OCT equations one uses Lagrange multipliers to consider both functions independent (Werschnik and Gross, 2007). Here we use an alternative derivation (Zhu et al., 1999) explicitly showing how they relate to each other via the TDSE (the dynamical constraint). The quantum dynamics of the system, including the variations, must follow the equation

$$\frac{d}{dt}(\psi(t)+\delta\psi(t)) = -\frac{i}{\hbar}[\mathbf{H}(t)-\mu(\epsilon(t)+\delta\epsilon(t))](\psi(t)+\delta\psi(t)). \tag{87}$$

As we only keep variations up to first order, we can drop terms of second or higher order from the equations,

$$\frac{d}{dt}\delta\psi(t) = -\frac{i}{\hbar}\mathbf{H}(t)\delta\psi(t) + \frac{i}{\hbar}\mu\delta\epsilon(t)\psi(t). \tag{88}$$

This is an inhomogeneous TDSE that connects $\delta\psi(t)$ with $\delta\epsilon(t)$ at all times, and in particular, at final time, as required in Eq. (86). Its formal solution is

$$\delta\psi(t) = \mathbf{U}(t,0;\epsilon)\delta\psi(0) + \frac{i}{\hbar}\int_0^t \mathbf{U}(t,t';\epsilon(t'))\mu\delta\epsilon(t')\psi(t')dt'. \tag{89}$$

We are not allowed to change the initial state. Thus, $\delta\psi(0) = 0$ and at final time

$$\delta\psi(T) = \frac{i}{\hbar}\int_0^T \mathbf{U}(T,t';\epsilon(t'))\mu\delta\epsilon(t')\psi(t')dt'. \tag{90}$$

Substituting Eq. (90) in Eq. (86) we obtain

$$\delta J = \int_0^T dt'\left\{\frac{2}{\hbar}\mathrm{Re}[i\langle\psi(T)|\mathbf{P}\mathbf{U}(T,t';\epsilon)\mu\delta\epsilon(t')|\psi(t')\rangle] - \frac{2}{Tf^2(t')}\epsilon(t')\delta\epsilon(t')\right\} \tag{91}$$

or, since $\delta\epsilon(t)$ is real

$$\delta J = -2\int_0^T dt'\left\{\mathrm{Im}\left[\langle\psi(T)|\mathbf{P}\mathbf{U}(T,t';\epsilon)\frac{\mu}{\hbar}|\psi(t')\rangle\right] + \frac{1}{Tf^2(t')}\epsilon(t')\right\}\delta\epsilon(t'). \tag{92}$$

We can define an instantaneous gradient $dJ_t/d\epsilon(t)$ such that

$$\delta J = \int_0^T \frac{dJ_t}{d\epsilon(t)} \delta\epsilon(t) dt, \tag{93}$$

where

$$\frac{dJ_t}{d\epsilon(t)} = -2\left\{ \mathrm{Im}\left[\langle \psi(T)|\mathbf{P}\mathbf{U}(T,t;\epsilon)\frac{\mu}{\hbar}|\psi(t)\rangle \right] + \frac{1}{Tf^2(t)}\epsilon(t) \right\}. \tag{94}$$

Next, we find a maximum of the functional making $dJ_t/d\epsilon(t) = 0$ at each time, t. This determines the equation obeyed by the optimal field,

$$\epsilon_{oc}(t) = -\frac{T}{\hbar} f^2(t) \mathrm{Im}[\langle \psi(T)|\mathbf{P}\mathbf{U}(T,t;\epsilon_{oc}(t))\mu|\psi(t)\rangle] \tag{95}$$

or

$$\epsilon_{oc}(t) = -\frac{T}{\hbar} f^2(t) \mathrm{Im}[\langle \psi(T)|\mathbf{P}\mathbf{U}(T,t;\epsilon_{oc}(t))\mu\mathbf{U}(t,0;\epsilon_{oc}(t))|\psi(0)\rangle]. \tag{96}$$

Eq. (96) is an implicit equation: $\epsilon_{oc}(t)$ depends on $\mathbf{U}(T,t;\epsilon_{oc}(t))$ which itself depends on $\epsilon_{oc}(t)$ in a complicated way. In particular, knowing $\epsilon_{oc}(t)$ requires knowledge of the whole history of the dynamics, from the past to the present (via $\mathbf{U}(t,0;\epsilon_{oc}(t))$) and from the future to the present (via $\mathbf{U}(T,t;\epsilon_{oc}(t))$). To solve the nonlinear equation one needs iterative procedures. Notice that, had we not included the quadratic penalty form of the field in the functional, the gradient (Eq. (94)) would not be an explicit function of the field.

It is customary to write Eq. (96) in more symmetric fashion. First we define the performance function, which can be identified with a Lagrange multiplier that forces the quantum unitary evolution of $\psi(t)$ in an unconstrained optimization (Werschnik and Gross, 2007),

$$\chi(T) = \mathbf{P}\psi(T). \tag{97}$$

The performance function can only be evaluated at the end of the dynamics (it is fixed at time $t = T$), and then we propagate it backwards in time with the optimal field. Since

$$\langle \psi(T)|\mathbf{P}\mathbf{U}(T,t;\epsilon_{oc}) = \langle \chi(T)|\mathbf{U}(T,t;\epsilon_{oc}) = \langle \chi(t)|, \tag{98}$$

we can write

$$\epsilon_{oc}(t) = -\frac{T}{\hbar} f^2(t) \mathrm{Im}[\langle \chi(t)|\mu|\psi(t)\rangle]. \tag{99}$$

This is the quantum OCT equation for the optimal field. It is very compact and deceivingly simple, but since both $\chi(t)$ and $\psi(t)$ depend on the field, the equation (obviously) remains nonlinear. Usually one defines a positive envelope function $S(t) \equiv f^2(t)$ and adds a scale factor α instead of T in the equation. On the other hand, it has been shown that often one obtains better results when instead of penalizing the fluence, one penalizes changes in the fluence with respect to some reference field, $\epsilon_{\text{ref}}(t)$. That is, one changes $\epsilon(t)^2$ for $[\epsilon(t) - \epsilon_{\text{ref}}(t)]^2$ in the penalty term of Eq. (84).

One can obtain similar quantum optimal control equations for more complex functionals. For instance, with cost terms involving time-dependent penalty functions (Kaiser and May, 2004; Ohtsuki et al., 2004; Serban et al., 2005; Sola et al., 1999b) or constrains in the optimal pulse spectra that imply only phase modulation of the optimal pulses (Gollub et al., 2008; Lapert et al., 2009; Werschnik and Gross, 2005)) or when the optimal pulse is parameterized (Shi and Rabitz, 1990; Sola et al., 1998a).

It is instructive to compare the LCT and OCT pulses. In LCT we force monotonic increase in P_{if} over time. We recall that $\mathbf{P}$ commutes with the molecular Hamiltonian, so that we can use Eq. (79) for the LCT solution. To compare with the OCT solution, we change $2f(t) \to Tf^2(t)$, rewriting Eq. (79) as

$$\epsilon_{lc}(t) = -\frac{T}{\hbar} f^2(t) \text{Im}(\langle \psi(t)|\mathbf{P}\mu|\psi(t)\rangle), \tag{100}$$

so that the field has the right dimensions. This looks very much as Eq. (99) except that $\langle\psi(t)|\mathbf{P}$ is not $\langle\chi(t)|$. Let us remember that from Eq. (98),

$$\langle\chi(t)| = \langle\psi(T)|\mathbf{P}\mathbf{U}(T, t; \epsilon_{oc}) = \langle\psi(t)|\mathbf{U}(t, T; \epsilon_{oc})\mathbf{P}\mathbf{U}(T, t; \epsilon_{oc}).$$

So that we can make the expressions of the LCT and OCT identical,

$$\epsilon_{oc}(t) = -\frac{T}{\hbar} f^2(t) \text{Im}\big(\langle \psi(t)|\widetilde{\mathbf{P}}(t)\mu|\psi(t)\rangle\big), \tag{101}$$

hiding the complexity of the OCT field in the time-dependent projection operator

$$\widetilde{\mathbf{P}}(t) \equiv \mathbf{U}(t, T; \epsilon_{oc})\mathbf{P}\mathbf{U}(T, t; \epsilon_{oc})$$

that takes into account all the dynamics of the system. $\widetilde{\mathbf{P}}(t)$ is an operator in the Heisenberg representation with the reference time defined in the future $t = T$, instead of $t = 0$. Only when $\mathbf{P}$ commutes with the time-evolution

operator ($\widetilde{\mathbf{P}} = \mathbf{P}$), LCT and OCT give identical results. Then, the instantaneous dipole that forces the monotonic increase in the population transfer, without care of the future dynamics, fully maximizes the population transfer at final time. Unfortunately, it can be shown that this condition only applies when the dynamics is trivial. The LCT field is (almost) never optimal. One can (almost) always improve its final yield with a OCT version. But then LCT is much faster and computationally friendly to use than OCT.

8.4 Finding the Optimal Pulses: Optimal Control Algorithms

As indicated, Eq. (99) (or the equivalent form (96)) is an implicit equation that can only be solved by iterative procedures. Many quantum optimal control algorithms have been proposed in the literature. Most use the gradient (Eq. 94) (Combariza et al., 1991; Shi and Rabitz, 1991; Sola et al., 1998b) or some generalization of the gradient that leads to fast monotonic increase of the functional at each iteration, as in the Krotov (Kosloff et al., 1992; Maday and Turinici, 2003; Ohtsuki et al., 2004, 2007; Palao and Kosloff, 2003; Somlói et al., 1993; Zhu and Rabitz, 1998), the Zhu–Rabitz (Werschnik and Gross, 2007; Zhu et al., 1998), and the two-point boundary-value quantum control paradigm (Ho and Rabitz, 2010; Liao et al., 2011). Taking into account the form of the landscapes, some global search algorithms as genetic algorithms have been proposed (Geremia et al., 2000; Turinici et al., 2004). However, in general these algorithms only use information of the observable at final time, throwing away the wealth of information contained in the dynamics, that is obtained by solving the TDSE. As a result, they are quite less efficient from a computational point of view. As we discuss in Section 8.6 these are the type of algorithms that are precisely needed to find optimal pulses in the laboratory, by adaptive learning.

In this section we focus on two algorithms that can be used as a motivation for the study and development of other algorithms: the gradient method and the Krotov method. Since they imply iterative procedures, we refer to $\epsilon^{(k)}(t)$ and $\epsilon^{(k+1)}(t)$ as two consecutive steps in the run to obtain good (optimal) solutions. To start the algorithm one always needs an initial guess $k = 0$ which is often physically motivated (e.g., from the open-loop approach). In some occasions a very non imaginative guess, $\epsilon^{(0)}(t) = 0$, suffices. On the other hand, the search must stop by imposing convergence conditions, for instance

$$\int_0^T dt \frac{\left[\epsilon^{(k+1)}(t) - \epsilon^{(k)}(t)\right]^2}{f(t)^2} \leq T\kappa \qquad \text{or} \qquad J^{(k+1)} - J^{(k)} \leq \kappa',$$

where κ (κ') are predetermined criteria for convergence.

To simplify the notation and use Eq. (99) we will call $\psi^{(k)}(t)$ to the wave function obtained by propagating with $\mathbf{U}\left(t, 0; \epsilon^{(k)}(t)\right)$ and likewise $\chi^{(k)}(t)$ to the performance function obtained by propagating with $\mathbf{U}^{\dagger}\left(t, T; \epsilon^{(k)}(t)\right)$.

8.4.1 The Gradient Method

The *gradient method* is based on choosing the field on step $k+1$ as the field on step k plus a contribution along the gradient obtained with the same k field. From Eq. (94), writing the gradient as a function of the performance function evaluated after iteration k, $\chi^{(k)}(T)$,

$$\frac{dJ_t^{(k)}}{d\epsilon(t)} = -2\left\{ \mathrm{Im}\left[\langle \chi^{(k)}(t)|\frac{\mu}{\hbar}|\psi^{(k)}(t)\rangle\right] + \frac{1}{Tf^2(t)}\epsilon(t)\right\}. \tag{102}$$

Then

$$\epsilon^{(k+1)}(t) = \epsilon^{(k)}(t) + \beta\frac{dJ_t^{(k)}}{d\epsilon(t)}, \tag{103}$$

where β (a small but unknown positive number) must be found by linear search. It is not difficult to prove that this choice makes $J^{(k+1)} \geq J^{(k)}$ at least for a certain range of β. Once the gradient at each iteration is known, alternative gradient-based search algorithms, such as the conjugate-gradient method, can be used as well.

8.4.2 The Krotov Method

The *Krotov method* is based on general (not differential) changes in the pulses from iteration to iteration that assure monotonic increase of $\Delta J = J^{(k+1)} - J^{(k)}$. In terms of the changes in the final state $\Delta\psi(T) = \psi^{(k+1)}(T) - \psi^{(k)}(T)$, and in the field, $\Delta\epsilon(t) = \epsilon^{(k+1)}(t) - \epsilon^{(k)}(t)$,

$$\begin{aligned}\Delta J = &\langle \Delta\psi(T)|\mathbf{P}|\Delta\psi(T)\rangle + 2\mathrm{Re}\left[\langle \psi^{(k)}(T)|\mathbf{P}|\Delta\psi(T)\rangle\right] \\ &-\frac{1}{T}\int_0^T dt\frac{\Delta\epsilon(t)^2 + 2\epsilon^{(k)}(t)\Delta\epsilon(t)}{f^2(t)}.\end{aligned} \tag{104}$$

Since the first term is always positive, one only has to evaluate changes in the fields that force the second and third term positiveness, for which we need to link changes in the final wave function with changes in the field. Using a TDSE similar to Eq. (87), we can write

$$\frac{d}{dt}\Delta\psi = -\frac{i}{\hbar}\left[\mathbf{H}_0 - \mu\epsilon^{(k)}\right]\Delta\psi + \frac{i}{\hbar}\mu\left[\epsilon^{(k+1)} - \epsilon^{(k)}\right]\psi^{(k+1)} \tag{105}$$

only that now we cannot drop terms that depend on second-order variations. Solving the inhomogeneous TDSE gives

$$\Delta\psi(T) = \frac{i}{\hbar}\int_0^T \mathbf{U}(T,t;\epsilon^{(k)}(t))\mu\Delta\epsilon(t)\psi^{(k+1)}(t)dt \tag{106}$$

and introducing Eq. (106) into Eq. (104) we obtain

$$\mathrm{Re}\left[\langle\psi^{(k)}(T)|\mathbf{P}|\Delta\psi(T)\rangle\right] = -\int_0^T \mathrm{Im}\left[\langle\chi^{(k)}(t)|\frac{\mu}{\hbar}|\psi^{(k+1)}(t)\rangle\right]\Delta\epsilon(t)dt. \tag{107}$$

We need to make the integrand,

$$I(t) = -2\mathrm{Im}\left[\langle\chi^{(k)}(t)|\frac{\mu}{\hbar}|\psi^{(k+1)}(t)\rangle\right]\Delta\epsilon(t) - \frac{1}{T}\frac{\Delta\epsilon(t)^2 + 2\epsilon^{(k)}(t)\Delta\epsilon(t)}{f^2(t)}$$

always positive. In the Krotov scheme we maximize it with respect to $\Delta\epsilon(t)$,

$$\frac{dI(t)}{d\Delta\epsilon(t)} = -2\mathrm{Im}\left[\langle\chi^{(k)}(t)|\frac{\mu}{\hbar}|\psi^{(k+1)}(t)\rangle\right] - \frac{2\Delta\epsilon(t) + 2\epsilon^{(k)}(t)}{f^2(t)T} = 0 \tag{108}$$

leading to

$$\Delta\epsilon(t) = -\epsilon^{(k)}(t) - 2\mathrm{Im}\left[\langle\chi^{(k)}(t)|\frac{\mu}{\hbar}|\psi^{(k+1)}(t)\rangle\right]. \tag{109}$$

The Krotov-optimized field for the step $k + 1$ is therefore

$$\epsilon^{(k+1)}(t) = \epsilon^{(k)}(t) + \Delta\epsilon(t) = -f^2(t)T\mathrm{Im}\left[\langle\chi^{(k)}(t)|\frac{\mu}{\hbar}|\psi^{(k+1)}(t)\rangle\right]. \tag{110}$$

This equation is very similar to Eq. (99), and the equation for $dI(t)/d\Delta\epsilon(t)$ (Eq. 108) is very similar to the gradient, Eq. (102), but notice that while $\chi^{(k)}(t)$ is propagated using the field obtained at the previous step (the only one that is known at all times), $\psi^{(k+1)}(t)$ is propagated with the new field. This implies immediate feedback and gives the faster convergence properties of Krotov or similar methods. It can also be proved that the Krotov method guarantees $J^{(k+1)} \geq J^{(k)}$ without needing any line search for β.

8.5 Geometrical Optimization

In OCT (or LCT) the initial wave function is fixed and the pulse is changed to maximize the probability of a given process. Alternatively, one can change the initial wave function (within some constrains in a subspace of

the Hilbert space so that the solution is not obvious) to maximize the probability for a given fixed field. Since the optimization amounts to finding a superposition state (a rotation in the Hilbert space not parameterized by the time), this approach is called a Geometrical Optimization.

Consider then again that we want to maximize the transition probability P_{if} for which we construct a functional $J = \langle\psi_i|\mathbf{U}^\dagger(0,\ T;\ \epsilon)\mathbf{P}\mathbf{U}(0,\ T;\ \epsilon)|\psi_i\rangle$ that depends on ψ_i. For brevity, we will omit the arguments of the time-evolution operator. Typically, $\mathbf{P} = |\psi_f\rangle\langle\psi_f|$ projects on a particular vibrational wave function in the electronic excited state. Alternatively, we may want to maximize the electronic absorption, for which $\mathbf{P} = \sum_f |\psi_f\rangle\langle\psi_f|$ where the summation runs over all the vibrational states of the excited electronic state.

On the other hand, ψ_i can be changed within a subset of vibrational levels in the electronic state, subject to norm conservation, $\langle\psi_i + \delta\psi_i|\psi_i + \delta\psi_i\rangle = 1$. Maximizing with constraints can be achieved by the technique of Lagrange multipliers.

We define the unconstrained functional as $J' = J - \chi_i(\langle\psi_i|\psi_i\rangle - 1)$, where χ_i is the Lagrange multiplier, and take variations on ψ_i ($\psi_i \to \psi_i + \delta\psi_i$). By formally deriving with respect to the initial bra ψ_i^* (the derivation with respect to the ket gives the conjugate gradient of the same expression), we obtain

$$\frac{\partial J'}{\partial \psi_i^*} = \mathbf{U}^\dagger\mathbf{P}\mathbf{U}|\psi_i\rangle - \chi_i|\psi_i\rangle.$$

Upon extremization (i.e., making the derivative equal to zero) we obtain the secular equation,

$$\mathbf{U}^\dagger\mathbf{P}\mathbf{U}|\psi_i\rangle = \chi_i|\psi_i\rangle, \tag{111}$$

which is an eigenvalue equation for the operator $\mathbf{P}_H \equiv \mathbf{U}(0,\ T;\ \epsilon)\mathbf{P}\mathbf{U}(T,\ 0;\ \epsilon)$, which is the transpose of the projection operator in the Heisenberg picture evaluated at final time. The eigenvalues give the probabilities of the transfer while the eigenfunctions give the superposition states that extremize the functional. Typically one is only interested in the maximum eigenvalue and eigenfunction, although for other operators it could be the minimum.

Expanding the initial wave function in the set of N allowed vibrational levels in the ground electronic state (where N could include all the bound vibrational levels in the ground electronic state or only a subset of them), $\psi_i = \sum_k^N a_{ki}\varphi_j$, and deriving J' with respect to the coefficients of the superposition a_j, we obtain Eq. (111) in matrix form (Chang et al., 2015e),

$$\sum_{k=1}^{N} P_{jk} a_{ki} = a_{ji} \chi_i, \tag{112}$$

where

$$P_{jk} = \langle \varphi_j | \mathbf{P}_H | \varphi_k \rangle. \tag{113}$$

Chang and coworkers have applied the Geometrical Optimization scheme to maximize electronic absorption (Chang et al., 2015d,e), selective excitation of entangled states and quasi-dark states (Chang et al., 2015c), multiphoton transitions (Sampedro et al., 2016b), and isomerization reactions (Chang et al., 2017a). In particular, it was shown that the preparation of specific superposition states was necessary to accelerate the absorption and achieve state-selective excitation with broadband pulses.

8.6 Pulse Shaping and Adaptive Learning

The solution of both OCT and LCT approaches gives typically complex pulses or pulse sequences. The optimal pulse must adjust its amplitude and phase at each time to maximally use the instantaneous transient dipole of the molecule; and for competing processes, it must generate dynamical phases that lead to constructive interference on the wanted state, and destructive interference in all other available states. With the development of pulse shaping techniques, these pulses are within the reach of most laser experimentalists. The starting point is the generation of ultrashort transformed-limited pulses. In a Fourier-transformed pulse all frequencies are locked. Manipulation of these frequencies in phase and amplitude constitutes the key tool for changing the temporal structure.

The basic idea is shown in Fig. 35. The short pulse is decomposed into its Fourier components. Then a mask is applied generating phases (and/or blocking components) that lead to the modification of the pulse after Fourier recombination. Mathematically, this process can be written as

$$\epsilon^{+}_{mod}(t) = \frac{1}{2\pi} \int_{-\infty}^{\infty} \widetilde{M}(\omega) \epsilon^{+}(\omega) e^{i\omega t} d\omega, \tag{114}$$

where $\widetilde{M}(\omega)$ is the complex optical transfer function (or spectral mask) that represents the passage of the pulse through a linear optical system, and $\epsilon^{+}(\omega)$ is the positive part of the initial pulse spectrum. Since Eq. (114) is a product in the frequency domain, the inverse Fourier transform is a convolution of the pulse and mask in the time domain.

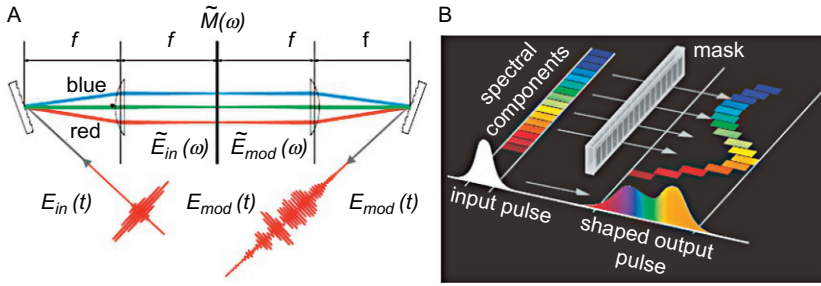

Fig. 35 (A) Basic layout for Fourier transform femtosecond pulse shaping. (B) Schematic illustration of shaping the temporal profile of an ultrashort laser pulse in a liquid crystal modulator. *Adapted from Stoian, R., Wollenhaupt, M., Baumert, T., Hertel, I.V., 2010. Temporal Pulse Tailoring in Ultrafast Laser Manufacturing Technologies. Springer, Berlin, Heidelberg. ISBN 978-3-642-10523-4, 121–144. https://doi.org/10.1007/978-3-642-10523-4_5 with permission.*

As an exercise in Fourier analysis, it is relatively simple to anticipate some interesting effects of pulse shaping on the original pulse, which we assume Gaussian. Consider a purely phase mask that does not change the spectrum. If the optical phase $\omega(t)$ is quadratically modulated it leads to linear chirping of the frequency and stretching of the pulse, as indicated in Section 6.2. Third-order dispersion breaks the symmetry of the system, generating weak sidepulses leading or trailing the main subpulse (McMullen, 1977). Phase jumps subdivide the pulse in two (Meshulach and Silberberg, 1999; Präkelt et al., 2004; Renard et al., 2004), whereas sinusoidal spectral phase modulation generates a train of pulses where one can control the amplitudes and time delays between the subpulses (Herek et al., 2002; Meshulach and Silberberg, 1998; Weiner et al., 1990).

In practice, the generation of complex shaped laser pulses is now regularly achieved on programmable pulse shaping techniques that control $\tilde{M}(\omega)$ based on liquid crystal spatial light modulators (Weiner, 1995, 2000) or acousto-optic modulators (Wefers and Nelson, 1995) among other possibilities. But, in many quantum control cases, $\tilde{M}(\omega)$ is parameterized in a very general way, without constraining the functional form. The parameters are then obtained by quantum control algorithms. Typically, a family of pulses is produced and its performance is checked by measuring the observable of interest. Then an evolutionary algorithm (or a different learning algorithm) is used to manipulate the pulse parameters (the Fourier amplitudes and phases) keeping the pulses that gave better performance and introducing randomized variations (or interchanged of parameters, etc.), so that a new family of pulses is generated and the procedure is iteratively continued until

convergence. This feedback learning or closed-loop approach to optimize light-induced processes, started a whole new class of experiments, that had a very strong impact on the evolution of the quantum control field, with applications ranging from selective nonlinear spectroscopy (e.g., high-harmonic generation) in atoms, multiphoton microscopy, photodissociation and isomerization reactions in complex molecules, or electron transfer, to even the control of the energy flow in biomolecular complexes, and applications in liquid phase and in semiconductors. We refer the interested reader to the general reviews that focus on the many experimental achievements of quantum control through adaptive learning (Brif et al., 2012; Brixner and Gerber, 2003; Gordon and Rice, 1997; Nuernberger et al., 2007; Rabitz et al., 2000) and the references therein.

9. SUMMARY AND OUTLOOK

In this chapter we have reviewed several general aspects of quantum control. Understanding how the different pulse parameters act driving the dynamics allows to motive different control setups for selective population transfer between quantum states and between manifolds of states (for instance, electronic states) that may serve as a doorway to design quantum information protocols, prepare quantum gates, optimize nonlinear spectroscopic methods, or control photochemical and photophysical processes. We have mainly used results from our research to illustrate how the methods work in simple scenarios.

Starting from the simplest example of a two-level system, we have commented on control mechanisms based on so-called π-pulses and on adiabatic evolution using two-photon transitions and geometric phases. As an example, we focused on preparing quantum gates where the qubit is implemented on the electron spin. Application of adiabatic passage using frequency chirped pulses to maximize the Raman coherence for CARS signal enhancement has been presented, introducing the roof method. Both STIRAP and their generalizations for sequentially coupled multilevel systems were explained, focusing on similarities and differences between S-STIRAP and A-STIRAP. We presented some results of the two-qubit system dynamics as an example of closed-loop system control using the relative phase between two quantum pathways. Collapse and revival of entanglement has been discussed addressing trapped ions state manipulation by external fields in two different excitation regimes. The important role of the relative phase between the pulses in the modified Mølner–Sørensen scheme of CNOT quantum gate implementation has been demonstrated.

We then studied how the previous solutions could be applied using pulses short enough that create wave packets, and the interplay between the dynamic dephasing (the evolution induced by the gradient of the potentials) and the excitation processes to control the position and width of the wave function. These schemes are extensions of the Tannor–Kosloff–Rice control setup. We analyzed the role of the pulse intensity in the control of the absorption spectra, lifetimes, geometry, photophysical (intersystem crossing, internal conversion), and photochemical properties of molecules under strong fields, where the dynamical properties can be better understood using light-induced potentials. Most of these schemes generalize the APLIP, LAMB, and NRDSE control setups that use the dynamical Stark effect to induce the desired dynamics or to decouple the unwanted processes. Finally, we briefly discussed how to maximally use all the physical resources in the pulse to optimally drive the dynamics, formulating the quantum optimal control problem. We mainly focused on connections between optimal control, local control, and tracking methods and described different algorithms. The important problems of controllability and quantum landscapes and their importance in deriving general properties of the control solutions were briefly mentioned.

Before ending, we would like to comment on some challenges and some motivations underlying many conceptual problems that are open.

Many quantum control experiments applied the closed-loop learning algorithm method of Judson and Rabitz to laser excitation with Ti-sapphire laser pulses, due to the nice shaping capabilities of femtosecond pulses. This approach artificially limits the systems that can be controlled to those that can be excited at 1.55 eV or their multiples (Lozovoy and Dantus, 2005). In spite of these constrains, in most experiments one routinely finds solutions to the point of raising the question of whether optimal control can be economically viable as a competing route for chemical reactions. However, it is difficult to assess how close or far are the solutions from global maxima. In addition, most experiments required maximizing yields or ratios of coarse-grained observables, where it is not so difficult to obtain reasonable yields almost by statistical sampling. The challenge remains in finding good controls of fine observables that integrate more information from the dynamics and particularly in addressing not only photodissociation or rearranging reactions, but also photoassociation processes, that can be used to synthesize a molecule in a quantum state. Several control mechanisms were proposed in cold conditions (Koch and Shapiro, 2012), but recently photoassociation at high temperature is being studied (Levin et al., 2015).

Other frontiers are in the timescale and the complexity. Controlling electronic or coupled nuclear-electronic processes in the attosecond scale is still in its infancy. More developed is the study in complex setups. There are remarkable results in the control of processes in liquid phase and with biomolecules (Brixner et al., 2001; Herek et al., 2002; Vogt et al., 2005), where dissipation or decoherent effects should pose insurmountable difficulties to quantum control. In current experiments, it is hard to assess to what degree the control uses quantum resources, as it is in general difficult to characterize the mechanism by which the control drives the dynamics, but some protocols for classifying the solutions have been proposed (Mitra et al., 2003; Rey-de Castro and Rabitz, 2010; Sharp et al., 2008).

In many ways the philosophy of quantum control is the opposite to that of Nanoscience. In Nanoscience one synthesizes a quantum system so that it behaves in the desired way (e.g., a catalyst of a chemical reaction) or has the demanded property (e.g., emits at a certain frequency). Essentially to manipulate the properties of a system one enlarges the Hilbert space adding particles, working with few states per particle or, in other words, staying at the lowest energy states. The setup is stable but not very flexible, and there are no good inversion or optimization algorithms that help us to fine the optimal Hamiltonian. In quantum control the complexity is given by the set of excited states and is temporally addressed by the external field, which must therefore be complex in most cases. This leads to very flexible and fast controls and fast algorithms that find optimal solutions, although they are often not very stable. One of the greater challenges in quantum control is the application of its techniques to optimize important processes in Nanoscience, for instance, forcing molecules to act as catalysts, or in Quantum Technology, for instance, finding quantum algorithms. From controllability and landscape theories we might expect that such solutions exist and maybe they are not so difficult to find (Russell and Rabitz, 2017). However, the picture is not clear in the presence of irreversible processes such as dissipation or the loss of particles as in fragmentation or ionization processes at strong fields. The challenge and the opportunities are still lying ahead.

ACKNOWLEDGMENTS

I.R.S. thanks the Spanish Government for support through the MICINN project CTQ2015-65033-P; B.Y.C. acknowledges the Korean Government through the Basic Science Research program (2017R1A2B1010215); S.A.M. acknowledges support from the U.S. National Science Foundation under Grant Nos. PHY11-25915 and PHY12-05454, and the Office of Naval Research under Award No. N00014-17-1-2523.

REFERENCES

Abe, M., Ohtsuki, Y., Fujimura, Y., Domcke, W., 2005. A new quantum control scheme for multilevel systems based on effective decomposition by intense laser fields. J. Chem. Phys. 123, 144508.

Abrashkevich, D.G., Averbukh, I.S.h., Shapiro, M., 1994. Optimal squeezing of vibrational wave packets in sodium dimers. J. Chem. Phys. 101 (11), 9295–9302. https://doi.org/10.1063/1.467960.

Albert, J., Kaiser, D., Engel, V., 2016. Communication: adiabatic and non-adiabatic electron-nuclear motion: quantum and classical dynamics. J. Chem. Phys. 144 (17), 171103.

Allendorf, S.W., Szöke, A., 1991. High-intensity multiphoton ionization of H_2. Phys. Rev. A 44 (1), 518–534. https://doi.org/10.1103/PhysRevA.44.518.

Amstrup, B., Henriksen, N.E., 1992. Control of HOD photodissociation dynamics via bond-selective infrared multiphoton excitation and a femtosecond ultraviolet laser pulse. J. Chem. Phys. 97 (11), 8285–8295. https://doi.org/10.1063/1.463399.

Assion, A., Baumert, T., Bergt, M., Brixner, T., Kiefer, B., Seyfried, V., Strehle, M., Gerber, G., 1998. Control of chemical reactions by feedback-optimized phase-shaped femtosecond laser pulses. Science 282, 919.

Aubanel, E.E., Conjusteau, A., Bandrauk, A.D., 1993a. Effect of rotations on stabilization in high-intensity photodissociation of H_2^+. Phys. Rev. A 48 (6), R4011–R4014. https://doi.org/10.1103/PhysRevA.48.R4011.

Aubanel, E.E., Gauthier, J.M., Bandrauk, A.D., 1993b. Molecular stabilization and angular distribution in photodissociation of H_2^+ in intense laser fields. Phys. Rev. A 48 (3), 2145–2152. https://doi.org/10.1103/PhysRevA.48.2145.

Averbukh, I., Shapiro, M., 1993. Optimal squeezing of molecular wave packets. Phys. Rev. A 47 (6), 5086–5092. https://doi.org/10.1103/PhysRevA.47.5086.

Balint-Kurti, G.G., Zou, S., Brown, A., 2008. Optimal Control Theory for Manipulating Molecular Processes. In: John Wiley & Sons, Inc.. ISBN: 9780470259474, pp. 43–94. https://doi.org/10.1002/9780470259474.ch2

Band, Y.B., Magnes, O., 1994. Chirped adiabatic passage with temporally delayed pulses. Phys. Rev. A 50 (1), 584–594. https://doi.org/10.1103/PhysRevA.50.584.

Bandrauk, A.D., Sink, M.L., 1981. Photodissociation in intense laser fields: predissociation analogy. J. Chem. Phys. 74 (2), 1110–1117. https://doi.org/10.1063/1.441217.

Bartana, A., Kosloff, R., Tannor, D.J., 1993. Laser cooling of molecular internal degrees of freedom by a series of shaped pulses. J. Chem. Phys 99 (1), 196–210. https://doi.org/10.1063/1.465797.

Bayer, M., Ortner, G., Stern, O., Kuther, A., Gorbunov, A.A., Forchel, A., Hawrylak, P., Fafard, S., Hinzer, K., Reinecke, T.L., Walck, S.N., Reithmaier, J.P., Klopf, F., Schäfer, F., 2002. Fine structure of neutral and charged excitons in self-assembled In(Ga)As/(Al)GaAs quantum dots. Phys. Rev. B 65, 195315.

Bayer, T., Wollenhaupt, M., Baumert, T., 2008. Strong-field control landscapes of coherent electronic excitation. J. Phys. B 41 (7), 074007. http://stacks.iop.org/0953-4075/41/i=7/a=074007.

Bergmann, K., Theuer, H., Shore, B.W., 1998. Coherent population transfer among quantum states of atoms and molecules. Rev. Mod. Phys. 70 (3), 1003–1025. https://doi.org/10.1103/RevModPhys.70.1003.

Berman, P.R., Malinovsky, V.S., 2011. Principles of Laser Spectroscopy and Quantum Optics. Princeton University Press, Princeton.

Bohm, A., Mostafazadeh, A., Koizumi, H., Niu, Q., Zwanziger, J., 2003. The Geometrical Phase in Quantum Systems. Springer, Berlin.

Botina, J., Rabitz, H., Rahman, N., 1995. A new approach to molecular classical optimal control: application to the reaction HCN→HC+N. J. Chem. Phys. 102 (1), 226–236. https://doi.org/10.1063/1.469395.

Botina, J., Rabitz, H., Rahman, N., 1996. A simplified approach to optimally controlled quantum dynamics. J. Chem. Phys. 104 (11), 4031–4040. https://doi.org/10.1063/1.471215.

Brif, C., Chakrabarti, R., Rabitz, H., 2012. Control of quantum phenomena, vol. 148. Wiley-Blackwell, Malden, pp. 1–76. ISBN 978-1-118-15871-5; 978-1-118-12235-8.

Brixner, T., Gerber, G., 2001. Femtosecond polarization pulse shaping. Opt. Lett. 26, 559.

Brixner, T., Gerber, G., 2003. Quantum control of gas-phase and liquid-phase femtochemistry. ChemPhysChem 4, 418.

Brixner, T., Damrauer, N.H., Niklaus, P., Gerber, G., 2001. Photoselective adaptive femtosecond quantum control in the liquid phase. Nature 414, 57.

Brixner, T., Krampert, G., Pfeifer, T., Selle, R., Gerber, G., Wollenhaupt, M., Graefe, O., Horn, C., Liese, D., Baumert, T., 2004. Quantum control by ultrafast polarization shaping. Phys. Rev. Lett. 92, 208301.

Brixner, T., Pfeifer, T., Gerber, G., Wollenhaupt, M., Baumert, T., 2005. Femtosecond Laser Spectroscopy. In: Springer Verlag(Chapter 9).

Brumer, P., Shapiro, M., 1986. Laser control of product quantum state populations in unimolecular reactions. J. Chem. Phys. 84, 4103.

Brumer, P., Shapiro, M., 1992. Laser control of molecular processes. Annu. Rev. Phys. Chem. 43 (1), 257–282. https://doi.org/10.1146/annurev.pc.43.100192.001353.

Bucksbaum, P.H., Zavriyev, A., Muller, H.G., Schumacher, D.W., 1990. Softening of the H_2^+ molecular bond in intense laser fields. Phys. Rev. Lett. 64 (16), 1883–1886. https://doi.org/10.1103/PhysRevLett.64.1883.

Calegari, F., Ayuso, D., Trabattoni, A., Belshaw, L., Camillis, S.D., Anumula, S., Frassetto, F., Poletto, L., Palacios, A., Decleva, P., Greenwood, J., Martín, F., Nisoli, M., 2014. Ultrafast electron dynamics in a biomolecule initiated by attosecond pulses. Science 346, 336. https://doi.org/10.1126/science.1254061.

Cao, J., Wilson, K.R., 1997. A simple physical picture for quantum control of wave packet localization. J. Chem. Phys. 107 (5), 1441–1450. https://doi.org/10.1063/1.475151.

Cao, J., Bardeen, C.J., Wilson, K.R., 1998. Molecular "π pulse" for total inversion of electronic state population. Phys. Rev. Lett. 80 (7), 1406–1409. https://doi.org/10.1103/PhysRevLett.80.1406.

Chang, B.Y., Sola, I.R., 2005. Pump-dump iterative squeezing of vibrational wave packets. J. Chem. Phys. 123 (24), 244101. https://doi.org/10.1063/1.2139091.

Chang, B.Y., Sola, I.R., Malinovsky, V.S., Santamaria, J., 2000. Selective excitation of diatomic molecules by chirped laser pulses. J. Chem. Phys. 113 (12), 4901–4911. https://doi.org/10.1063/1.1289248.

Chang, B.Y., Sola, I.R., Santamaria, J., 2001a. High vibrational excitation and bond breaking by generalized raman ladder climbing. Chem. Phys. Lett. 341 (3), 373–381. https://doi.org/10.1016/S0009-2614(01)00485-7. http://www.sciencedirect.com/science/article/pii/S0009261401004857.

Chang, B.Y., Sola, I.R., Santamaria, J., 2001b. Optimizing Raman ladder climbing: Theory and application in Na_2. J. Phys. Chem. A 105 (39), 8864–8870. https://doi.org/10.1021/jp011077s.

Chang, B.Y., Sola, I.R., Santamaria, J., Malinovsky, V.S., Krause, J.L., 2001c. Transferring vibrational population between electronic states of diatomic molecules via light-induced-potential shaping. J. Chem. Phys. 114 (20), 8820–8830. https://doi.org/10.1063/1.1368130.

Chang, B.Y., Kim, B., Sola, I.R., 2003a. Electronic and vibrational population transfer in diatomic molecules as a function of chirp for different pulse bandwidths. J. Chem. Phys. 118 (14), 6270–6279. https://doi.org/10.1063/1.1559009.

Chang, B.Y., Rabitz, H., Sola, I.R., 2003b. Light-induced trapping of molecular wave packets in the continuum. Phys. Rev. A 68 (3), 031402. https://doi.org/10.1103/PhysRevA.68.031402.

Chang, B.Y., Lee, S., Sola, I.R., 2004. Stationary molecular wave packets at nonequilibrium nuclear configurations. J. Chem. Phys. 121 (22), 11118–11128. https://doi.org/10.1063/1.1811077.

Chang, B.Y., Lee, S., Sola, I.R., Santamari, J., 2005. Adiabatic squeezing of molecular wave packets by laser pulses. J. Chem. Phys. 122 (20), 204316. https://doi.org/10.1063/1.1904593.

Chang, B.Y., Lee, S., Sola, I.R., Santamari, J., 2006a. Wave-packet squeezing by iterative pump-dump control in diatomic molecules. Phys. Rev. A 73 (2), 023407. https://doi.org/10.1103/PhysRevA.73.023407.

Chang, B.Y., Lee, S., Sola, I.R., Santamaria, J., 2006b. Squeezing the ground vibrational state of diatomic molecules. J. Photochem. Photobio. A: Chem. 180 (3), 241–247. https://doi.org/10.1016/j.jphotochem.2006.02.006. http://www.sciencedirect.com/science/article/pii/S1010603006000463.

Chang, B.Y., Shin, S., Sola, I.R., 2010. Inducing changes in the bond length of diatomic molecules by time-symmetric chirped pulses. Phys. Rev. A 82 (6), 063414. https://doi.org/10.1103/PhysRevA.82.063414.

Chang, B.Y., Shin, S., Santamaria, J., Sola, I.R., 2011. Laser adiabatic manipulation of the bond length of diatomic molecules with a single chirped pulse. J. Chem. Phys. 134 (14), 144303. https://doi.org/10.1063/1.3574837.

Chang, B.Y., Shin, S., Santamaria, J., Sola, I.R., 2012. Ultrafast control of the internuclear distance with parabolic chirped pulses. J. Phys. Chem. A 116 (11), 2691–2697. https://doi.org/10.1021/jp2076484.

Chang, B.Y., Shin, S., Palacios, A., Martin, F., Sola, I.R., 2013. Two-pulse control of large-amplitude vibrations in H2+. Chemphyschem 14 (7), 1405–1412. https://doi.org/10.1002/cphc.201201078.

Chang, B.Y., Shin, S., Malinovsky, V.S., Sola, I.R., 2015a. The Hydrogen molecular cation as a molecular antenna. J. Phys. B 48 (17), 174005. http://stacks.iop.org/0953-4075/48/i=17/a=174005.

Chang, B.Y., Shin, S., Palacios, A., Martin, F., Sola, I.R., 2015b. Oscillating molecular dipoles require strongly correlated electronic and nuclear motion. J. Phys. B 48 (4), 043001. http://stacks.iop.org/0953-4075/48/i=4/a=043001.

Chang, B.Y., Shin, S., Sola, I.R., 2015c. State-selective excitation of quantum systems via geometrical optimization. J. Chem. Theor. Comp. 11 (9), 4005–4010. https://doi.org/10.1021/acs.jctc.5b00522.

Chang, B.Y., Shin, S., Sola, I.R., 2015d. "Stirred, not shaken": vibrational coherence can speed up electronic absorption. J. Phys. Chem. A 119 (34), 9091–9097. https://doi.org/10.1021/acs.jpca.5b05994.

Chang, B.Y., Shin, S., Sola, I.R., 2015e. Ultrafast population inversion without the strong field catch: the parallel transfer. J. Phys. Chem. Lett. 6 (9), 1724–1728. https://doi.org/10.1021/acs.jpclett.5b00651.

Chang, B.Y., Shin, S., Engel, V., Sola, I.R., 2017a. Geometrical optimization approach to isomerization: models and limitations. J. Phys. Chem. A 121 (43), 8280–8287. https://doi.org/10.1021/acs.jpca.7b08767.

Chang, B.Y., Shin, S., Park, Y.C., Lee, Y.S., Sola, I.R., 2017b. Laser control of the RbCs bond. Eur. Phys. J. D 71 (6), 167. https://doi.org/10.1140/epjd/e2017-80137-3.

Chelkowski, S., Bandrauk, A.D., 1997. Raman chirped adiabatic passage: a new method for selective excitation of high vibrational states. J. Ram. Spectr. 28 (6), 459–466. https://doi.org/10.1002/(sici)1097-4555(199706)28:6⟨459::Aid-jrs124⟩3.0.Co;2-y.

Chelkowski, S., Gibson, G.N., 1995. Adiabatic climbing of vibrational ladders using Raman transitions with a chirped pump laser. Phys. Rev. A 52 (5), R3417–R3420. https://doi.org/10.1103/PhysRevA.52.R3417.

Chelkowski, S., Bandrauk, A.D., Corkum, P.B., 1990. Efficient molecular dissociation by a chirped ultrashort infrared laser pulse. Phys. Rev. Lett. 65 (19), 2355–2358. https://doi.org/10.1103/PhysRevLett.65.2355.

Chen, Y., Gross, P., Ramakrishna, V., Rabitz, H., Mease, K., 1995. Competitive tracking of molecular objectives described by quantum mechanics. J. Chem. Phys. 102 (20), 8001–8010. https://doi.org/10.1063/1.468998.

Chen, P., Piermarocchi, C., Sham, L.J., Gammon, D., Steel, D.G., 2004. Theory of quantum optical control of a single spin in a quantum dot. Phys. Rev. B 69, 075320.

Chiara, G.D., Palma, G.M., 2003. Berry phase for a spin 1/2 particle in a classical fluctuating field. Phys. Rev. Lett. 91, 090404.

Combariza, J.E., Just, B., Manz, J., Paramonov, G.K., 1991. Isomerizations controlled by ultrashort infrared laser pulses: model simulations for the inversion of ligands (H) in the double-well potential of an organometallic compound, [(C5H5)(CO) 2FePH2]. J. Phys. Chem. 95 (25), 10351–10359. https://doi.org/10.1021/j100178a022.

Corrales, M.E., Gonzalez-Vazquez, J., Balerdi, G., Sola, I.R., de Nalda, R., Bañares, L., 2014. Control of ultrafast molecular photodissociation by laser-field-induced potentials. Nat. Chem. 6, 785. https://doi.org/10.1038/nchem.2006.

Corrales, M.E., de Nalda, R., Bañares, L., 2017. Strong laser field control of fragment spatial distributions from a photodissociation reaction. Nat. Commun. 8 (1), 1345. https://doi.org/10.1038/s41467-017-01139-6.

Csehi, A., Halász, G.J., Cederbaum, L.S., Vibók, A., 2017. Competition between light-induced and intrinsic nonadiabatic phenomena in diatomics. J. Phys. Chem. Lett. 8 (7), 1624–1630. https://doi.org/10.1021/acs.jpclett.7b00413.

Cubel, T., Teo, B.K., Malinovsky, V.S., Guest, J.R., Reinhard, A., Knuffman, B., Berman, P.R., Raithel, G., 2005. Coherent population transfer of ground-state atoms into Rydberg states. Phys. Rev. A 72, 023405.

D'Alessandro, D., 2007. Introduction to Quantum Control and Dynamics. Chapman & Hall.

Daniel, C., Full, J., González, L., Lupullescu, C., Manz, J., Merli, A., Vajda, S., Wöste, L., 2003. Deciphering the reaction dynamics underlying optimal control laser fields. Science 299, 536.

Davis, J.C., Warren, W.S., 1999. Selective excitation of high vibrational states using Raman chirped adiabatic passage. J. Chem. Phys. 110 (9), 4229–4237. https://doi.org/10.1063/1.478305.

Demekhin, P.V., Cederbaum, L.S., 2013. Light-induced conical intersections in polyatomic molecules: general theory, strategies of exploitation, and application. J. Chem. Phys 139 (15), 154314. https://doi.org/10.1063/1.4826172.

Deutsch, D., Barenco, A., Ekert, A., 1995. Universality in quantum computation. Proc. R. Soc. Lond. A 449, 669–677.

DiVincenzo, D.P., 2000. The physical implementation of quantum computation. Fortschr. Phys. 48, 771–783.

Economou, S.E., Reinecke, T.L., 2007. Theory of fast optical spin rotation in a quantum dot based on geometric phases and trapped states. Phys. Rev. Lett. 99, 217401.

Elghobashi, N., González, L., 2004. Breaking the strong and weak bonds of OHF^- using few-cycle IR + UV laser pulses. Phys. Chem. Chem. Phys. 6 (16), 4071–4073. https://doi.org/10.1039/B409446H.

Engel, V., Meier, C., Tannor, D.J., 2009. Local Control Theory: Recent Applications to Energy and Particle Transfer Processes in Molecules, vol. 141. John Wiley & Sons, Inc. ISBN: 9780470431917, pp. 29–101. https://doi.org/10.1002/9780470431917.ch2.

Falci, G., Fazio, R., Palma, G.M., Siewert, J., Vedral, V., 2000. Detection of geometric phases in superconducting nanocircuits. Nature 407, 355–358.

Falge, M., Engel, V., Gräfe, S., 2012a. Fingerprints of adiabatic versus diabatic vibronic dynamics in the asymmetry of photoelectron momentum distributions. J. Phys. Chem. Lett. 3 (18), 2617–2620.

Falge, M., Engel, V., Lein, M., Vindel-Zandbergen, P., Chang, B.Y., Sola, I.R., 2012b. Quantum wave-packet dynamics in spin-coupled vibronic states. J. Phys. Chem. A 116 (46), 11427–11433. https://doi.org/10.1021/jp306566x.

Falge, M., Vindel-Zandbergen, P., Engel, V., Lein, M., Chang, B.Y., Sola, I.R., 2014. The time-scale of nonlinear events driven by strong fields: can one control the spin coupling before ionization runs over? J. Phys. B 47 (12), 124027. http://stacks.iop.org/0953-4075/47/i=12/a=124027.

Falvo, C., Debnath, A., Meier, C., 2013. Vibrational ladder climbing in carboxy-hemoglobin: effects of the protein environment. J. Chem. Phys. 138 (14), 145101. https://doi.org/10.1063/1.4799271.

Friedrich, B., Herschbach, D., 1995. Alignment and trapping of molecules in intense laser fields. Phys. Rev. Lett. 74, 4623–4626. https://doi.org/10.1103/PhysRevLett.74.4623.

Garraway, B.M., Suominen, K.A., 1995. Wave-packet dynamics: new physics and chemistry in femto-time. Rep. Progr. Phys. 58 (4), 365. http://stacks.iop.org/0034-4885/58/i=4/a=001.

Garraway, B.M., Suominen, K.A., 1998. Adiabatic passage by light-induced potentials in molecules. Phys. Rev. Lett. 80 (5), 932–935. https://doi.org/10.1103/PhysRevLett.80.932.

Gaubatz, U., Rudecki, P., Schiemann, S., Bergmann, K., 1990. Population transfer between molecular vibrational levels by stimulated Raman scattering with partially overlapping laser fields. a new concept and experimental results. J. Chem. Phys. 92, 5363.

Geppert, D., de Vivie-Riedle, R., 2005. Reaction velocity control by manipulating the momentum of a nuclear wavepacket with phase-sensitive optimal control theory. Chem. Phys. Lett. 404, 289.

Geremia, J.M., Zhu, W., Rabitz, H., 2000. Incorporating physical implementation concerns into closed loop quantum control experiments. J. Chem. Phys. 113 (24), 10841–10848. https://doi.org/10.1063/1.1326905.

Giusti-Suzor, A., Mies, F.H., 1992. Vibrational trapping and suppression of dissociation in intense laser fields. Phys. Rev. Lett. 68 (26), 3869–3872. https://doi.org/10.1103/PhysRevLett.68.3869.

Giusti-Suzor, A., Mies, F.H., DiMauro, L.F., Charron, E., Yang, B., 1995. Dynamics of H_2^+ in intense laser fields. J. Phys. B 28 (3), 309. http://stacks.iop.org/0953-4075/28/i=3/a=006.

Glushko, B., Kryzhanovsky, B., 1992. Radiative and collisional damping effects on efficient population transfer in a three-level system driven by two delayed laser pulses. Phys. Rev. A 46, 2823–2830.

Gollub, C., Kowalewski, M., de Vivie-Riedle, R., 2008. Monotonic convergent optimal control theory with strict limitations on the spectrum of optimized laser fields. Phys. Rev. Lett. 101 (7), 073002. https://doi.org/10.1103/PhysRevLett.101.073002.

Gonzalez-Vazquez, J., Sola, I.R., Santamaria, J., 2006a. Adiabatic passage by light-induced potentials in polyatomic molecules. J. Phys. Chem. A 110 (4), 1586–1593. https://doi.org/10.1021/jp0539021.

Gonzalez-Vazquez, J., Sola, I.R., Santamaria, J., Malinovsky, V.S., 2006b. Optical control of the singlet-triplet transition in Rb_2. J. Chem. Phys. 125 (12), 124315. https://doi.org/10.1063/1.2355492.

Gonzalez-Vazquez, J., Sola, I.R., Santamaria, J., Malinovsky, V.S., 2006c. Quantum control of spin-orbit coupling by dynamic Stark-shifts induced by laser fields. Chem. Phys. Lett. 431 (4), 231–235. https://doi.org/10.1016/j.cplett.2006.09.085. http://www.sciencedirect.com/science/article/pii/S0009261406014473.

Gonzalez-Vazquez, J., Sola, I.R., Santamaria, J., Malinovsky, V.S., 2007. Vibrationally state-selective spin-orbit transfer with strong nonresonant pulses. J. Phys. Chem. A 111 (14), 2670–2678. https://doi.org/10.1021/jp066825y.

Gonzalez-Vazquez, J., González, L., Sola, I.R., Santamaria, J., 2009. Laser control of conical intersections: quantum model simulations for the averaged loss-gain strategies of fast electronic deactivation in 1,1-difluoroethylene. J. Chem. Phys. 131 (10), 104302. https://doi.org/10.1063/1.3223998.

Gordon, R.J., Rice, S.A., 1997. Active control of the dynamics of atoms and molecules. Annu. Rev. Phys. Chem. 48 (1), 601. http://search.ebscohost.com/login.aspx?direct=true&db=a9h&AN=5364962&site=ehost-live.

Goswami, D., 2003. Optical pulse shaping approaches to coherent control. Phys. Rep. 374 (6), 385–481. https://doi.org/10.1016/S0370-1573(02)00480-5. http://www.sciencedirect.com/science/article/pii/S0370157302004805.

Gräfe, S., Marquetand, P., Engel, V., Henriksen, N.E., Müller, K.B., 2004. Quantum control fields from instantaneous dynamics. Chem. Phys. Lett. 398 (1), 180–185. https://doi.org/10.1016/j.cplett.2004.09.050. http://www.sciencedirect.com/science/article/pii/S0009261404014356.

Greilich, A., Yakovlev, D.R., Shabaev, A., Efros, A.L., Yugova, I.A., Oulton, R., Stavarache, V., Wieck, A., Bayer, M., 2006. Mode locking of electron spin coherences in singly charged quantum dots. Science 313, 341–345.

Gross, P., Singh, H., Rabitz, H., Mease, K., Huang, G.M., 1993. Inverse quantum-mechanical control: a means for design and a test of intuition. Phys. Rev. A 47 (6), 4593–4604. https://doi.org/10.1103/PhysRevA.47.4593.

Guérin, S., 1997. Complete dissociation by chirped laser pulses designed by adiabatic Floquet analysis. Phys. Rev. A 56 (2), 1458–1462. https://doi.org/10.1103/PhysRevA.56.1458.

Guhr, M., Ibrahim, H., Schwentner, N., 2004. Controlling vibrational wave packet revivals in condensed phase: dispersion and coherence for Br_2 in solid Ar. Phys. Chem. Chem. Phys. 6 (23), 5353–5361. https://doi.org/10.1039/B413635G.

Halász, G.J., Sindelka, M., Moiseyev, N., Cederbaum, L.S., Vibók, A., 2012a. Light-induced conical intersections: topological phase, wave packet dynamics, and molecular alignment. J. Phys. Chem. A 116 (11), 2636–2643. https://doi.org/10.1021/jp206860p.

Halász, G.J., Vibók, A., Sindelka, M., Cederbaum, L.S., Moiseyev, N., 2012b. The effect of light-induced conical intersections on the alignment of diatomic molecules. Chem. Phys. 399, 146.

Halász, G.J., Vibók, A., Meyer, H.D., Cederbaum, L.S., 2013a. Effect of light-induced conical intersection on the photodissociation dynamics of the D_2^+ molecule. J. Phys. Chem. A 117, 8497.

Halász, G.J., Vibók, A., Moiseyev, N., Cederbaum, L.S., 2013b. Nuclear-wave-packet quantum interference in the intense laser dissociation of the D_2^+ molecule. Phys. Rev. A 88 (4), 043413. https://doi.org/10.1103/PhysRevA.88.043413.

Halász, G.J., Csehi, A., Vibók, A., Cederbaum, L.S., 2014. Influence of light-induced conical intersection on the photodissociation dynamics of D_2^+ starting from individual vibrational levels. J. Phys. Chem. A 118 (51), 11908–11915. https://doi.org/10.1021/jp504889e.

Halász, G.J., Vibók, A., Cederbaum, L.S., 2015. Direct signature of light-induced conical intersections in diatomics. J. Phys. Chem. Lett. 6 (3), 348–354. https://doi.org/10.1021/jz502468d.

Hawkins, P.E., Malinovskaya, S.A., Malinovsky, V.S., 2012. Ultrafast geometric control of a single qubit using chirped pulses. Phys. Scr. T147, 014013.

Herek, J.L., Wohlleben, W., Cogdell, R.J., Zeidler, D., Motzkus, M., 2002. Quantum control of energy flow in light harvesting. Nature 417, 533. https://doi.org/10.1038/417533a.

Hess, C., Wolf, M., Bonn, M., 2000. Direct observation of vibrational energy delocalization on surfaces: CO on Ru(001). Phys. Rev. Lett. 85 (20), 4341–4344. https://doi.org/10.1103/PhysRevLett.85.4341.

Hill, S., Wootters, W.K., 1997. Entanglement of a pair of quantum bits. Phys. Rev. Lett. 78, 5022–5025.

Ho, T.S., Rabitz, H., 2006. Why do effective quantum controls appear easy to find? J. Photochem. Photobiol. A: Chem. 180 (3), 226–240. https://doi.org/10.1016/j.jphotochem.2006.03.038. http://www.sciencedirect.com/science/article/pii/S1010603006001948.

Ho, T.S., Rabitz, H., 2010. Accelerated monotonic convergence of optimal control over quantum dynamics. Phys. Rev. E 82 (2), 026703. https://doi.org/10.1103/PhysRevE.82.026703.

Ho, T.S., Rabitz, H., Chu, S.I., 2014. Theoretical foundations for exploring quantum optimal control of molecules. In: World Sci.. ISBN: 9780470259474, pp. 1–57. https://doi.org/10.1142/9789814619042_0001

Huang, G.M., Tarn, T.J., Clark, J.W., 1983. On the controllability of quantum-mechanical systems. J. Math. Phys. 24 (11), 2608–2618. https://doi.org/10.1063/1.525634.

Jaksch, D., Cirac, J.I., Zoller, P., Rolston, S.L., Côté, R., Lukin, M.D., 2000. Fast quantum gates for neutral atoms. Phys. Rev. Lett. 85, 2208–2211.

Jaynes, E.T., Cummings, F.W., 1963. Comparison of quantum and semiclassical radiation theories with application to the beam maser. Proc. IEEE 51, 89–109.

Jiménez-Galán, A., Argenti, L., Martín, F., 2014. Modulation of attosecond beating in resonant two-photon ionization. Phys. Rev. Lett. 113, 263001. https://doi.org/10.1103/PhysRevLett.113.263001.

Joe-Wong, C., Ho, T.S., Rabitz, H., 2016. On choosing the form of the objective functional for optimal control of molecules. J. Math. Chem. 54 (1), 1–9. https://doi.org/10.1007/s10910-015-0558-7.

Jolicard, G., Atabek, O., 1992. Above-threshold-dissociation dynamics of H_2^+ with short intense laser pulses. Phys. Rev. A 46 (9), 5845–5855. https://doi.org/10.1103/PhysRevA.46.5845.

Jones, J.A., Vedral, V., Ekert, A., Castagnoli, G., 2000. Geometric quantum computation using nuclear magnetic resonance. Nature 403, 869–871.

Judson, R.S., Rabitz, H., 1992. Teaching lasers to control molecules. Phys. Rev. Lett. 68, 1500.

Kaiser, A., May, V., 2004. Optimal control theory for a target state distributed in time: Optimizing the probe-pulse signal of a pump-probe-scheme. J. Chem. Phys. 121 (6), 2528–2535. https://doi.org/10.1063/1.1769370.

Kallush, S., Band, Y.B., 2000. Short-pulse chirped adiabatic population transfer in diatomic molecules. Phys. Rev. A 61 (4), 041401. https://doi.org/10.1103/PhysRevA.61.041401.

Khaneja, N., Glaser, S.J., 2001. Cartan decomposition of SU(2n) and control of spin systems. Chem. Phys. 267 (1), 11–23. https://doi.org/10.1016/S0301-0104(01)00318-4. http://www.sciencedirect.com/science/article/pii/S0301010401003184.

Khaneja, N., Brockett, R., Glaser, S.J., 2001. Time optimal control in spin systems. Phys. Rev. A 63 (3), 032308. https://doi.org/10.1103/PhysRevA.63.032308.

Kim, J., Tao, H., White, J.L., Petrovi, V.S., Martinez, T.J., Bucksbaum, P.H., 2012. Control of 1,3-cyclohexadiene photoisomerization using light-induced conical intersections. J. Phys. Chem. A 116 (11), 2758–2763. https://doi.org/10.1021/jp208384b.

Koch, C.P., Shapiro, M., 2012. Coherent control of ultracold photoassociation. Chem. Rev. 112 (9), 4928–4948. https://doi.org/10.1021/cr2003882.

Kosloff, R., Rice, S.A., Gaspard, P., Tersigni, S., Tannor, D.J., 1989. Wavepacket dancing: achieving chemical selectivity by shaping light pulses. Chem. Phys. 139 (1), 201–220.

https://doi.org/10.1016/0301-0104(89)90012-8. http://www.sciencedirect.com/science/article/pii/0301010489900128.
Kosloff, R., Hammerich, A.D., Tannor, D., 1992. Excitation without demolition: radiative excitation of ground-surface vibration by impulsive stimulated Raman scattering with damage control. Phys. Rev. Lett. 69 (15), 2172–2175. https://doi.org/10.1103/PhysRevLett.69.2172.
Krause, J.L., Whitnell, R.M., Wilson, K.R., Yan, Y., Mukamel, S., 1993. Optical control of molecular dynamics: molecular cannons, reflectrons, and wave-packet focusers. J. Chem. Phys. 99 (9), 6562–6578. https://doi.org/10.1063/1.465848.
Kuklinski, J.R., Gaubatz, U., Hioe, F.T., Bergmann, K., 1989. Adiabatic population transfer in a three-level system driven by delayed laser pulses. Phys. Rev. A 40, 6741–7644.
Ladd, T.D., Jelezko, F., Laflamme, R., Nakamura, Y., Monroe, C., O'Brien, J.L., 2010. Quantum computers. Nature 464, 45–53.
Lapert, M., Tehini, R., Turinici, G., Sugny, D., 2009. Monotonically convergent optimal control theory of quantum systems with spectral constraints on the control field. Phys. Rev. A 79 (6), 063411. https://doi.org/10.1103/PhysRevA.79.063411.
Leibfried, D., DeMarco, B., Meyer, V., Lucas, D., Barrett, M., Britton, J., Itano, W.M., Jelenkovic, B., Langer, C., Rosenband, T., Wineland, D.J., 2003. Experimental demonstration of a robust, high-fidelity geometric two ion-qubit phase gate. Nature 422, 412–415.
Levin, L., Skomorowski, W., Rybak, L., Kosloff, R., Koch, C.P., Amitay, Z., 2015. Coherent control of bond making. Phys. Rev. Lett. 114, 233003. https://doi.org/10.1103/PhysRevLett.114.233003.
Levis, R.J., Menkir, G.M., Rabitz, H., 2001. Selective bond dissociation and rearrangement with optimally tailored, strong-field laser pulses. Science 292, 709.
Lewenstein, M., Balcou, P., Ivanov, M.Y., L'Huillier, A., Corkum, P.B., 1994. Theory of high-harmonic generation by low-frequency laser fields. Phys. Rev. A 49 (3), 2117–2132. https://doi.org/10.1103/PhysRevA.49.2117.
Li, X., Wu, Y., Steel, D., Gammon, D., Stievater, T.H., Katzer, D.S., Park, D., Piermarocchi, C., Sham, L.J., 2003. An all-optical quantum gate in a semiconductor quantum dot. Science 301, 809–811.
Liao, S.L., Ho, T.S., Chu, S.I., Rabitz, H., 2011. Fast-kick-off monotonically convergent algorithm for searching optimal control fields. Phys. Rev. A 84 (3), 031401. https://doi.org/10.1103/PhysRevA.84.031401.
Liu, R.B., Yao, W., Sham, L.J., 2010. Quantum computing by optical control of electron spins. Adv. Phys. 59, 703–802.
Lloyd, S., 1995. Almost any quantum logic gates is universal. Phys. Rev. Lett. 75, 346–349.
Lozovoy, V.V., Dantus, M., 2005. Systematic control of nonlinear optical processes using optimally shaped femtosecond pulses. ChemPhysChem 6 (10), 1970–2000. https://doi.org/10.1002/cphc.200400342.
Lukin, M.D., Fleischhauer, M., Cote, R., Duan, L.M., Jaksch, D., Cirac, J.I., Zoller, P., 2001. Dipole blockade and quantum information processing in mesoscopic atomic ensembles. Phys. Rev. Lett 87, 037901.
Lupo, C., Aniello, P., 2009. Robustness of the geometric phase under parametric noise. Phys. Scr. 79, 065012.
Maas, D.J., Duncan, D.I., Vrijen, R.B., van der Zande, W.J., Noordam, L.D., 1998. Vibrational ladder climbing in no by (sub)picosecond frequency-chirped infrared laser pulses. Chem. Phys. Lett. 290 (1), 75–80. https://doi.org/10.1016/S0009-2614(98)00531-4. http://www.sciencedirect.com/science/article/pii/S0009261498005314.
Maday, Y., Turinici, G., 2003. New formulations of monotonically convergent quantum control algorithms. J. Chem. Phys. 118 (18), 8191–8196. https://doi.org/10.1063/1.1564043.

Malinovskaya, S.A., 2006. Mode selective excitation using ultrafast chirped laser pulses. Phys. Rev. A. 73, 033416.
Malinovskaya, S.A., 2007. Chirped pulse control methods for imaging of biological structure and dynamics. Int. J. Quant. Chem. 107, 3151–3158.
Malinovskaya, S.A., 2009. Optimal coherence via adiabatic following. Opt. Comm. 282, 3527–3529.
Malinovskaya, S.A., Malinovsky, V.S., 2007. Chirped-pulse adiabatic control in coherent anti-Stokes Raman scattering for imaging of biological structure and dynamics. Opt. Lett. 32, 707–709.
Malinovsky, V.S., Krause, J.L., 2001a. General theory of population transfer by adiabatic rapid passage with intense, chirped laser pulses. Eur. Phys. J. D: At. Mol. Opt. Plas. Phys. 14 (2), 147–155. https://doi.org/10.1007/s100530170212.
Malinovsky, V.S., Krause, J.L., 2001b. Efficiency and robustness of coherent population transfer with intense, chirped laser pulses. Phys. Rev. A 63, 043415.
Malinovsky, V.S., Rudin, S., 2012a. Geometric single-qubit gates for an electron spin in a quantum dot. Int. J. Quant. Chem. 112, 3744–3749.
Malinovsky, V.S., Rudin, S., 2012b. Ultrafast control of electron spin in a quantum dot using geometric phase. Solid State Electron. 78, 28–33.
Malinovsky, V.S., Sola, I.R., 2006. Phase-controlled collapse and revival of entanglement of two interacting qubits. Phys. Rev. Lett. 96, 050502.
Malinovsky, V.S., Tannor, D.J., 1997. Simple and robust extension of the stimulated Raman adiabatic passage technique to *N*-level systems. Phys. Rev. A 56 (6), 4929–4937. https://doi.org/10.1103/PhysRevA.56.4929.
Malinovsky, V.S., Meier, C., Tannor, D.J., 1997. Optical paralysis in electronically congested systems: application to large-amplitude vibrational motion of ground state Na_2. Chem. Phys. 221 (1), 67–76. https://doi.org/10.1016/S0301-0104(97)00126-2. http://www.sciencedirect.com/science/article/pii/S0301010497001262.
Malinovsky, V.S., Santamaria, J., Sola, I.R., 2003. Controlling non-FranckCondon transitions: Counterintuitive schemes of population transfer in the adiabatic and strong adiabatic regimes. J. Phys. Chem. A 107 (40), 8259–8270. https://doi.org/10.1021/jp0226477.
Malinovsky, V.S., Sola, I.R., Vala, J., 2014. Phase-controlled two-qubit quantum gates. Phys. Rev. A 89, 032301.
Manz, J., Sundermann, K., de Vivie-Riedle, R., 1998. Quantum optimal control strategies for photoisomerization via electronically excited states. Chem. Phys. Lett. 290 (4), 415–422. https://doi.org/10.1016/S0009-2614(98)00472-2. http://www.sciencedirect.com/science/article/pii/S0009261498004722.
Marquetand, P., Engel, V., 2005. Predissociation and dissociation dynamics in quantum control fields. Chem. Phys. Lett. 407 (4), 471–476. https://doi.org/10.1016/j.cplett.2005.03.136. http://www.sciencedirect.com/science/article/pii/S0009261405005105.
Marquetand, P., Engel, V., 2007. Local control theory applied to molecular photoassociation. J. Chem. Phys. 127 (8), 084115. https://doi.org/10.1063/1.2762222.
McMullen, J.D., 1977. Chirped-pulse compression in strongly dispersive media. J. Opt. Soc. Am. 67 (11), 1575–1578. https://doi.org/10.1364/JOSA.67.001575. http://www.osapublishing.org/abstract.cfm?URI=josa-67-11-1575.
Melinger, J.S., Hariharan, A., Gandhi, S.R., Warren, W.S., 1991. Adiabatic population inversion in I_2 vapor with picosecond laser pulses. J. Chem. Phys. 95 (3), 2210–2213. https://doi.org/10.1063/1.460971.
Meshulach, D., Silberberg, Y., 1998. Coherent quantum control of two-photon transitions by a femtosecond laser pulse. Nature 396, 239. https://doi.org/10.1038/24329.
Meshulach, D., Silberberg, Y., 1999. Coherent quantum control of multiphoton transitions by shaped ultrashort optical pulses. Phys. Rev. A 60 (2), 1287–1292. https://doi.org/10.1103/PhysRevA.60.1287.

Meyer, S., Engel, V., 1997. Vibrational revivals and the control of photochemical reactions. J. Phys. Chem. A 101 (42), 7749–7753. https://doi.org/10.1021/jp971247u.

Mitra, A., Sola, I.R., Rabitz, H., 2003. Revealing quantum-control mechanisms through Hamiltonian encoding in different representations. Phys. Rev. A 67, 043409. https://doi.org/10.1103/PhysRevA.67.043409.

Moiseyev, N., Sindelka, M., Cederbaum, L.S., 2008. Laser-induced conical intersections in molecular optical lattices. J. Phys. B 41 (22), 221001. http://stacks.iop.org/0953-4075/41/i=22/a=221001.

Mølmer, K., Sørensen, A., 1999. Multiparticle entanglement of hot trapped ions. Phys. Rev. Lett. 82, 1835–1838.

Moore, K.W., Rabitz, H., 2011. Exploring quantum control landscapes: topology, features, and optimization scaling. Phys. Rev. A 84 (1), 012109. https://doi.org/10.1103/PhysRevA.84.012109.

Nägerl, H.C., Mark, M.J., Haller, E., Gustavsson, M., Hart, R., Danzl, J.G., 2011. Ultracold and dense samples of ground-state molecules in lattice potentials. J. Phys.: Conf. Ser. 264, 012015.

Nakahara, M., Ohmi, T., 2008. Quantum Computing. CRC Press, Boca Raton.

Nguyen-Dang, T.T., Chatelas, C., Tanguay, D., 1995. Time-resolved laser control of vibrational excitations in molecules. J. Chem. Phys. 102 (4), 1528–1539. https://doi.org/10.1063/1.468885.

Nielsen, M.A., Chuang, I.L., 2006. Quantum Computation and Quantum Information. Cambridge University Press.

Niikura, H., Villeneuve, D.M., Corkum, P.B., 2004. Stopping a vibrational wave packet with laser-induced dipole forces. Phys. Rev. Lett. 92 (13), 133002. https://doi.org/10.1103/PhysRevLett.92.133002.

Nuernberger, P., Vogt, G., Brixner, T., Gerber, G., 2007. Femtosecond quantum control of molecular dynamics in the condensed phase. Phys. Chem. Chem. Phys. 9 (20), 2470–2497. https://doi.org/10.1039/B618760A.

Nuernberger, P., Wolpert, D., Weiss, H., Gerber, G., 2010. Femtosecond quantum control of molecular bond formation. Proc. Nat. Acad. Sci. USA 107, 10366.

Ohtsuki, Y., Kono, H., Fujimura, Y., 1998. Quantum control of nuclear wave packets by locally designed optimal pulses. J. Chem. Phys. 109 (21), 9318–9331. https://doi.org/10.1063/1.477593.

Ohtsuki, Y., Turinici, G., Rabitz, H., 2004. Generalized monotonically convergent algorithms for solving quantum optimal control problems. J. Chem. Phys. 120 (12), 5509–5517. https://doi.org/10.1063/1.1650297.

Ohtsuki, Y., Teranishi, Y., Saalfrank, P., Turinici, G., Rabitz, H., 2007. Monotonically convergent algorithms for solving quantum optimal control problems described by an integrodifferential equation of motion. Phys. Rev. A 75 (3), 033407. https://doi.org/10.1103/PhysRevA.75.033407.

Ortigoso, J., Rodriguez, M., Gupta, M., Friedrich, B., 1999. Time evolution of pendular states created by the interaction of molecular polarizability with a pulsed nonresonant laser field. J. Chem. Phys. 110 (8), 3870–3875. https://doi.org/10.1063/1.478241.

Palao, J.P., Kosloff, R., 2002. Quantum computing by an optimal control algorithm for unitary transformations. Phys. Rev. Lett. 89 (18), 188301. https://doi.org/10.1103/PhysRevLett.89.188301.

Palao, J.P., Kosloff, R., 2003. Optimal control theory for unitary transformations. Phys. Rev. A 68 (6), 062308. https://doi.org/10.1103/PhysRevA.68.062308.

Paloviita, A., Suominen, K.A., Stenholm, S., 1995. Molecular excitation by chirped pulses. J. Phys. B 28 (8), 1463. http://stacks.iop.org/0953-4075/28/i=8/a=011.

Peirce, A.P., Dahleh, M.A., Rabitz, H., 1988. Optimal control of quantum-mechanical systems: existence, numerical approximation, and applications. Phys. Rev. A 37 (12), 4950–4964. https://doi.org/10.1103/PhysRevA.37.4950.

Präkelt, A., Wollenhaupt, M., Sarpe-Tudoran, C., Baumert, T., 2004. Phase control of a two-photon transition with shaped femtosecond laser-pulse sequences. Phys. Rev. A 70 (6), 063407. https://doi.org/10.1103/PhysRevA.70.063407.

Press, D., Ladd, T.D., Zhang, B., Yamamoto, Y., 2008. Complete quantum control of a single quantum dot spin using ultrafast optical pulses. Nature 456, 218–221.

Rabitz, H., de Vivie-Riedle, R., Motzkus, M., Kompa, K., 2000. Whither the future of controlling quantum phenomena? Science 288 (5467), 824–828. https://doi.org/10.1126/science.288.5467.824. http://science.sciencemag.org/content/sci/288/5467/824.full.pdf.

Rabitz, H.A., Hsieh, M.M., Rosenthal, C.M., 2004. Quantum optimally controlled transition landscapes. Science 303 (5666), 1998–2001. https://doi.org/10.1126/science.1093649. http://science.sciencemag.org/content/sci/303/5666/1998.full.pdf.

Rabitz, H., Hsieh, M., Rosenthal, C., 2005. Landscape for optimal control of quantum-mechanical unitary transformations. Phys. Rev. A 72 (5), 052337. https://doi.org/10.1103/PhysRevA.72.052337.

Rabitz, H., Ho, T.S., Hsieh, M., Kosut, R., Demiralp, M., 2006. Topology of optimally controlled quantum mechanical transition probability landscapes. Phys. Rev. A 74 (1), 012721. https://doi.org/10.1103/PhysRevA.74.012721.

Ramakrishna, V., Salapaka, M.V., Dahleh, M., Rabitz, H., Peirce, A., 1995. Controllability of molecular systems. Phys. Rev. A 51 (2), 960–966. https://doi.org/10.1103/PhysRevA.51.960.

Rangan, C., Bloch, A.M., Monroe, C., Bucksbaum, P.H., 2004. Control of trapped-ion quantum states with optical pulses. Phys. Rev. Lett. 92 (11), 113004. https://doi.org/10.1103/PhysRevLett.92.113004.

Renard, M., Chaux, R., Lavorel, B., Faucher, O., 2004. Pulse trains produced by phase-modulation of ultrashort optical pulses: tailoring and characterization. Opt. Expr. 12 (3), 473–482. https://doi.org/10.1364/OPEX.12.000473. http://www.opticsexpress.org/abstract.cfm?URI=oe-12-3-473.

Rey-de Castro, R., Rabitz, H., 2010. Laboratory implementation of quantum-control-mechanism identification through hamiltonian encoding and observable decoding. Phys. Rev. A 81, 063422. https://doi.org/10.1103/PhysRevA.81.063422.

Rice, S.A., Zhao, M., 2000. Optical Control of Molecular Dynamics. Wiley.

Robiscoe, R.T., 1983. Perturbative solution to the time-dependent two-level problem and the validity of the rosen-zener conjecture. Phys. Rev. A 27 (3), 1365–1372. https://doi.org/10.1103/PhysRevA.27.1365.

Rodriguez, M., Suominen, K.A., Garraway, B.M., 2000. Tailoring of vibrational state populations with light-induced potentials in molecules. Phys. Rev. A 62 (5), 053413. https://doi.org/10.1103/PhysRevA.62.053413.

Rosen, N., Zener, C., 1932. Double Stern-Gerlach experiment and related collision phenomena. Phys. Rev. 40 (4), 502–507. https://doi.org/10.1103/PhysRev.40.502.

Rosker, M.J., Dantus, M., Zewail, A.H., 1988. Femtosecond real-time probing of reactions. I. The technique. J. Chem. Phys. 89, 6113.

Roslund, J., Rabitz, H., 2009. Experimental quantum control landscapes: inherent monotonicity and artificial structure. Phys. Rev. A 80, 013408.

Rothman, A., Ho, T.S., Rabitz, H., 2005. Quantum observable homotopy tracking control. J. Chem. Phys. 123 (13), 134104. https://doi.org/10.1063/1.2042456.

Rothman, A., Ho, T.S., Rabitz, H., 2006. Exploring the level sets of quantum control landscapes. Phys. Rev. A 73 (5), 053401. https://doi.org/10.1103/PhysRevA.73.053401.

Ruhman, S., Kosloff, R., 1990. Application of chirped ultrashort pulses for generating large-amplitude ground-state vibrational coherence: a computer simulation. J. Opt. Soc. Am. B 7 (8), 1748–1752. https://doi.org/10.1364/JOSAB.7.001748. http://josab.osa.org/abstract.cfm?URI=josab-7-8-1748.

Rungta, P., Buzek, V., Caves, C.M., Hillery, M., Milburn, G.J., 2001. Universal state inversion and concurrence in arbitrary dimensions. Phys. Rev. A 64, 042315.
Russell, B., Rabitz, H., 2017. Common foundations of optimal control across the sciences: evidence of a free lunch. Phil. Trans. R. Soc. A 375 (2088), 20160210. https://doi.org/10.1098/rsta.2016.0210.
Salomon, J., Turinici, G., 2006. On the relationship between the local tracking procedures and monotonic schemes in quantum optimal control. J. Chem. Phys. 124 (7), 074102. https://doi.org/10.1063/1.2170085.
Sampedro, P., Chang, B.Y., Sola, I.R., 2016a. Nonresonant electronic transitions induced by vibrational motion in light-induced potentials. Phys. Chem. Chem. Phys. 18 (36), 25265–25270. https://doi.org/10.1039/C6CP04761K.
Sampedro, P., Chang, B.Y., Sola, I.R., 2016b. Protecting and accelerating adiabatic passage with time-delayed pulse sequences. Phys. Chem. Chem. Phys. 18 (19), 13443–13448. https://doi.org/10.1039/C6CP01680D.
Schirmer, S.G., Fu, H., Solomon, A.I., 2001. Complete controllability of quantum systems. Phys. Rev. A 63 (6), 063410. https://doi.org/10.1103/PhysRevA.63.063410.
Schirmer, S.G., Andrew, D.G., Viswanath, R., Herschel, R., 2002. Constructive control of quantum systems using factorization of unitary operators. J. Phys. A 35 (39), 8315. http://stacks.iop.org/0305-4470/35/i=39/a=313.
Schmidt-Kaler, F., Häffner, H., Riebe, M., Gulde, S., Lancaster, G.P.T., Deuschle, T., Becher, C., Roos, C.F., Eschne, J., Blatt, R., 2003. Realization of the Cirac-Zoller controlled-not quantum gate. Narture 422, 408–411.
Seideman, T., Hamilton, E., 2005. Nonadiabatic alignment by intense pulses. concepts, theory, and directions. Adv. Atom. Mol. Opt. Phys. 52, 289–329.
Seideman, T., Ivanov, M.Y., Corkum, P.B., 1995. Role of electron localization in intense-field molecular ionization. Phys. Rev. Lett. 75 (15), 2819–2822. https://doi.org/10.1103/PhysRevLett.75.2819.
Serban, I., Werschnik, J., Gross, E.K.U., 2005. Optimal control of time-dependent targets. Phys. Rev. A 71 (5), 053810. https://doi.org/10.1103/PhysRevA.71.053810.
Shapiro, M., Brumer, P., 1999. Coherent control of atomic, molecular, and electronic processes. Adv. Atom. Mol. Opt. Phys. 42, 287.
Shapiro, M., Brumer, P., 2003. Principles of the Quantum Control of Molecular Processes. Wiley & Sons, Hoboken.
Sharp, R., Mitra, A., Rabitz, H., 2008. Principles for determining mechanistic pathways from observable quantum control data. J. Math. Chem. 44 (1), 142–171. https://doi.org/10.1007/s10910-007-9298-7.
Shen, Z., Hsieh, M., Rabitz, H., 2006. Quantum optimal control: Hessian analysis of the control landscape. J. Chem. Phys. 124 (20), 204106. https://doi.org/10.1063/1.2198836.
Shi, S., Rabitz, H., 1990. Optimal control of selective vibrational excitation of harmonic molecules: analytic solution and restricted forms for the optimal fields. J. Chem. Phys. 92 (5), 2927–2937. https://doi.org/10.1063/1.457940.
Shi, S., Rabitz, H., 1991. Optimal control of bond selectivity in unimolecular reactions. Comp. Phys. Commun. 63 (1), 71–83. https://doi.org/10.1016/0010-4655(91)90239-H. http://www.sciencedirect.com/science/article/pii/001046559190239H.
Shi, S., Woody, A., Rabitz, H., 1988. Optimal control of selective vibrational excitation in harmonic linear chain molecules. J. Chem. Phys. 88 (11), 6870–6883. https://doi.org/10.1063/1.454384.
Shore, B.W., 2011. Manipulating Quantum Structures Using Laser Pulses. Cambridge University Press, Cambridge.
Shore, B.W., Knight, P.L., 1993. The Jaynes-Cummings model. J. Mod. Opt. 40, 1195–1238.

Shore, B.W., Bergmann, K., Oreg, J., Rosenwaks, S., 1991. Multilevel adiabatic population transfer. Phys. Rev. A 44, 7442.

Silberberg, Y., 2009. Quantum coherent control for nonlinear spectroscopy and microscopy. Annu. Rev. Phys. Chem. 60 (1), 277–292. https://doi.org/10.1146/annurev.physchem.040808.090427. http://www.annualreviews.org/doi/abs/10.1146/annurev.physchem.040808.090427.

Sindelka, M., Moiseyev, N., Cederbaum, L.S., 2011. Strong impact of light-induced conical intersections on the spectrum of diatomic molecules. J. Phys. B 44 (4), 045603. http://stacks.iop.org/0953-4075/44/i=4/a=045603.

Sola, I.R., 2004. Laser-assisted molecular engineering of bond lengths and vibrational motion. Phys. Rev. A 69 (3), 033401. https://doi.org/10.1103/PhysRevA.69.033401.

Sola, I.R., Malinovsky, V.S., 2003. Collapse of the stimulated Raman adiabatic passage due to geometrical factors and how to overcome it. Phys. Rev. A 68 (1), 013412. https://doi.org/10.1103/PhysRevA.68.013412.

Sola, I.R., Muñoz-Sanz, R., Santamaria, J., 1998a. Survival of molecular reaction control in a bistable system in condensed phase. J. Phys. Chem. A 102 (23), 4321–4327. https://doi.org/10.1021/jp973278v.

Sola, I.R., Santamaria, J., Tannor, D.J., 1998b. Optimal control of multiphoton excitation: a black box or a flexible toolkit? J. Phys. Chem. A 102 (23), 4301–4309. https://doi.org/10.1021/jp980281l.

Sola, I.R., Malinovsky, V.S., Chang, B.Y., Santamaria, J., Bergmann, K., 1999a. Coherent population transfer in three-level λ systems by chirped laser pulses: minimization of the intermediate-level population. Phys. Rev. A 59, 4494–4501.

Sola, I.R., Malinovsky, V.S., Tannor, D.J., 1999b. Optimal pulse sequences for population transfer in multilevel systems. Phys. Rev. A 60 (4), 3081–3090. https://doi.org/10.1103/PhysRevA.60.3081.

Sola, I.R., Chang, B.Y., Santamaria, J., Malinovsky, V.S., Krause, J.L., 2000a. Selective excitation of vibrational states by shaping of light-induced potentials. Phys. Rev. Lett. 85 (20), 4241–4244. https://doi.org/10.1103/PhysRevLett.85.4241.

Sola, I.R., Santamaria, J., Malinovsky, V.S., 2000b. Efficiency and robustness of adiabatic passage by light-induced potentials. Phys. Rev. A 61 (4), 043413. https://doi.org/10.1103/PhysRevA.61.043413.

Sola, I.R., Gonzalez-Vazquez, J., Malinovsky, V.S., 2006. Optical control of a spin switch in the weak spin-orbit coupling limit. Phys. Rev. A 74 (4), 043418. https://doi.org/10.1103/PhysRevA.74.043418.

Sola, I.R., Shin, S., Chang, B.Y., 2011. Bond lengths of diatomic molecules periodically driven by light: the p-LAMB scheme. J. Chem. Phys. 134 (10), 104301. https://doi.org/10.1063/1.3562123.

Somlói, J., Kazakov, V.A., Tannor, D.J., 1993. Controlled dissociation of I_2 via optical transitions between the X and B electronic states. Chem. Phys. 172 (1), 85–98. https://doi.org/10.1016/0301-0104(93)80108-L. http://www.sciencedirect.com/science/article/pii/030101049380108L.

Spano, F., Hares, M., Warren, W.S., 1987. Spectroscopic demonstration of picosecond, phase-shifted laser multiple-pulse sequences. Chem. Phys. Lett. 135, 97.

Sørensen, A., Mølmer, K., 1999. Quantum computation with ions in thermal motion. Phys. Rev. Lett. 82, 1971–1974.

Sørensen, A., Mølmer, K., 2000. Entanglement and quantum computation with ions in thermal motion. Phys. Rev. A. 62, 022311.

Stapelfeldt, H., Seideman, T., 2003. Colloquium: aligning molecules with strong laser pulses. Rev. Mod. Phys. 75 (2), 543–557. https://doi.org/10.1103/RevModPhys.75.543.

Sugawara, M., Yoshizawa, S., Yabushita, S., 2001. Coherent control of wavepacket dynamics by locally designed external field. Chem. Phys. Lett. 350 (3), 253–259. https://doi.

org/10.1016/S0009-2614(01)01259-3. http://www.sciencedirect.com/science/article/pii/S0009261401012593.
Sukharev, M., Seideman, T., 2004. Optimal control approach to suppression of radiationless transitions. Phys. Rev. Lett. 93 (9), 093004. https://doi.org/10.1103/PhysRevLett.93.093004.
Sun, Y., Metcalf, H., 2014. Nonadiabaticity in stimulated Raman adiabatic passage. Phys. Rev. A 90, 033408.
Suominen, K.A., 2014. Multistate APLIP and VibLIP: from molecular bond extension to atomic transport. J. Mod. Opt. 61 (10), 851–856. https://doi.org/10.1080/09500340.2013.854423.
Sussman, B.J., Townsend, D., Ivanov, M.Y., Stolow, A., 2006. Dynamic Stark control of photochemical processes. Science 314 (5797), 278–281. https://doi.org/10.1126/science.1132289. http://science.sciencemag.org/content/sci/314/5797/278.full.pdf.
Tamura, H., Nanbu, S., Ishida, T., Nakamura, H., 2006. Ab initio nonadiabatic quantum dynamics of cyclohexadiene/hexatriene ultrafast photoisomerization. J. Chem. Phys. 124, 084313.
Tang, H., Kosloff, R., Rice, S.A., 1996. A generalized approach to the control of the evolution of a molecular system. J. Chem. Phys. 104 (14), 5457–5471. https://doi.org/10.1063/1.471785.
Tannor, D.J., Rice, S.A., 1985. Control of selectivity of chemical reaction via control of wave packet evolution. J. Chem. Phys 83 (10), 5013–5018. https://doi.org/10.1063/1.449767.
Tannor, D., Kosloff, R., Rice, S.A., 1986. Coherent pulse sequence induced control of selectivity of reactions: exact quantum mechanical calculations. J. Chem. Phys. 85, 5805.
Tavis, M., Cummings, F.W., 1968. Exact solution for an N-molecule-radiation-field Hamiltonian. Phys. Rev. 170, 379–384.
Tesch, C.M., de Vivie-Riedle, R., 2002. Quantum computation with vibrationally excited molecules. Phys. Rev. Lett. 89 (15), 157901. https://doi.org/10.1103/PhysRevLett.89.157901.
Thomas, E.F., Henriksen, N.E., 2016. Non-resonant dynamic Stark control of vibrational motion with optimized laser pulses. J. Chem. Phys. 144 (24), 244307. https://doi.org/10.1063/1.4954663.
Townsend, D., Sussman, B.J., Stolow, A., 2011. A Stark future for quantum control. J. Phys. Chem. A 115 (4), 357–373. https://doi.org/10.1021/jp109095d.
Trallero, C., Pearson, B.J., Weinacht, T., Gillard, K., Matsika, S., 2008. Interpreting ultrafast molecular fragmentation dynamics with ab initio electronic structure calculations. J. Chem. Phys. 128, 124107.
Troppmann, U., Gollub, C., de Vivie-Riedle, R., 2006. The role of phases and their interplay in molecular vibrational quantum computing with multiple qubits. New J. Phys. 8 (6), 100. http://stacks.iop.org/1367-2630/8/i=6/a=100.
Turinici, G., Herschel, R., 2003. Wavefunction controllability for finite-dimensional bilinear quantum systems. J. Phys. A 36 (10), 2565. http://stacks.iop.org/0305-4470/36/i=10/a=316.
Turinici, G., Rabitz, H., 2001. Quantum wavefunction controllability. Chem. Phys. 267 (1), 1–9. https://doi.org/10.1016/S0301-0104(01)00216-6. http://www.sciencedirect.com/science/article/pii/S0301010401002166.
Turinici, G., Le Bris, C., Rabitz, H., 2004. Efficient algorithms for the laboratory discovery of optimal quantum controls. Phys. Rev. E 70 (1), 016704. https://doi.org/10.1103/PhysRevE.70.016704.
Vindel-Zandbergen, P., Meier, C., Sola, I.R., 2016. Local control approach to ultrafast electron transfer. Chem. Phys. 478, 97–102. https://doi.org/10.1016/j.chemphys.2016.04.015. http://www.sciencedirect.com/science/article/pii/S0301010416301574.

Vitanov, N.V., Stenholm, S., 1996. Non-adiabatic effects in population transfer in three-level systems. Opt. Commun. 127, 215–222.
Vitanov, N.V., Stenholm, S., 1997. Analytic properties and effective two-level problems in stimulated Raman adiabatic passage. Phys. Rev. A 55, 648–660.
Vitanov, N.V., Shore, B.W., Bergmann, K., 1998. Adiabatic population transfer in multistate chains via dressed intermediate states. Eur. Phys. J. D 4, 15–29.
Vitanov, N.V., Halfmann, T., Shore, B.W., Bergmann, K., 2001. Laser-induced population transfer by adiabatic passage techniques. Ann. Rev. Phys. Chem. 52 (1), 763–809. https://doi.org/10.1146/annurev.physchem.52.1.763.
Vitanov, N.V., Rangelov, A.A., Shore, B.W., Bergmann, K., 2017. Stimulated Raman adiabatic passage in physics, chemistry, and beyond. Rev. Mod. Phys. 89, 015006.
Vogt, G., Krampert, G., Niklaus, P., Nuernberger, P., Gerber, G., 2005. Optimal control of photoisomerization. Phys. Rev. Lett. 94, 068305.
Wefers, M.M., Nelson, K.A., 1995. Analysis of programmable ultrashort waveform generation using liquid-crystal spatial light modulators. J. Opt. Soc. Am. B 12 (7), 1343–1362. https://doi.org/10.1364/JOSAB.12.001343. http://josab.osa.org/abstract.cfm?URI=josab-12-7-1343.
Weiner, A.M., 1995. Femtosecond optical pulse shaping and processing. Prog. Quant. Electr. 19 (3), 161–237. https://doi.org/10.1016/0079-6727(94)00013-O. http://www.sciencedirect.com/science/article/pii/007967279400013O.
Weiner, A.M., 2000. Femtosecond pulse shaping using spatial light modulators. Rev. Sci. Instr. 71 (5), 1929–1960. https://doi.org/10.1063/1.1150614.
Weiner, A.M., Heritage, J.P., Thurston, R.N., 1986. Synthesis of phase-coherent, picosecond optical square pulses. Opt. Lett. 11, 153.
Weiner, A.M., Leaird, D.E., Wiederrecht, G.P., Nelson, K.A., 1990. Femtosecond pulse sequences used for optical manipulation of molecular motion. Science 247 (4948), 1317–1319. https://doi.org/10.1126/science.247.4948.1317. http://science.sciencemag.org/content/sci/247/4948/1317.full.pdf.
Wells, E., Rallis, C.E., Zohrabi, M., Siemering, R., Jochim, B., Andrews, P.R., Ablikim, U., Gaire, B., De, S., Carnes, K.D., Bergues, B., de Vivie-Riedle, R., Kling, M.F., Ben-Itzhak, I., 2013. Adaptive strong-field control of chemical dynamics guided by three-dimensional momentum imaging. Nature Comm. 4:2895. https://doi.org/10.1038/ncomms3895.
Werschnik, J., Gross, E.K.U., 2005. Tailoring laser pulses with spectral and fluence constraints using optimal control theory. J. Opt. B: Quant. Sem. Opt. 7 (10), S300. http://stacks.iop.org/1464-4266/7/i=10/a=014.
Werschnik, J., Gross, E.K.U., 2007. Quantum optimal control theory. J. Phys. B 40 (18), R175. http://stacks.iop.org/0953-4075/40/i=18/a=R01.
Witte, T., Hornung, T., Windhorn, L., Proch, D., de Vivie-Riedle, R., Motzkus, M., Kompa, K.L., 2003. Controlling molecular ground-state dissociation by optimizing vibrational ladder climbing. J. Chem. Phys. 118 (5), 2021–2024. https://doi.org/10.1063/1.1540101.
Wollenhaupt, M., Baumert, T., 2006. Ultrafast strong field quantum control on K_2 dimers. J. Photochem. Photobiol. A: Chem. 180 (3), 248–255. https://doi.org/10.1016/j.jphotochem.2006.03.010. http://www.sciencedirect.com/science/article/pii/S1010603006001444.
Wollenhaupt, M., Engel, V., Baumert, T., 2005. Femtosecond laser photoelectron spectroscopy on atoms and small molecules: prototype studies in quantum control. Annu. Rev. Phys. Chem. 56, 25–56. https://doi.org/10.1146/annurev.physchem.56.092503.141315.
Wollenhaupt, M., Liese, D., Prkelt, A., Sarpe-Tudoran, C., Baumert, T., 2006. Quantum control by ultrafast dressed states tailoring. Chem. Phys. Lett. 419 (1), 184–190. https://

doi.org/10.1016/j.cplett.2005.11.079. http://www.sciencedirect.com/science/article/pii/S0009261405018166.
Wollenhaupt, M., Bayer, T., Vitanov, N.V., Baumert, T., 2010. Three-state selective population of dressed states via generalized spectral phase-step modulation. Phys. Rev. A 81 (5), 053422. https://doi.org/10.1103/PhysRevA.81.053422.
Wootters, W.K., 1998. Entanglement of formation of an arbitrary state of two qubits. Phys. Rev. Lett. 80, 2245–2248.
Worth, G.A., Richings, G.W., 2013. Optimal control by computer. Annu. Rep. Sect. C Phys. Chem. 109, 113–139. https://doi.org/10.1039/C3PC90003G.
Wu, R., Rabitz, H., Turinici, G., Sola, I., 2004. Connectivity analysis of controlled quantum systems. Phys. Rev. A 70 (5), 052507. https://doi.org/10.1103/PhysRevA.70.052507.
Yakovlev, V.V., Bardeen, C.J., Che, J., Cao, J., Wilson, K.R., 1998. Chirped pulse enhancement of multiphoton absorption in molecular iodine. J. Chem. Phys. 108 (6), 2309–2313. https://doi.org/10.1063/1.475615.
Yang, B., Saeed, M., DiMauro, L.F., Zavriyev, A., Bucksbaum, P.H., 1991. High-resolution multiphoton ionization and dissociation of H_2 and D_2 molecules in intense laser fields. Phys. Rev. A 44 (3), R1458–R1461. https://doi.org/10.1103/PhysRevA.44.R1458.
Yao, G., Chu, S.I., 1992. Laser-induced molecular stabilization and trapping and chemical bond hardening in intense laser fields. Chem. Phys. Lett. 197 (4), 413–418. https://doi.org/10.1016/0009-2614(92)85793-A. http://www.sciencedirect.com/science/article/pii/000926149285793A.
Yu, T., Eberly, J.H., 2002. Phonon decoherence of quantum entanglement: robust and fragile states. Phys. Rev. B 66, 193306.
Yu, T., Eberly, J.H., 2003. Qubit disentanglement and decoherence via dephasing. Phys. Rev. B 68, 165322.
Yuan, J.M., George, T.F., 1978. Semiclassical theory of unimolecular dissociation induced by a laser field. J. Chem. Phys. 68 (7), 3040–3052. https://doi.org/10.1063/1.436170.
Zanardi, P., Rasetti, M., 1999. Holonomic quantum computation. Phys. Lett. A 264, 94–99.
Zavriyev, A., Bucksbaum, P.H., Muller, H.G., Schumacher, D.W., 1990. Ionization and dissociation of H_2 in intense laser fields at 1.064 μm, 532 nm, and 355 nm. Phys. Rev. A 42 (9), 5500–5513. https://doi.org/10.1103/PhysRevA.42.5500.
Zavriyev, A., Bucksbaum, P.H., Squier, J., Saline, F., 1993. Light-induced vibrational structure in H_2^+ and D_2^+ in intense laser fields. Phys. Rev. Lett. 70 (8), 1077–1080. https://doi.org/10.1103/PhysRevLett.70.1077.
Zewail, A.H., 1988. Laser Femtochemistry. Science 242, 1645.
Zewail, A.H., 2000. Femtochemistry: atomic-scale dynamics of the chemical bond. J. Phys. Chem. A 104, 5660.
Zhang, J., Vala, J., Sastry, S., Whaley, K.B., 2003. Geometric theory of nonlocal two-qubit operations. Phys. Rev. A 67, 042313.
Zhu, W., Rabitz, H., 1998. A rapid monotonically convergent iteration algorithm for quantum optimal control over the expectation value of a positive definite operator. J. Chem. Phys. 109 (2), 385–391. https://doi.org/10.1063/1.476575.
Zhu, W., Rabitz, H., 2003. Quantum control design via adaptive tracking. J. Chem. Phys. 119 (7), 3619–3625. https://doi.org/10.1063/1.1582847.
Zhu, W., Botina, J., Rabitz, H., 1998. Rapidly convergent iteration methods for quantum optimal control of population. J. Chem. Phys. 108 (5), 1953–1963. https://doi.org/10.1063/1.475576.
Zhu, W., Smit, M., Rabitz, H., 1999. Managing singular behavior in the tracking control of quantum dynamical observables. J. Chem. Phys. 110 (4), 1905–1915. https://doi.org/10.1063/1.477857.